UNIVERSITY OF CALIFORNIA SAN DIEGO

A Seed Resource for Screening Functionally Redundant Genes

&

Isolation of Novel Mutants Impaired in Abiotic Responses

A dissertation submitted in partial satisfaction of the

requirements for the degree of Doctor of Philosophy

in

Biology

by

Paulo Henrique de Oliveira Ceciliato

Committee in charge:

Professor Julian I. Schroeder, Chair
Professor Mark Estelle
Professor Randolph Hampton
Professor Ralph F. Keeling
Professor Sergey Kryazhimskiy

2019

The dissertation of Paulo Henrique de Oliveira Ceciliato is approved, and it is acceptable in quality and form for publication on microfilm and electronically:

_____

_____

_____

_____

_____

Chair

University of California San Diego

2019

DEDICATION

I dedicate this dissertation to my family, my friends and my co-workers who have helped me during these past few years. In special, I dedicate this dissertation to the love of my life, Keini Dressano, who is my endless source of inspiration and strength.

To my parents, Carlos and Gisele, to my grandparents Maria Amalia and Franklin and to my siblings Carlos and Fernanda who even hundreds of miles away, are always there for me providing unconditional love and support.

EPIGRAPH

Imagination is more important than knowledge.

For knowledge is limited, whereas imagination embraces the entire world.

Albert Einstein

TABLE OF CONTENTS

LIST OF ABBREVIATIONS

βCA	Beta Carbonic Anhydrase
[CO_2]	CO_2 Concentration
ABA	Abscisic Acid
ABI1/2	ABA-Insensitive 1/2
ABI4/5	ABA-Insensitive 4/5
ABRC	Arabidopsis Biological Resource Center
AHG1/3	ABA-Hypersensitive Germination 1/3
AIG	Avirulence-induced gene 2
amiRNA	Artificial MicroRNA
BiFC	Bimolecular Florescence Complementation
BPM3/5	BTB/POZ and Math Domain 3/5
CBC1/2	Convergence of Blue Light and CO_2
Ci	Internal concentration of CO_2
Col-0	Columbia-0
CRISPR/Cas9	Clustered Regularly Interspaced Short Palindromic Repeats Cas9 (CRISPR associated protein 9)
EMS	Ethyl methanesulfonate
ERA1	Enhanced Response to ABA 1
Flg22	Flagellin 22
FLS2	Flagellin-Sensitive 2
GA	Gibberellic Acid
Gs	Stomatal Conductance

HAB1/2	ABA-Hypersensitive 1/2
HAI1/2/3	Higly ABA-Induced 1/2/3
HsMYO	*Homo sapiens* Myosin 2
HT1	High Leaf Temperature 1
IP/MS	Spectrometry-based Immuno-Precipitation
LB	Luria-Bertani-Miller medium
Mpk4/12	Mitogen-Activated Protein Kinase 4/12
MS	Murashige and Skoog
OD	Optical Density
OST1	Open Stomata 1
PAB	Proteasome Alpha Subunit B
PAG	Proteasome Alpha Subunit G
PIP	Plasma Membrane Intrinsic Protein
PP2C	Protein Phosphatase Type 2C
PPM	Parts Per Million
PUB12/13	Plant U-Box 12/13
PYL	Pyrabactin Resistance 1(PYR1)-Like
PYR	Pyrabactin Resistance 1
RAB18	Responsive to ABA 18
RCAR	Regulatory Components of ABA Receptors
RGKG1	Ring Domain Ligase 1
RopGEF1	ROP (Rho of Plants) Guanine nucleotide Exchange Factor 1
RPM	Rotations per Minute

SCF	Skp1- Rbx1-Cul1-F-box protein
SLAC1	Slow Anion Channel-Associated 1
SnRK2	Sucrose Nonfermenting1-Related Subfamily 2
WGS	Whole Genome Sequencing
WMD3	Web MicroRNA Designer
WT	Wild Type
Y2H	Yeast-two-Hybrid

LIST OF FIGURES

LIST OF TABLES

ACKNOWLEDGEMENTS

More experienced scientists once told me that teamwork is key to success, and these past few years as a PhD student proved them right. I would never be where I am or even be who I am, if it was not for the amazing people I have had the privilege to work with. First of all, I thank my advisor Julian I. Schroeder for giving me this great opportunity. Julian taught me so much about what being a good scientist and a good team leader means, I will be forever grateful. But Julian was not the only one teaching me all of this. Special thanks to my committee members: Mark Estelle, Randy Hampton, Ralph Keeling and Sergey Kryazhimskiy. It was a privilege to have you mentoring me for these past four-and-half years. Please do not become strangers!

Sometimes things go wrong in life… if you are a PhD student, this happens quite often. But if you surround yourself with great scientists, troubleshooting becomes so much easier. Thanks to my wonderful lab members, I have always had someone helping me when I needed. Thank you to all the members of the Schroeder lab. Of course, a more than special thanks to my dearest friends Guillaume Dubeaux, Sebastian Schulze and Klara Kernig. Team optimistic forever!! And, of course, how would I ever survive without my amazing and more experienced PhD student friends?! I do not know. Andrew Cooper and Diane Pater, thank you for everything you taught me and all the pain you saved me from with your priceless advice and input.

This paragraph is now dedicated to people outside the lab who I had the pleasure to work with. Thank you, Marty Yanofsky, Yunde Zhao and Cindy Gustafson-Brown for everything you taught me when I was teaching with you. The Division grad office, especially Marifel Alfaro, Suzi Harlow and Melody Bazyar. My classmates for making me feel so welcome and motivated. My dear Alyona Bobkova, who makes me feel home with all her kindness. To my former PI, Daniel

Scherer de Moura, who was and still is more important to me as a scientist model than I will ever be able to describe.

Thanks to the Brachypodium team, Felipe Rangel, Morgana Sidhom, Bryn Lopez and Li Zhang.

I would like to acknowledge the financial support of the Ciencias sem Fronteiras CNPq/CAPES fellowship from Brazil.

Chapter 1, in full, is published as it may appear in Journal of Experimental Botany, Hauser, F; Ceciliato, PHO; Lin, YC; Guo, D; Gregerson, JD; Abbasi, N; Youhanna, D; Park, J; Dubeaux, G; Shani, E; Poomchongkho, N; Schroeder, JI. The dissertation author was the primary investigator and author of this paper.

Chapter 2 is coauthored with Hauser, G; Gendron, J; Schroeder, JI. The dissertation author was the primary author of this chapter.

Chapter 3, in full, is published as it may appear in Plant Methods, Ceciliato, PHO; Zhang, J; Liu, Q; Shen, X; Hu, H; Liu, C; Schäffner, AR; Schroeder JI. The dissertation author was the primary investigator and author of this paper.

Chapter 4 is coauthored with Sidhom, M; Rangel, F; Zhang, L; Lopez, B; Schroeder, JI. The dissertation author was the primary author of this chapter.

VITA

EDUCATION

2013 Bachelor of Biological Sciences

Universidade de São Paulo -ESALQ/USP, Brazil (2009-2013).

2015 Masters of Genetics and Plant Breeding

Universidade de São Paulo -ESALQ/USP, Brazil (2013-2015).

2019 Doctor of Philosophy, Biology

University of California San Diego -UCSD, USA (2015-2019).

PUBLICATIONS

- **Paulo H. O. Ceciliato**, Jingbo Zhang, Qing Liu, Xin Shen, Honghong Hu, Chen Liu, Anton R. Schäffner, Julian I. Schroeder. Intact leaf gas exchange provides a robust method for measuring the kinetics of stomatal conductance responses to abscisic acid and other small molecules in *Arabidopsis* and grasses. *Plant Methods* **(2019)**. https://doi.org/10.1186/s13007-019-0423-y.

- Jiyoung Park, Tae-Houn Kim, Yohei Takahashi, Rebecca Schwab, Keini Dressano, Aaron B. Stephan, **Paulo H. O. Ceciliato**, Eduardo Ramirez, Vince Garin, Alisa Huffaker, Julian I. Schroeder. Chemical genetic identification of a lectin receptor kinase that transduces immune responses and interferes with abscisic acid signaling. *The Plant Journal* **(2019)**. https://doi.org/10.1111/tpj.14232.

- Felix Hauser*****, **Paulo H. O. Ceciliato***, Yi-Chen Lin, DanDan Guo, JD Gregerson, Nazia Abbasi, Diana Youhanna, Jiyoung Park, Guillaume Dubeaux, Eilon Shani, Nusra Poomchongkho, Julian I. Schroeder. A seed resource for screening functionally redundant genes and isolation of new mutants impaired in CO_2 and ABA responses. *Journal of Experimental Botany* **(2019)**. https://doi.org/10.1093/jxb/ery363 *****Authors contributed equally to this work.

- Jingbo Zhang, **Paulo H. O. Ceciliato**, Yohei Takahashi, Sebastian Schulze, Tamar Shemer, Guillaume Dubeaux, Felix Hauser, Wouter-Jan Rappel, Hannes Kollist and Julian Schroeder. Insights into the Molecular Mechanisms of CO2-Mediated Regulation of Stomatal Movements **(2018)**. *Current Biology*. https://doi.org/10.1016/j.cub.2018.10.015.

- Kadri Tõldsepp, Jingbo Zhang, Yohei Takahashi, Yana Sindarovska, Hanna Hõrak, **Paulo H. O. Ceciliato**, Kaspar Koolmeister, Yuh-Shuh Wang, Lauri Vaahtera, Liina Jakobson, Chung-Yueh Yeh, Jiyoung Park, Mikael Brosche, Julian I. Schroeder, Hannes Kollist. Mitogen-activated protein kinases MPK4 and MPK12 are key components mediating CO_2-induced stomatal movements **(2018)**. *The Plant Journal*. https://doi.org/10.1111/tpj.14087.

- Aparecida L Silva, Keini Dressano, **Paulo H. O. Ceciliato,** Juan Carlos Guerrero-Abad, Daniel S Moura. Evaluation of Root pH Change Through Gel Containing pH-sensitive Indicator Bromocresol Purple **(2018)**. *Bio-protocol*. https://10.21769/BioProtoc.2796.

- Wellington F Campos*, Keini Dressano*, **Paulo H. O. Ceciliato*,** Juan Carlos Guerrero-Abad, Aparecida L Silva, Celso S Fiori, Amanda Morato do Canto, Tábata Bergonci, Lucas AN Claus, Marcio C Silva-Filho, Daniel S Moura. Arabidopsis thaliana rapid alkalinization factor 1-mediated root growth inhibition is dependent on calmodulin-like protein 38 **(2017)**. *Journal of Biological Chemistry* https://10.1074/jbc.M117.808881. *Authors contributed equally to this work.

- Keini Dressano, **Paulo H. O. Ceciliato**, Aparecida L Silva, Juan Carlos Guerrero-Abad, Tábata Bergonci, Fausto Andrés Ortiz-Morea, Marco Bürger, Marcio C Silva-Filho, Daniel S Moura et al. **(2017)**. *PLOS Genetics.* https://doi.org/10.1371/journal.pgen.1007053

- Amanda Morato do Canto*, **Paulo H. O. Ceciliato***, Bianca Ribeiro*, Fausto Andrés Ortiz Morea, Antonio Augusto Franco Garcia, Marcio C Silva-Filho, Daniel S Moura. Biological activity of nine recombinant AtRALF peptides: Implications for their perception and function in Arabidopsis. *Plant Physiology and Biochemistry* **(2014)**. https://doi.org/10.1016/j.plaphy.2013.12.005. *Authors contributed equally to this work.

- Tábata Bergonci, Bianca Ribeiro, **Paulo H. O. Ceciliato**, Juan Carlos Guerrero-Abad, Marcio C Silva-Filho, Daniel S Moura. *Arabidopsis thaliana* RALF1 opposes brassinosteroid effects on root cell elongation and lateral root formation **(2014)**. *Journal of Experimental Botany*. https://doi.org/10.1093/jxb/eru099.

AWARDS

- Excellence in Teaching award (UC San Diego) (2019).
- Goeddel Endowed Award (UC San Diego).
- Excellence in Teaching award (UC San Diego) (2017).
- Ciência sem Fronteiras Fellowship, CNPq. PhD research (2015 – 2019).
- CAPES Fellowship. Master's research (2013-2015).
- FAPESP Fellowship. Scientific initiation research (2012-2013).
- CNPq Fellowship. Scientific initiation research (2010-2012).
- RUSP Fellowship. Scientific initiation research (2009-2010).

ABSTRACT OF THE DISSERTATION

A Seed Resource for Screening Functionally Redundant Genes

&

Isolation of Novel Mutants Impaired in Abiotic Responses

by

Paulo Henrique de Oliveira Ceciliato

Doctor of Philosophy in Biology

University of California San Diego, 2019

Professor Julian I. Schroeder, Chair

Overview: The global atmospheric CO_2 concentration is rising and in 2013 it surpassed 400 parts per million for the first time in human history. Plants can sense CO_2 concentrations in leaves and adapt transpiration accordingly. Ultimately, plants control gas exchange by opening and closing stomatal pores, which are highly responsive to changes in CO_2 concentration, and CO_2-mediated regulation of stomatal conductance has profound effects on plants. Among several signals that regulate stomatal movements, the stress hormone Abscisic Acid (ABA) plays a critical role in plant responses to abiotic stresses such as drought. The molecular signaling mechanisms and network principles by which CO_2 and ABA control plant gas exchange were investigated. Three unbiased forward genetic screens were pursued and, after screening over 10,000 artificial

microRNA lines and over 1,000 EMS mutagenized Brachypodium lines, partially ABA or CO_2 insensitive lines were isolated and are currently being characterized.

Major Goal: Due to the rising atmospheric CO_2 concentration, CO_2 control of gas exchange in plants will have profound effects on global water-transpiration, plant water use efficiency, leaf heat stress and optimal stomatal conductance of plants, including crops. Elevated CO_2 concentrations in leaves cause stomatal closure, whereas reduced CO_2 concentrations result in stomatal opening. However, little is known about the molecular signal transduction mechanisms that mediate CO_2-induced stomatal movements, especially in grasses. Besides, the stress hormone ABA plays a key role in drought-induced stomatal closure, and the molecular pathways of CO_2 and ABA converge, fine tuning stomatal movements in plants. My main goal was to identify and characterize new genes/proteins that play a role in CO_2 and ABA signaling in plants, further elucidating these complex molecular pathways.

Specific Goals: Three extensive forward genetic screens were pursued: 1- over 10,000 amiRNA lines were screened for ABA sensitivity, leading to the isolation of partially insensitive lines, 2- over 10,000 amiRNA lines were screened for low [CO_2] sensitivity, leading to the isolation and characterization of lines and 3- over 1,000 EMS mutagenized Brachypodium lines were screened, leading to the isolation of two [CO_2]-insensitive lines. As some of these finding have already been published (Hauser and Ceciliato et al., 2018 *Journal of Experimental Botany*), the other most relevant lines are being further investigated.

Chapter 1:

A seed resource for screening functionally redundant genes and isolation of new mutants impaired in CO_2 and ABA responses

Abstract

The identification of homologous genes with functional overlap in forward genetic screens is severely limited. Here, we report the generation of over 14,000 artificial microRNA (amiRNA)-expressing plants that enable screens of the functionally redundant gene space in Arabidopsis. A protocol was developed for isolating robust and reproducible amiRNA mutants. Examples of validation approaches and essential controls are presented for two new amiRNA mutants that exhibit genetically redundant phenotypes and circumvent double mutant lethality. In a forward genetic screen for abscisic acid (ABA)-mediated inhibition of seed germination, amiRNAs that target combinations of known redundant ABA receptor and *SnRK2* kinase genes were rapidly isolated, providing a strong proof of principle for this approach. A new ABA-insensitive amiRNA line that targets three *avirulence-induced gene 2(-like)* genes was isolated. A thermal imaging screen for plants with impaired stomatal opening in response to low CO_2 exposure led to the isolation of a new amiRNA targeting two essential proteasomal subunits, *PAB1* and *PAB2*. The seed library of 11,000 T2 amiRNA lines (with 3000 lines in progress) generated here provides a new platform for forward genetic screens and has been made available to the Arabidopsis Biological Resource Center (ABRC). Optimized procedures for amiRNA screening and controls are described. This work was published at Journal of Experimental Botany (**https://doi.org/10.1093/jxb/ery363**)

Introduction

The presence of large gene families in plants, including Arabidopsis (Lindsey *et al.*, 2017), leads to functional genetic redundancies or partial functional overlap among closely related genes. Functional overlap and partial or complete redundancy between different family members has been proposed to provide a buffer for loss or gain of function mutation events and mechanistic robustness of cellular networks (Wagner, 2005) . This is considered to be a main reason for the lack of observable phenotypes in single-gene deletion mutants and increasing severity of phenotypes in higher order mutants of homologous genes (Ma *et al.*, 2009; Park *et al.*, 2009). Identification and characterization of functionally overlapping genes in genetic screens is limited, as is evident from the relatively low number (591 of all Arabidopsis genes) of genes not associated with a single mutant phenotype (Koncz and Schell, 1986). Analysis of genome-wide gene family definitions showed that the Arabidopsis genome includes over 22,000 genes belonging to gene families (Hauser *et al.*, 2013). Strategies and tools have been developed to enable screens of the functionally redundant gene space. Recently, an artificial microRNA (amiRNA)-based computational design approach was introduced (Hauser *et al.*, 2013). AmiRNAs designed to specifically target diverse combinations of gene family members or combinations of subfamily members enable the screening of partial overlapping homologous gene functions at a genome-wide scale (Hauser *et al.*, 2013). The presented platform also provides an approach for the capture of homologous gene silencing phenotypes, for which higher order loss of function mutants would lead to lethality, as illustrated by a mutant identified here.

Here, we report the generation of over 11,000 T2 amiRNA lines and 3000 additional amiRNA lines by transformation of Arabidopsis Col-0 with a previously published amiRNA library and screening of T2 amiRNA lines for abscisic acid (ABA)-insensitive seed germination

phenotypes or plants with low-CO_2-insensitive high-leaf-temperature phenotypes. Methods are described to identify robust amiRNA mutants and how to avoid pitfalls of this approach. The screen rapidly identified two amiRNAs that target three *PYR/RCAR* ABA receptor (Ma *et al.*, 2009; Park *et al.*, 2009) or six SNF1-related kinase- (*SnRK2*; (Mustilli *et al.*, 2002; Yoshida *et al.*, 2002; Fujii and Zhu, 2009) encoding genes known to be involved in ABA-mediated control of seed germination. One candidate line that shows an ABA-insensitive seed germination phenotype contains an amiRNA that targets three genes of unknown function, which are annotated as *Avirulence-induced gene 2* (*AIG2A*; AT3G28930), *Avirulence-induced gene 2-like protein A* (*AIG2LA*; AT5G39720), and *Avirulence-induced gene 2-like protein B* (*AIG2LB*; AT5G39730). One amiRNA that causes a low-CO_2-insensitive high-leaf-temperature phenotype targets two genes encoding proteasomal α2-subunits, annotated as *PAB1* (AT1G16470) and *PAB2* (AT1G79210), for which double mutation causes lethality. New amiRNA lines that target the gene for proteasomal α7-subunit, annotated as *PAG1* (AT2G27027), were constructed resulting in a similar stomatal phenotype. Together these observations indicate a rate-limiting role of the intact proteasome for stomatal opening responses.

Materials and methods

Plant material, growth conditions and transformation

Arabidopsis accession Columbia-0 was used as the background for all amiRNA transformations of the library. Surface-sterilized seeds (15 min 70% ethanol, 0.1% sodium dodecyl sulfate; three to four washes with ~100% ethanol; alternatively 10 min 50% bleach, 0.05% Tween-20; four to six washes with water; (Lindsey *et al.*, 2017)) of Arabidopsis were cold-treated for 2–5 d at 4 °C and germinated on half-strength Murashige and Skoog basal medium supplemented with Gamborg's vitamins (Sigma-Aldrich (Murashige and Skoog, 1962; Gamborg *et al.*, 1968) 0.8% Phytoagar (Difco, Franklin Lakes, NJ, USA) and pH adjusted (pH 5.8; 2.6 mM MES titrated with potassium hydroxide). After 5–7 d, plants were transferred to plastic pots containing sterilized premixed soil (Sunshine Professional Blend LC1 RS; Sunshine; supplemented with an appropriate amount of insecticide (Marathon, Gnatrol)) and propagated under the following conditions: long day (16 h light/8 h dark); 23–27 °C; 20–70% humidity, 60–100 mmol m^{-2} s^{-1} light.

Plant transformation by floral dip was performed as described elsewhere(Clough and Bent, 1998) with the following modifications. *Agrobacterium tumefaciens* GV3101::pMP90 (Koncz and Schell, 1986) was grown under selection of all markers, i.e. genomic (rifampicin), Ti-plasmid (gentamicin), pSOUP (tetracycline) and T-DNA plasmid (spectinomycin). The infiltration medium for resuspension of the bacteria and floral dip contained 5% sucrose (w/v) and 0.02% (v/v) Silwet L-77 (Clough and Bent, 1998).

Large scale transformation with the amiRNA library pools (Hauser *et al.*, 2013) was performed as described elsewhere (Cutler *et al.*, 2000) with the following modifications. One microgram of DNA of each amiRNA sublibrary (Hauser *et al.*, 2013) was electroporated into a total of 500 µl electrocompetent *A. tumefaciens* cells. The 20 bp and 21 bp amiRNA sublibrary

variants for each pool were individually electroporated and combined at this stage. After 2 h at 30 °C in non-selective Luria–Bertani–Miller medium (LB, Teknova), the cells were spread on 20 LB plates (1.5% agar; 150 mm diameter) containing all the appropriate antibiotics (rifampicin, gentamycin, tetracycline, spectinomycin) and grown for 3 d at 30 °C. The bacteria were scraped from the plates, resuspended in 5 ml LB and concentrated by centrifugation for 20 min at 5855 *g*. Plants were transformed by spraying the flowers with this suspension of the bacteria in infiltration medium (adjusted to an optical density at 600 nm of 0.5) twice with 1 week between the treatments. T1 plants were selected on plates supplemented with 75 μM phosphinotricin or directly on soil by spraying diluted herbicide (1000× dilution, Finale®; Bayer, Research Triangle Park, NC, USA) four times with 2–7 d between the treatments. Herbicide-resistant plants were transferred to soil and grown to full maturity and T2 seeds collected from individual plants. When appropriate, media for growth of bacteria or plant selection contained the following concentrations of antibiotics (mg ml^{-1}): carbenicillin 100, gentamycin 25, kanamycin 30, rifampicin 50, spectinomycin 100, tetracycline 10, and phosphinotricin 15.

Screen for abscisic acid-insensitive cotyledon emergence phenotype

T2 plants were screened individually for insensitivity of seed germination to ABA in 96-well plates (100 μl 0.1% agarose supplemented with 2 μM (±)-ABA, Sigma-Aldrich). Approximately 10–20 seeds were used from each T2 plant. For the pooled screening, approximately 10–50 seeds of 90 individual T2 plants were mixed, surface sterilized and sprinkled onto agar plates (3 μM (±)-ABA; Sigma-Aldrich). As control for ABA insensitivity, *abi4-1* (ABRC, CS8104) or *abi5-1* (ABRC, CS8105) was used and Col-0 was used as a wild-type control. A putative ABA-insensitive phenotype was scored in a binary manner for similarity to

the *abi4-1* or *abi5-1*phenotype and difference from wild-type after 5–8 d using green cotyledons as indicator (Kuhn *et al.*, 2006). For lines that showed a putative ABA insensitivity, the seed germination assay was repeated by propagating individual T2 seedlings to the next generation (T3) and using seeds of the T3 generation for ABA sensitivity assays. This time, seeds were placed on plates with and without ABA (2 µM (±)-ABA; Sigma-Aldrich) and images were taken daily for 7 d and emergence of radicles and cotyledons was counted manually using Fiji (Schindelin *et al.*, 2012). For candidates of the individual screen the T2 seeds were used for the repetition of the germination assay.

For candidates of the pooled screen ABA-insensitive seedlings were transferred to plates containing 75 µM phosphinotricin, and after 7–10 d resistant seedlings were transferred to soil, grown up to full maturity, and the T3 seeds used for the validation of the ABA-insensitive germination phenotype.

Screen for CO_2-insensitive leaf temperature phenotype

Seeds of T2 plants were germinated in 96-pot-flats (254 mm×508 mm; East Jordan Plastics, East Jordan, MI, USA) on soil with each pot containing seeds from one plant. After 7 d, seedlings were sprayed with a 1000× dilution of Finale® (Bayer), and 2–3 d later pale seedlings were removed and only one healthy dark green seedling was left per pot. After 19 d under standard growth conditions, the plants were exposed to 150 ppm CO_2 for 2 h in a Percival growth chamber. A first set of thermal images was taken with a FLIR A320 thermal imaging camera (FLIR, Wilsonville, OR, USA). Subsequently the plants were exposed to ≥ 800 ppm CO_2 and after 2 h a second set of thermal images was taken. Control plants included in the experiments were *ht1-2* (Hashimoto *et al.*, 2006), *ost1-3* and wild-type Col-0. Thermal images were converted into

Flexible Image Transport System format (fits) using the ExaminIR software (FLIR). For the screen using the 96-pot-flat format, the temperature of plant leaves and the surrounding soil were measured using Fiji. The soil temperature served as a location-specific reference to compensate for temperature variation depending on the position in the 96-pot flat. Either the temperature difference between plant leaves and surrounding soil or the average temperature of plant leaves was used as a quantitative measure. Plants with more than 1 °C difference from soil were considered as primary candidates and subject to further testing. The high-temperature leaf phenotype of *ht1-2* was used as a reference for CO_2 insensitivity. To test the reproducibility of the CO_2-dependent leaf temperature phenotype of putative candidates, T2 plants were grown in triplicate and assayed again alongside with *ht1-2* and wild-type control plants.

Identification of amiRNA sequences and testing reproducibility

Genomic DNA from candidates with a robust and reproducible phenotype was isolated as described elsewhere (Edwards *et al.*, 1991) and the sequence of the amiRNA present was determined by sequencing of the PCR product (primers pha2804f and pha3479r; see Supplementary Table S1 at *JXB* online). Using the Target Search function available on the WMD3 website (Warthmann *et al.*, 2008), putative amiRNA target genes were predicted. For independent confirmation of the phenotype, independent lines were generated by cloning the identified amiRNA into pFH0032 (Supplementary Table S2) and transforming it into Arabidopsis Col-0. Confirmed phenotypes were further analyzed by using single knock-out mutants, higher order mutants generated by crossing and/or generating amiRNAs that target subsets of the initial target genes (see Supplementary Table S3).

Gas exchange analyses

Stomatal conductance of H_2O (g_s) was measured in leaves of 5- to 6-week-old plants using portable gas exchange systems (LI-6400 and LI-6800, LI-COR, Lincoln, NE, USA), starting 2 h after growth chamber light onset. For intact single leaf ABA treatments, a LED light source set at 150 µmol m^{-2} s^{-1} (10% blue) and a chamber temperature of 21 °C was used. Leaves were equilibrated for 1 h at a relative humidity of 70–72%, airflow of 200 rpm and CO_2 concentration of 400 ppm. After 1 h, steady-state stomatal conductance was recorded 10 min before the addition of ABA to the petioles submerged in water at the indicated concentration. For light-response measurements, plants were kept in the dark for 18 h prior to experiments. Stomatal conductance of a single intact leaf in the dark was recorded for 10 min, followed by red light treatment of 600 µmol m^{-2} s^{-1}. After 20 min of red light treatment, additional blue light was applied at 10 µmol m^{-2} s^{-1}. The incoming air humidity was kept at 62–65% and air flow at 200 rpm. For stomatal conductance measurements of single intact leaf CO_2 responses, incoming relative air humidity was kept at 62–65% and the imposed changes in CO_2 concentration were applied as indicated. Leaves were attached to intact plants and were equilibrated for 1 h before the measurements. The data presented represent $n \geq 3$ leaves with each leaf from independent plants per genotype per treatment.

qRT-PCR analysis

Total RNA (500 ng) was reverse transcribed using the first-strand cDNA synthesis kit (GE Healthcare). qRT-PCR analyses were performed using 3-fold-diluted cDNA (Maxima SYBR Green Rox/qPCR Master Mix; Thermo Fisher Scientific) on a CFX Connect PCR cycler (BioRad). The housekeeping *PDF2* gene was used as an internal control (Czechowski et al 2005). The threshold cycle (C_T) was determined by the instrument (CFX Manager Software, BioRad), and the

$\Delta\Delta C_T$ method was used to calculate the fold change in each gene (Livak and Schmittgen, 2001). For *RAB18* gene expression measurements, total RNA was extracted from 2-week-old seedlings that were treated with ABA for 9 h and final concentration of 20 μM.

Results

Generation of amiRNA library plants.

We have previously described the generation of an amiRNA library consisting of 10 sublibraries that represent 22,000 individual amiRNA designs (Hauser *et al.*, 2013). Deep sequencing of these 10 sublibraries showed that ≥95% of the designed amiRNAs were present in these sublibraries. The amiRNA library was transformed first into *Agrobacterium tumefaciens* and then into Arabidopsis Col-0. Over a period of over 4 years, the amiRNA library consisting of 10 sublibraries was transformed and T1 seeds harvested. Using plate- or soil-based selection methods, herbicide-resistant T1 plants were grown and T2 seeds from over 14,000 individual plants were harvested (Table 1). The transformation rate varied over a range from 0.08% to 0.76% with an average of 0.25%. During the course of this research, approximately 3,000 additional T2 lines were generated expressing amiRNAs that target homologous transporter-encoding gene family members. These 3,000 lines will also be made available to the ABRC, such that in the end over 14,000 total T2 lines will be submitted for use by the community.

Screen for ABA-insensitive seed germination phenotype.

In total over 2,500 T2 amiRNA lines were screened individually and over 5,000 T2 amiRNA lines were screened in pools for ABA-insensitive germination phenotypes (Fig. 1). In the primary screen using individual plants in a 96-well plate format, 59 putative candidates were identified. In the primary screen using pools of 90 plants with 25–80 seeds per line, approximately 340 putative candidates representing an unknown number of lines were identified (Fig. 1). These candidates were subjected to further analysis in a secondary screen (Fig. 2). The cotyledon emergence phenotype of 24 T3 seedlings from a total of 76 retested plants showed a more reduced

ABA sensitivity that was clearly different from wild-type and less severe than the *abi4-1* and *abi5-1* controls (Fig. 2A). From the 59 putative candidates identified using the individual screening approach, the amiRNA line p8l1257 showed a reproducible partial insensitivity to ABA in the T3 generation (Fig. 3). Only the amiRNA in candidates with the most robust phenotypes was determined by sequencing. Two of the amiRNA-targeted gene sets identified in 24 seedlings with reproducible phenotypes are known core components of the ABA signal transduction cascade (Fig. 2; Table 2). These include amiRNA lines that target the three ABA receptors PYR1 (RCAR11), PYL4 (RCAR10), and PYL6 (RCAR9) (Fig. 2B, C; Table 2). Furthermore, amiRNA-expressing plants that target six members of the SnRK2 protein kinase family (Mustilli *et al.*, 2002; Yoshida *et al.*, 2002; Fujii and Zhu, 2009) were isolated in this screen, including the three SnRK2 protein kinases, SnRK2.2, SnRK2.3, and SnRK2.6 (OST1), that are known to be required for abscisic acid signaling (Fig. 2B, C; Table 2; (Mustilli *et al.*, 2002; Yoshida *et al.*, 2002; Fujii and Zhu, 2009). Notably, Fig. 2D shows a strong variation in the cotyledon emergence phenotype among plants expressing the same amiRNA that targets six *SnRK2* kinase transcripts. This variation might be responsible for the high number of variable candidates that did not show a robust phenotype following the primary screen. Additional amiRNA lines were isolated as putative mutants and the amiRNA sequence was determined (Supplementary Table S4). Although some of the predicted targets might be expected to affect abscisic acid responses, rescreening of these putative mutants did not show consistently robust reproducible phenotypes. Thus, amiRNAs appear to produce phenotypes that may be variable even within the same line. These findings led us to develop a protocol in which: (i) only putative mutants that showed a consistent phenotype when screening seeds from the next generation of plants were selected, and (ii) Only lines that showed similar phenotypes upon re-transformation with new amiRNAs that are predicted to target the same genes

were selected. Furthermore, based on the variation observed here in the secondary screen it is advisable to investigate over 10 independent transformed lines (Schwab *et al.*, 2006; Hauser *et al.*, 2013) in the future to determine which amiRNAs produce phenotypes that can be carried forward.

The isolation of amiRNA lines targeting functionally overlapping *PYR*/*RCAR* ABA receptor and *SnRK2* protein kinase genes, which could not be isolated in traditional forward genetic mutant screens, provides a proof of principle that functionally redundant genes can be isolated in forward genetic screening using this new amiRNA resource. The inclusion of control lines and the validation steps described above should enable screening for diverse phenotypes using the lines generated here that are being provided to ABRC.

AmiRNA lines targeting three avirulence-induced genes show partial insensitivity to ABA inhibition of seed germination but not to ABA-induced stomatal closure.

The amiRNA in line p8l1257 isolated in the present screen targets a new set of three genes (Fig. 3A, 3B). Previous research annotated these genes based on their mRNA upregulation in a transcriptomic study after infection with *Pseudomonas syringae* pv *maculicola* carrying avrRpt2 (avrRpt2-induced gene, *AIG2*) (Reuber and Ausubel, 1996). However, these genes have not been previously described to be involved in ABA-mediated control of seed germination or other phenotypic responses in plants.

The line p8l1257 was named *amiRNA-AIG* here and was further tested by analysing seed germination with additional T2 generation seeds from the original p8l1257 stock (Fig. 3). Germination properties were compared with a control amiRNA line targeting the human myosin 2 (*amiRNA-HsMYO*), which has no targeted genes in Arabidopsis (Hauser *et al.*, 2013). After 12 d on plates containing 2 µM ABA, the *amiRNA-AIG* line showed cotyledon greening in contrast

to the control *amiRNA-HsMYO* line (Fig. 3A). The effect of the *amiRNA-AIG* on the expression of a known ABA-induced gene, *RAB18*, was analysed by qRT-PCR (see Supplementary Fig. S1). The ABA-mediated induction of *RAB18* expression was substantially reduced in the *amiRNA-AIG* line indicating a role of the targeted avirulence-induced genes (*AIG2s*) in ABA signal transduction.

Since two out of the three genes are tandemly repeated, generation of double mutants using T-DNA insertion knockouts would be limited. Therefore, five new amiRNA lines were generated that target subsets of genes targeted by the original *amiRNA-AIG* to verify the relevance of the predicted *AIG2* target genes. *AmiRNA1*, *2*and *3* targeted each a single *AIG2* (Fig. 3B; Supplementary Table S3). *AmiRNA4*targeted two tandem-repeat *AIG2* genes and *amiRNA5* targeted all three *AIG* genes targeted in the original *amiRNA-AIG* line, but with a different amiRNA sequence (Fig. 3B; Supplementary Table S3 for amiRNA sequences). When the T2 seeds expressing these five new amiRNAs were tested in a seed germination assay with 0.5 µM ABA, only the *amiRNA4* and *amiRNA5*-expressing lines showed less sensitivity to ABA compared with the control *amiRNA-HsMYO* line in cotyledon greening (Fig. 3C). The expression of all three putative target genes (AT5G39720, AT5G39730, AT3G28930) was analysed using qRT-PCR in the originally isolated *amiRNA-AIG* line and in all the *amiRNA* lines 1–5 (see Supplementary Fig. S2). The amiRNA efficiency of transcriptional inhibition varies between the lines, target transcript(s) and amiRNA sequence. Note that microRNA silencing in plants occurs via two mechanisms, (i) the degradation of transcripts and (ii) inhibition of translation (Brodersen *et al.*, 2008). Thus, quantification of targeted transcripts may not fully show the degree of silencing of target genes. Combined, these data provide evidence that the original *amiRNA-AIG* phenotype

is attributable to silencing of more than one *AIG2* gene, suggesting overlapping homologous gene functions.

The original *amiRNA-AIG* line was also investigated to determine if it affects ABA-induced stomatal closure using an intact leaf gas exchange analysis approach. When ABA was applied to the transpiration stream of intact leaves at a final concentration of 2 μM, both the control *amiRNA-HsMYO* line and the *amiRNA-AIG* line showed an ABA-induced decrease in stomatal conductance to H_2O (g_s, Fig. 4A). Normalization of the stomatal conductance data showed no dramatic difference in ABA-induced stomatal closure between *amiRNA-HsMYO* and *amiRNA-AIG* (Fig. 4B). Together, the present data show that the isolated *amiRNA-AIG* line is less sensitive to ABA inhibition of seed germination.

The *AIG2* genes are functionally annotated as putative γ-glutamyl cyclotransferases (GGCTs, EC:4.3.2.9) based on their similarity to the human orthologue (HsGGCT; O75223). AIG2LA and AIG2LB share only 16% and 17% identity, respectively, to the human orthologue. GGCTs have been described to cleave γ-glutamyl-amino acid dipeptides to release the free amino acid and 5-oxoproline (Oakley *et al.*, 2008). Further research will be required to determine the mechanism by which AIG2s affect ABA inhibition of seed germination.

Screen for CO_2-insensitive leaf temperature phenotype.

In total, over 2,500 T2 amiRNA lines were screened individually for an altered leaf temperature response to a low CO_2 concentration (150 ppm) by infra-red thermal imaging (Fig. 5). Leaf temperature depends on various parameters including radiation absorption, air temperature, and humidity (Merlot *et al.*, 2002). Low ambient CO_2 concentration leads to stomatal opening in Arabidopsis, causing an increased transpiration rate and thus a decrease in leaf temperature

compared with the surrounding air. Mutants impaired in CO_2-induced stomatal opening appear warmer compared with wild-type plants. In the screen, we used the soil temperature as reference to compensate for the local temperature differences due to various factors including humidity of the soil. Wild-type plants and plants of the HIGH LEAF TEMPERATURE1-2 (*ht1-2*) mutant (Hashimoto *et al.*, 2006; Matrosova *et al.*, 2015) were included in all trays as controls. Based on visual inspection of the thermal images, plants with relatively higher leaf temperature under low [CO_2] compared with the other plants in the same image were selected and the difference between the average leaf temperature and the surrounding soil was determined. The difference between leaf temperature and soil temperature was determined as reference for overall temperature and to compensate for local temperature differences. A set of 106 plants with more than one-degree difference between the leaf temperature and the surrounding soil was defined as initial putative candidates for further testing (see Methods for details). For the rescreening of putative mutants, we set a high threshold for temperature differences in the selection of mutants compared with the wild-type strain of 1 °C. The constitutive CO_2 response mutant *ht1-2*, when exposed to low [CO_2], shows a delta temperature above 1 °C between leaf and soil. Rescreening of these candidates in the T2 generation revealed an amiRNA line (p9l22) with a robust and reproducible impaired response to low CO_2 (Fig. 5B).

After exposure to low [CO_2], the leaf temperature of the p9l22 line was compared with wild-type (Col-0) and with the constitutive high-CO_2-response mutant *ht1-2* (Fig. 6A; Hashimoto et al., 2006). The leaves of the p9l22 line had a higher temperature than wild-type leaves and a similar temperature to *ht1-2* leaves (Fig. 6A). Stomatal index (SI) and density (SD) were calculated for wild-type, the control amiRNA-HsMYO, and p9l22 lines. No noteworthy differences were

found between the genotypes (Supplementary Fig. S3; amiRNA-HsMYO versus p9l22 line, one-way ANOVA, P>0.05 for SI and SD).

To measure [CO_2] responses in a time-resolved fashion, we measured stomatal conductance (g_s) using a gas exchange analyser. In the *amiRNA-HsMYO* control line, the shift from ambient (400 ppm) to low (150 ppm) [CO_2] led to a rapid increase in stomatal conductance (Fig. 6B). *AmiRNA* line *p9l22* responded to the same treatment with a lower magnitude of stomatal opening (Fig. 6B). Both lines showed stomatal closure in response to high (800 ppm) [CO_2] exposure at similar rates (Fig. 6B). To test whether line *p9l22* is defective in response to other stimuli that cause stomatal opening, light-induced g_s responses were investigated (Fig. 6C). The control *amiRNA-HsMYO* and *p9l22* lines were kept in the dark for 18 h prior to the experiments and steady-state g_s was measured. When red light (at 600 µmol m^{-2} s^{-1}) was applied, the *p9l22* line showed a reduced rate of g_s increase when compared with the control line. The same was observed when blue light (at 10 µmol m^{-2} s^{-1}) was superimposed on the red light background (Fig. 6C). Thus, the amiRNA line *p9l22*causes reduced responses to low CO_2 concentration, red light, and blue light.

The amiRNA in the *p9l22* line was sequenced and is predicted to target two homologous proteasomal subunit genes (*PAB1*, AT1G16470; and *PAB2*, AT1G79210). *PAB1* and *PAB2* are the sole genes that encode the 20S proteasome α2 subunit (Baumeister *et al.*, 1998). First, we attempted to isolate a double mutant (*pab1 pab2*) using T-DNA insertion lines (SALK_099950 and SALK_144987; (Alonso *et al.*, 2003). After genotyping over 100 plants in the F2 generation, no homozygous double mutant was recovered. We concluded that the double mutant is very likely lethal.

Alternatively, a new amiRNA sequence targeting solely the *PAB1* gene was cloned and transformed into the *pab2-1* single mutant (SALK_144987). This new amiRNA line, *pab2-1*mut *pab1amiRNA*, was investigated in stomatal conductance analyses of [CO_2] responses (Fig. 7). Leaves were first exposed to high (900 ppm) [CO_2] for 1 h and steady-state g_s was recorded. Shifts to low (150 ppm) [CO_2] led to an increase in g_s in both the *pab2-1*mut *pab1amiRNA* line and the control *amiRNA-HsMYO* line (Fig. 7A). The normalized stomatal conductance data show that the *pab2-1 amiRNA-PAB1* line responds to low [CO_2] with a reduced magnitude compared with the control line (Fig. 7B).

Initial experiments were pursued to determine if modifications in the α-ring of the 20S proteasome might be linked to the above phenotypes, or whether this mutation is specific to only α2 subunit mutations of the proteasome. The α-ring of the 20S proteasome is composed of seven α-subunits (Kurepa and Smalle, 2008). The *p9l22 amiRNA* targets the only two genes that encode the α2 subunit of the proteasome (Fig. 7, inset highlighted in red). To determine whether other α-subunits also affect the response to low [CO_2], a second amiRNA line was generated, which targets the *PAG1* gene (α7 subunit, inset in Fig. 7 highlighted in green), named *amiRNA-PAG1*. The α7 subunit is encoded by a single gene in Arabidopsis (Kurepa and Smalle, 2008). When an *amiRNA-PAG1* line was tested in g_s responses to [CO_2] shifts, it showed a lower rate of stomatal opening when compared with the control *amiRNA-HsMYO* line (Fig. 7C, D; one-way ANOVA $P>0.05$). The expression levels of *PAB1*, *PAB2*, and *PAG1*were analysed in the *p9l22* amiRNA line and also in *pab2-1*mut *pab1amiRNA* and *amiRNA-PAG1* lines using qRT-PCR (see Supplementary Fig. S4). With the exception of the severely reduced *PAB2* expression in the *pab2-1*mut *pab1amiRNA* line when compared with control lines, no clear evidence for knock down at

the transcriptional level could be detected in the amiRNA lines, which may point to amiRNA-mediated inhibition of translation (Brodersen *et al.*, 2008).

The present findings show that the *p9l22* amiRNA line is also partially impaired in red light-induced stomatal opening. Red light mediates stomatal opening in part via activation of photosynthesis and the resulting drop in internal concentration of CO_2 (C_i) (Roelfsema *et al.*, 2002; Matrosova *et al.*, 2015). In addition, the *p9l22* line is also partially impaired in blue light-induced stomatal opening. This suggests that a general regulator of stomatal opening is impaired in this line. As the proteasome mediates the degradation of proteins and reduced functions of α-ring subunits are predicted to increase protein levels, it is tempting to speculate that the phenotype observed might be correlated with an increased abundance of a negative regulator of stomatal opening. Further research will be required to test this or other hypotheses. In other studies, the 26S α2 subunit, when overexpressed, enhanced thermotolerance and adaptation in rice and Arabidopsis, suggesting that proteasomal subunits can have rate-limiting roles in regulating plant physiological responses.

Discussion

A library of over 11,000 plus 3,000 additional T2 generation amiRNA lines was created as a new resource to screen the redundant gene space in Arabidopsis. These amiRNA-expressing lines are being provided as individual lines to the Arabidopsis Biological Resource Center (ABRC). Given the observations and findings in the present study, lines will be available for high-throughput screening in pools of 90 lines per pool with approximately 25–50 seeds per individual amiRNA line in each pool. In each pool, the pooled seeds for screening will originate from one of the 10 sublibraries that target gene family members with defined functional annotations (Table 1; Hauser *et al.*, 2013). This approach will increase the probability of identifying interesting putative mutants in future screens despite the biological variability in amiRNA silencing lines found here (Fig. 2D).

The screen for ABA-insensitive seed germination phenotypes identified two amiRNAs targeting *PYR*/*RCAR* ABA receptor genes and *SnRK2* genes, which are both known groups of redundant key genes and proteins required for ABA signal transduction (Ma *et al.*, 2009; Park *et al.*, 2009). Isolating amiRNA lines in these known components serves as proof of principle for our approach. Moreover, screening this amiRNA population enables the identification of mutants that require co-silencing of homologous gene family members, which are less likely to be found in forward genetic screens of ethyl methanesulfonate or T-DNA mutagenized seed populations. Overall the presented amiRNA screen shows that amiRNA lines are prone to showing a high rate of variable candidates with weak or non-robust phenotypes. Nevertheless, as shown here new mutants can be isolated. Furthermore, during the course of this research, this amiRNA library resource has been used to isolate long-sought functionally redundant auxin transporter genes (e.g. *ABCB6*, *ABCB20*). Approaches to circumvent the inherent limitations of forward genetic

screening with amiRNAs were developed in the present study. As a first step, it is recommended to rescreen the next generation to identify robust and reproducible phenotypes in individually isolated putative mutant lines. As a second step, the amiRNA sequence of confirmed mutant lines needs to be determined (see Methods). AmiRNA sequences linked to the observed phenotypes are retransformed and testing over 10 independent lines for the phenotype is recommended. Alternatively, amiRNA on one line without break that target a subset of the initially predicted targets can be used to narrow down the causative genes (e.g. Fig. 3). For cases where only two to three genes are targeted, T-DNA lines or CRISPR/Cas9 mutants can be used to narrow down the genes relevant for the phenotype.

Over 95% of the amiRNAs in this library were designed to target only two to five genes (Hauser *et al.*, 2013), meaning that identification of causal genes is facilitated. Using the above approach, we report on two newly identified mutants: (i) amiRNA lines targeting three genes encoding avirulence induced gene (2-like) proteins show an ABA-insensitive seed germination phenotype; and (ii) amiRNA lines targeting two proteasomal subunits show insensitivity to low-CO_2-induced stomatal opening. Further analyses of the two targeted genes in this amiRNA line suggest that stronger T-DNA alleles result in lethality. This indicates the usefulness of the generated amiRNA lines for forward genetic isolation of higher order mutants that would be lethal upon knock-out. Our data suggest that the wild-type expression levels of two α-subunits of the 20S proteasome, α2 and α7, are required for fully functional stomatal opening mediated by physiological stimulation. This indicates that the proteasomal subunits are likely controlling an unknown general negative regulator of stomatal opening. The amiRNA seed resource generated here provides a new and potent tool to identify redundant genes and also lethality causing higher order mutants in many biological processes in Arabidopsis.

In conclusion, the amiRNA library resource is well suited for screening of phenotypes that can be easily verified in subsequent generations. This population may be best suited for screens that permit high throughput or medium throughput screening for phenotypes with a large dynamic range. Many such powerful screens have been performed in classical Arabidopsis mutant screens that were previously not designed to identify functionally redundant genes.

Chapter 1, in full, is published as it may appear in Journal of Experimental Botany, Hauser, F; Ceciliato, PHO; Lin, YC; Guo, D; Gregerson, JD; Abbasi, N; Youhanna, D; Park, J; Dubeaux, G; Shani, E; Poomchongkho, N; Schroeder, JI. The dissertation author was the primary investigator and author of this paper.

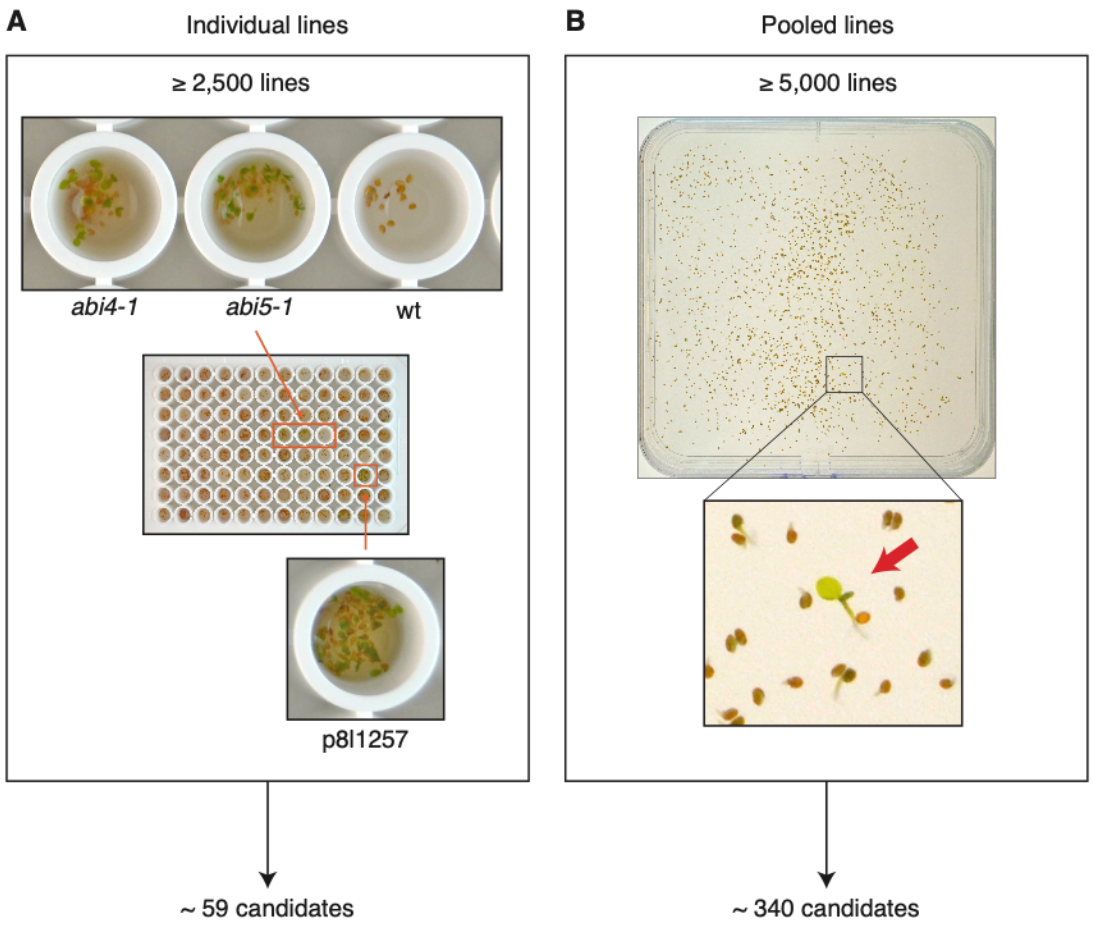

Figure 1.1 - Overview of primary screen performed with over 7500 T2 amiRNA lines. (A) Approximately 2500 T2 amiRNA lines were screened individually by adding seeds to 96-well plates each well containing 100 µl 0.1% agarose supplemented with 2 µM ABA and approximately 10–20 seeds from one plant. Wild-type (Col-0), *abi4-1*, and *abi5-1* were used as controls. Based on visual inspection of cotyledon greening, around 59 lines were considered as candidates for further testing in the T3 generation. (B) Approximately 5,000 T2 amiRNA lines were screened in pools. Each pool contained 10–50 seeds from 90 individually stored amiRNA lines (see main text). Approximately 340 lines were selected for further testing in the T3 generation.

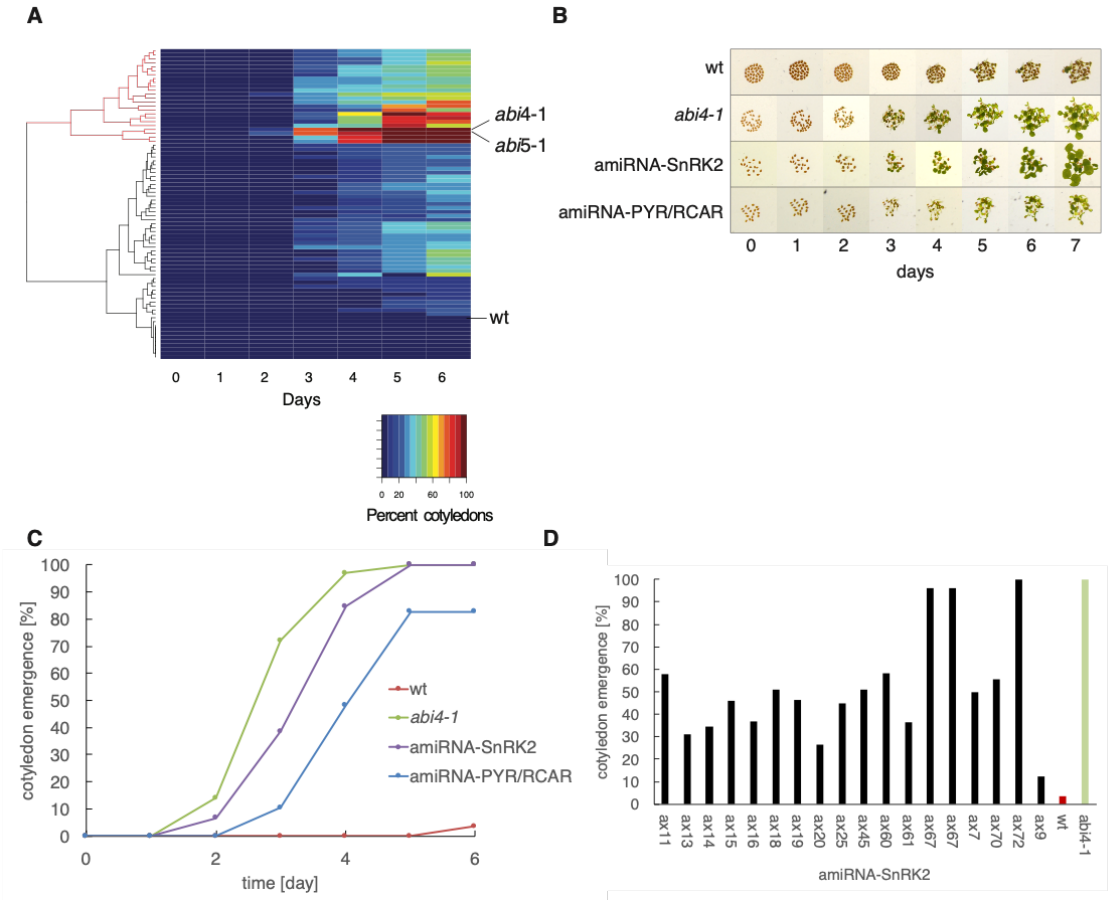

Figure 1.2 - Overview of secondary ABA insensitivity screen performed with T3 candidate amiRNA lines identified in the primary screen that targets known genes involved in ABA signal transduction. (A) Heat map representation of cotyledon emergence time course of the T3 generation obtained from candidates with putative ABA-insensitive seed germination or cotyledon emergence phenotypes. Each row represents the percentage of cotyledon emergence of one individual line. The rows are ordered by hierarchical clustering. Wild-type control (WT, Col-0) and *abi4-1* and *abi5*-1 as reference for ABA insensitivity are shown. (B) Images of seeds germinating on plates in secondary screen containing 2 µM ABA at the indicated time points. Shown are representative plants of amiRNA plants targeting a set of six *SnRK2* kinase genes (*amiRNA-SnRK2*) or a set of three *PYR/RCAR* ABA receptor genes (*amiRNA-PYR/RCAR*; see Table 2). Wild-type control (Col-0) and *abi4-1* and *abi5-1* as reference for insensitivity are shown in the other two rows. (C) Time course of cotyledon emergence in the presence of ABA for wild-type control (wt), *abi4-1* as a reference for ABA insensitivity and two representative amiRNA lines that target a set of six *SnRK2* protein kinase genes (*amiRNA-SnRK2*) or a set of three *PYR/RCAR* ABA receptor genes (*amiRNA-PYR/RCAR*). Per genotype 74 ± 46 seeds were phenotyped. (D) Bar plot of variation of cotyledon emergence phenotype (day 6; 2 µM ABA) in the T3 generation of plants isolated in the primary screen that were selected as candidates based on their seed germination phenotype in the T2 generation. Sequencing of the amiRNA confirmed that all 18 of these amiRNA-expressing plants contain an amiRNA that targets a set of six *SnRK2* kinase genes (*amiRNA-SnRK2*; see Table 2). Wild-type control (wt, Col-0) and *abi4-1* as reference for ABA insensitivity are shown.

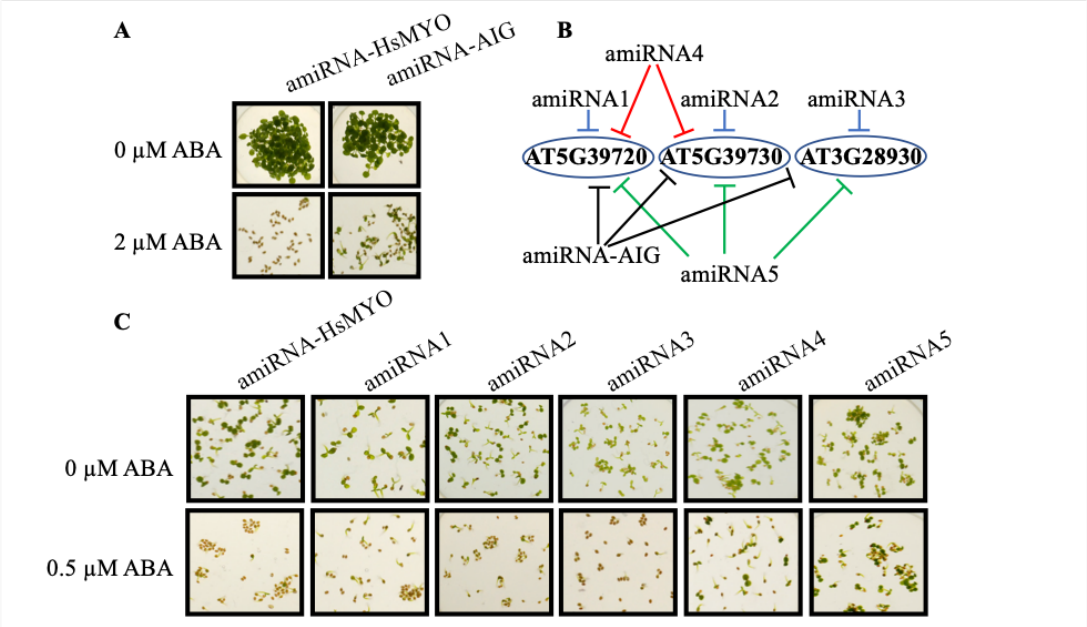

Figure 1.3 - Avirulence-induced genes (*AIG2*s) targeted by an amiRNA cause a reduced ABA sensitivity in cotyledon emergence assays. (A) Seedlings of the control amiRNA line, which has no target gene in Arabidopsis (*amiRNA-HsMYO* control), and an amiRNA line that targets three *AIG2* genes (*amiRNA-AIG*) germinated in the presence of 0 or 2 µM ABA. Photographs were taken after 12 d of exposure. (B) Five new amiRNAs were designed to target the three *AIG2(-like)* genes. Three of these amiRNAs, amiRNA1, 2 and 3, target a single gene each. AmiRNA4 targets two tandem-repeat *AIG2(-like)* genes and amiRNA5 targets all three genes at non-identical nucleotides compared with the original amiRNA isolated in the primary screen (*amiRNA-AIG*, see Supplementary Table S2 for amiRNA sequences). (C) The new T2 amiRNA lines were tested in cotyledon emergence assays. Seedlings were germinated in the presence of 0 or 0.5 µM ABA. Photographs were taken after 4 d of incubation.

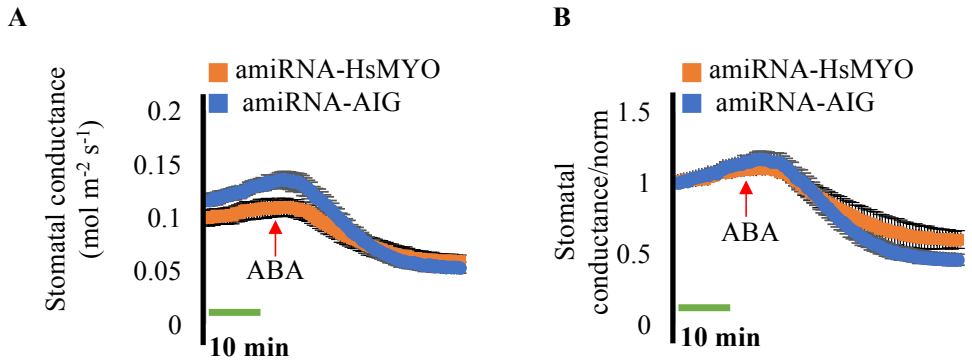

Figure 1.4 - The isolated amiRNA line targeting three *AIG2* genes (*amiRNA-AIG*) responds to ABA in whole leaf gas exchange analyses. Time-resolved stomatal conductance to H_2O (g_s) in response to application of 2 µM ABA to the transpiration stream (red arrows) is shown in the amiRNA control line (*amiRNA-HsMYO*) and in the amiRNA line targeting three *AIG2* genes (*amiRNA-AIG*). Stomatal conductance was analysed using whole leaf gas exchange. (A) Stomatal conductance in mol m^{-2} s^{-1}. (B) Data from (A) were normalized to stomatal conductance at the beginning of the experiment. Data are the mean of n=3 leaves per genotype ±SEM.

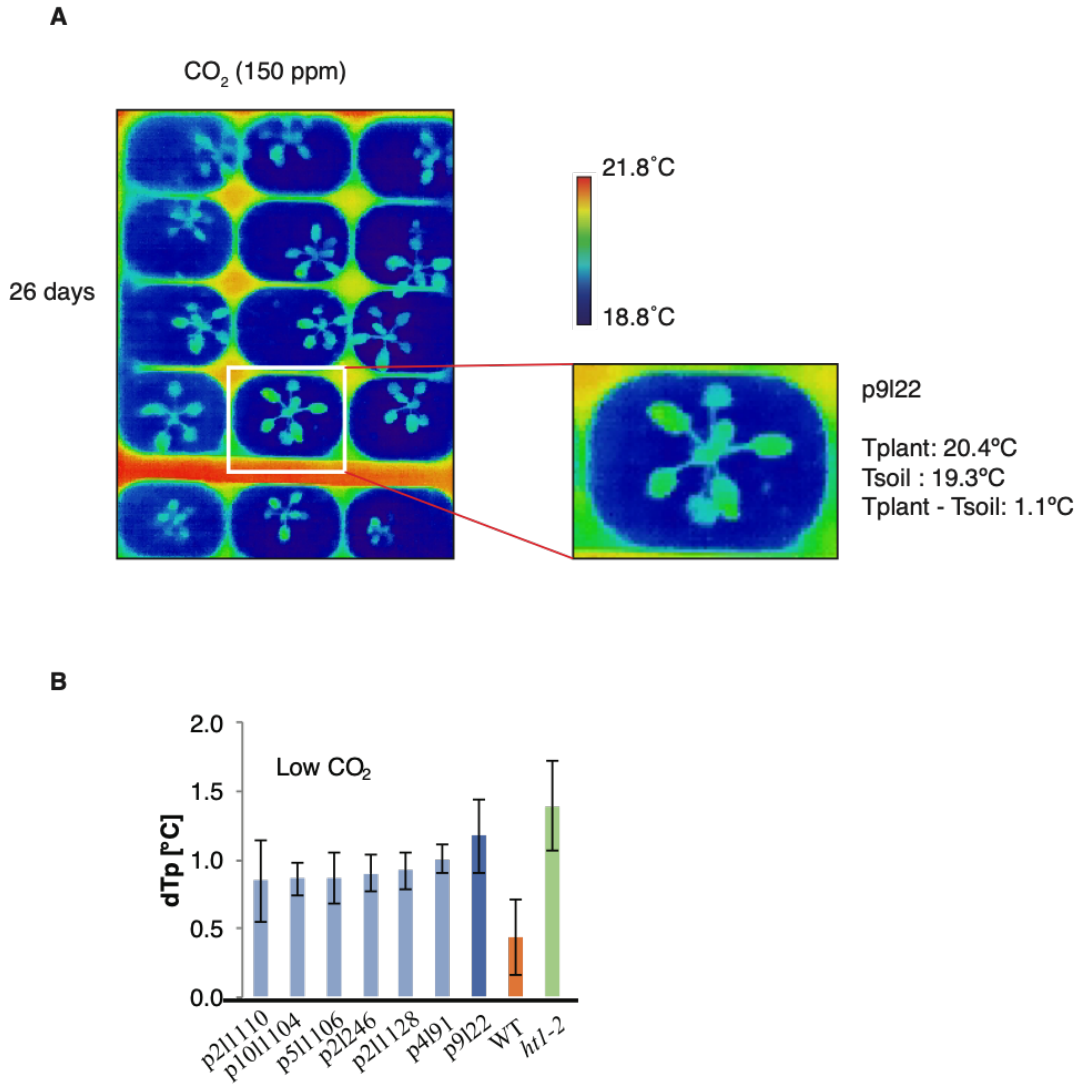

Figure 1.5 - Thermal imaging screen for mutants with impaired response to low CO_2 identified the amiRNA line *p9l22*. (A) Thermal images of amiRNA lines in the primary screen after exposure to low CO_2 (150 ppm). Plants were grown in 96-pot flats under ambient CO_2 and after 26 d exposed to low (150 ppm) CO_2 for 2 h and then thermal images of the entire flat were taken in eight separate images per flat. An image is shown from the primary screen in which the plant *p9l22* (white box) was flagged as a candidate with a putative altered response to CO_2 based on the leaf temperature. The average leaf temperature was computationally calculated across all rosette leaves for flagging putative mutants. (B) Differences of leaf temperature (T_{plant}) and surrounding soil (T_{soil}) for putative mutants exposed to low [CO_2] (150 ppm) for 2 h. Average leaf temperature was computed by image analysis of the most fully expanded rosette leaves. Bars show average ±SD (n=3–5 leaves). WT (Col-0) (orange) and *ht1-2* (green) were used as control.

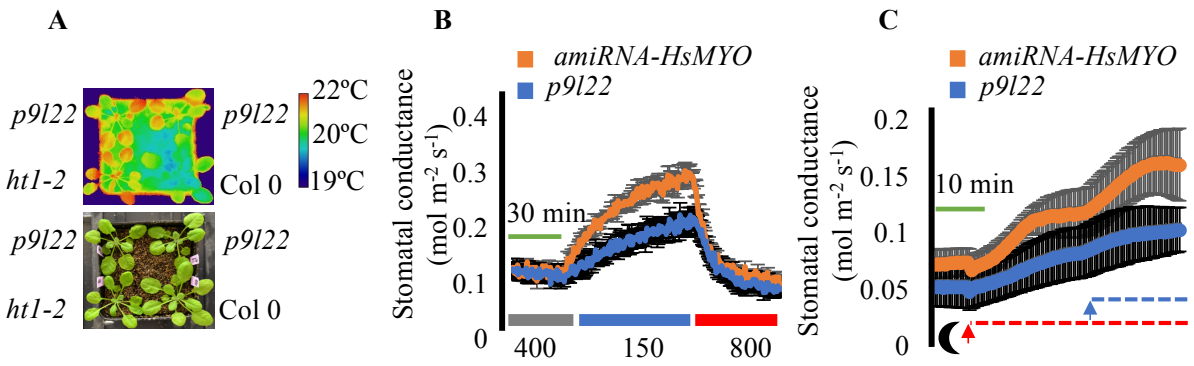

Figure 1.6 - The amiRNA line *p9l22* is defective in light- and low-CO_2-induced stomatal opening. (A) The *p9l22* line shows an elevated leaf temperature phenotype at low ambient [CO_2] treatment (150 ppm). Top, thermal imaging; bottom, image of the same plants. The calibration bar shows the pseudo-colored scale for temperature. (B) Time-resolved stomatal conductance responses at the imposed [CO_2] shifts (bottom in ppm) in the control *amiRNA-HsMYO* line and in the *p9l22* line were analysed using intact whole-leaf gas exchange. The plots represent average ±SEM (*n*=4 leaves from four plants per genotype). (C) Time-resolved stomatal conductance responses from darkness to the imposed light intensity and light quality shifts (bottom moon shape: darkness; red dashed line: red light at 600 µmol m^{-2} s^{-1}; and blue dashed line: blue light at 10 µmol m^{-2} s^{-1}) in the control *amiRNA-HsMYO* line and in the *p9l22* line were analysed using intact whole-leaf gas exchange. The plots represent average ±SEM (*n*=3 leaves from three plants per genotype).

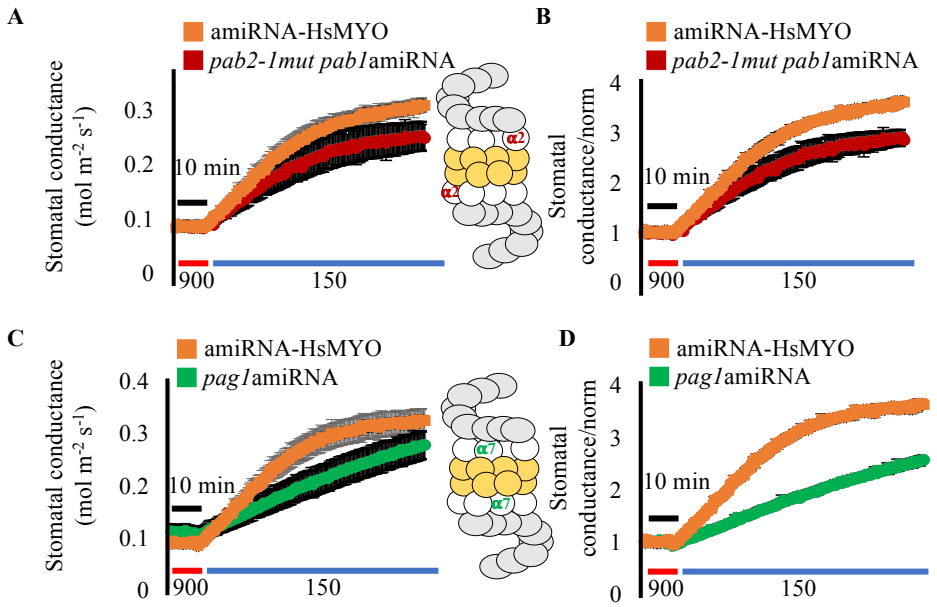

Figure 1.7 - New amiRNA lines targeting the two *PAB* genes (α2 subunit) and *PAG1* gene (α7 subunit) of the 26S proteasome show partial impairment in low-CO_2-induced stomatal opening. (A, C) Time-resolved stomatal conductance responses at the imposed [CO_2] shifts (bottom in ppm) in the control line *amiRNA-HsMYO* and (A) in the *pab2-1mut pab1amiRNA* line (*pab2* gene T-DNA knockout and *pab1*gene amiRNA knockdown, α2 subunit) and (C) *amiRNA-PAG1* line (*pag1* gene amiRNA knockdown, α7 subunit) were analysed using intact whole-leaf gas exchange. The plots represent average ±SEM (n=3–4 leaves from different plants per genotype). (B, D) Data from (A, C) were normalized to the average stomatal conductance of the first 10 min. Inserts show a representation of the 26S proteasome, with the α2 subunits highlighted in red and α7 subunits highlighted in green. The initial slope of g_s response for *amiRNA-HsMYO* and *amiRNA-PAG1* was calculated and one-way ANOVA was used to compare the values (P>0.05).

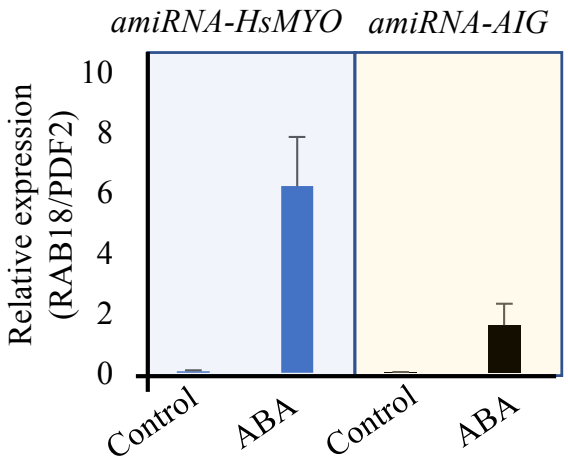

Figure 1.8 – (Figure S1): ABA-induction of *RAB18* gene expression is lower in the amiRNA-AIGs line. The expression of *RAB18* gene was measured in Arabidopsis seedlings (two-week-old) nine hours after ABA treatment (ABA) or ethanol (Control). qRT-PCR was performed using total RNA from seedlings and the *PDF2* gene expression was used as an internal control. The graph shows data from three biological replicates with two technical replicates each. Bars show mean ± SD.

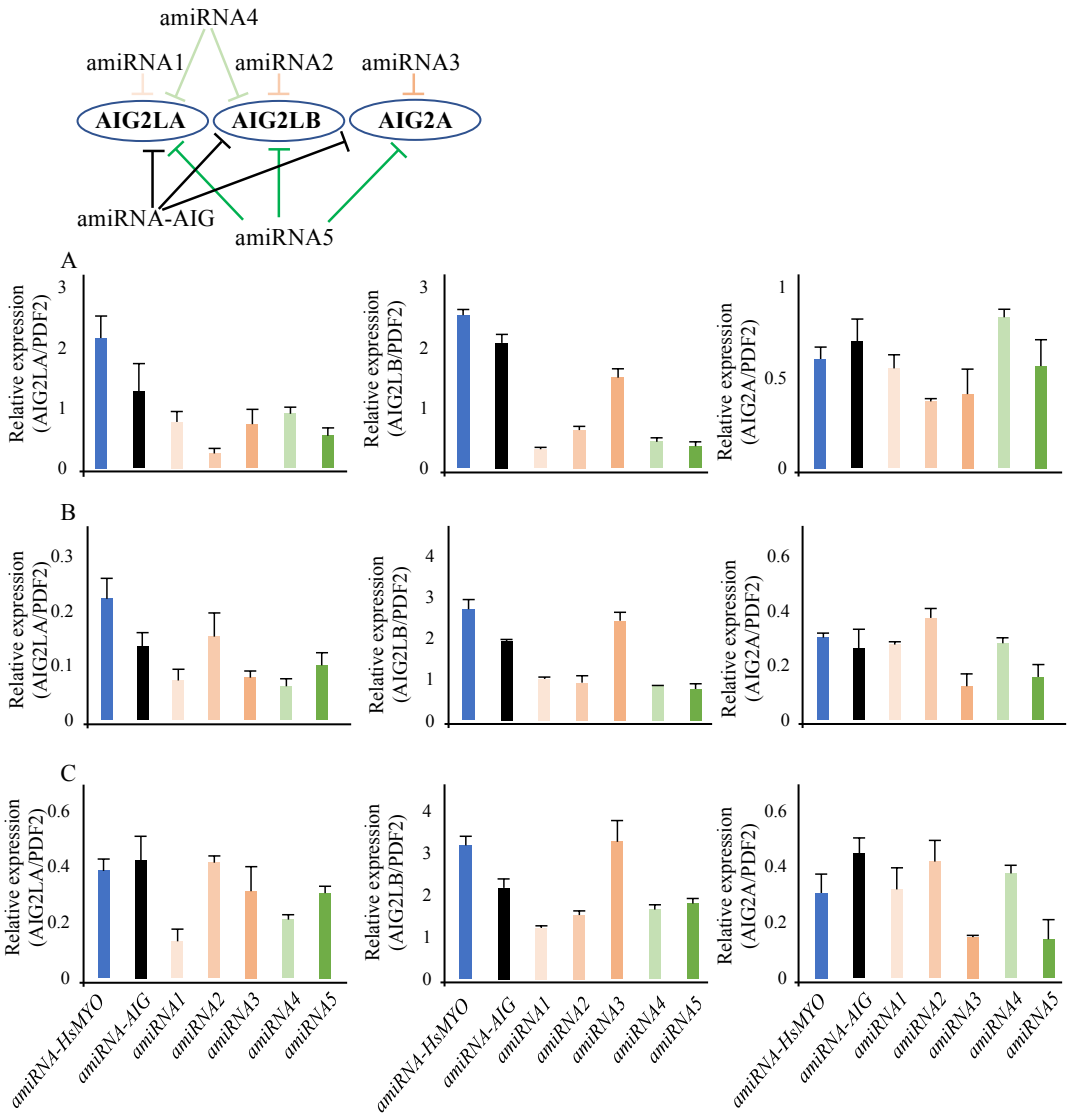

Figure 1.9 – (Figure S2): The expression of *AIGL* genes in amiRNA-AIGs lines. The expression of three *AIGL* genes was evaluated in *Arabidopsis* seedlings (two-week-old). qRT-PCR was performed using total RNA from seedlings. The *PDF2* gene expression was used as an internal control. Panels "A", "B" and "C" represent three biological replicates with three technical replicates for each biological replicate. AIG2LA (AT5G39720), AIG2LB (AT5G39730), AIG2A (AT3G28930).

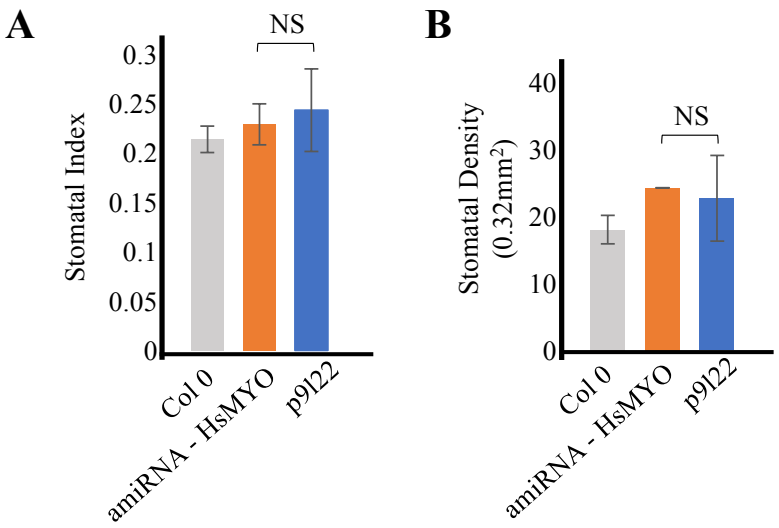

Figure 1.10 – (Figure S3): The *p9l22* amiRNA line has normal stomatal indices and density when compared to the *amiRNA- HsMYO* control line. Stomatal index **(A)** and stomatal density **(B)** measurements of the abaxial side of the fifth true leaf of 3 to 4-week-old plants. Wild type (Col 0), *amiRNA-HsMYO* and *p9l22* lines were evaluated. Data represent average of stomatal indices and density ± SD (n= 3 plants / three images per plant). NS, not significant (One-Way ANOVA $p>0.05$).

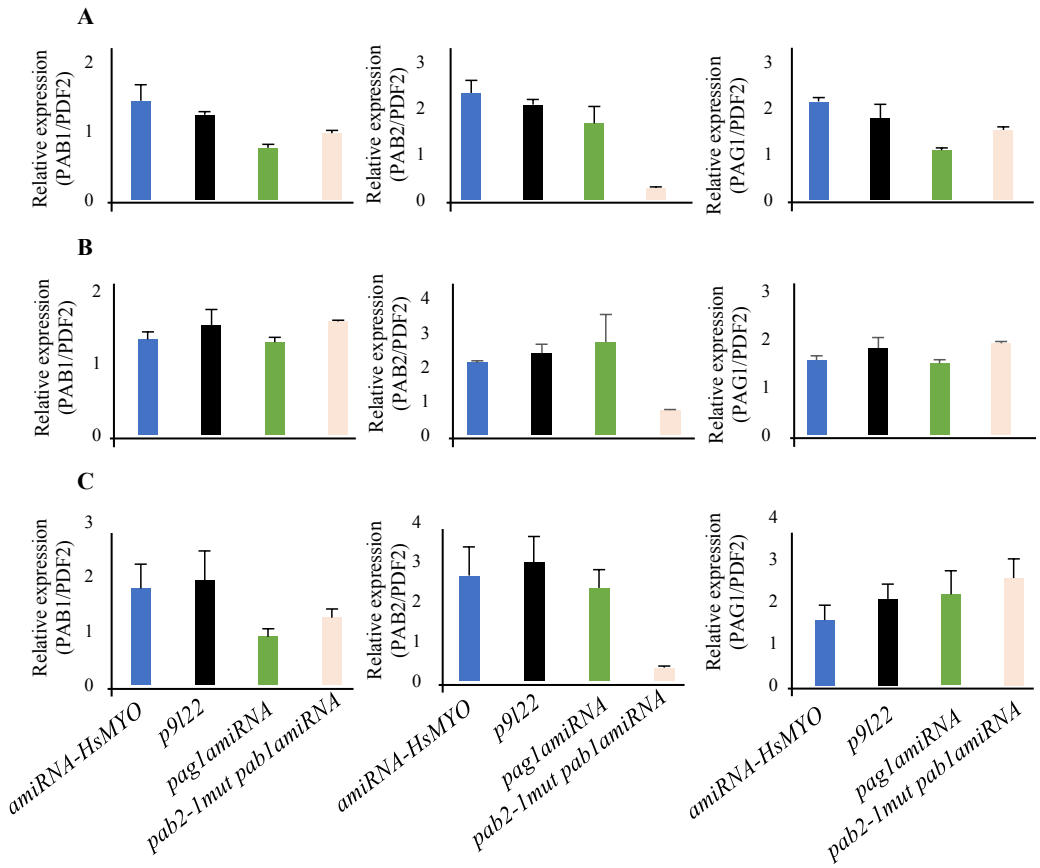

Figure 1.11 – (Figure S4): The expression of *PAB1, PAB2* and *PAG1* genes in amiRNA lines. The expression of three proteasomal subunits genes was evaluated in Arabidopsis seedlings (two-week-old). qRT-PCR was performed using total RNA from seedlings. The *PDF2* gene expression was used as an internal control. Panels "A", "B" and "C" represent three biological replicates with three technical replicates for each biological replicate. PAB1 (AT1G16470), PAB2 (AT1G79210), PAG1 (AT2G27020).

Table 1.1 - Overview of the ten amiRNA libraries as described by Hauser et. al. (2013), the number of amiRNAs designed for each library and the number of individual T2 amiRNA transformants that were generated here. Note that for the generation of each pool the 20bp and 21bp libraries were combined (see Hauser et. al. 2013 for details). All T2 lines have been submitted to the Arabidopsis Biological Resource Center (ABRC).

Pool name	Pool description	amiRNA designs	T2 lines
kinase receptor (PKR)	Protein kinases, protein phosphatases, receptors and their ligands	1860	817
binding (BNO)	Proteins binding small molecules	1968	1771
protein (CSI)	Proteins that form or interact with protein complexes including stabilization of those	2313	842
rna dna (TFB)	Transcriptionfactors and other RNA and DNA binding proteins	2964	831
metabolism (TEC)	Metabolic and other enzymes catalyzing transfer reactions (EC: 2)	1521	1548
diverse enzymes (PEC)	Catalytic active proteins, mainly enzymes	1881	1113
non-classified (UNC)	Genes for which the function is not known or cannot be inferred	4082	1387
diverse molfun (DMF)	Protein with diverse functional annotation not found in the other categories	1505	1152
hydrolase (HEC)	Hydrolytic enzymes (EC class 3), excluding protein phosphatases	2129	971
transporter (TRP)	Proteins that transport molecules across membranes	1777	3844
TOTAL			14276

Table 1.2 - AmiRNA sequences and predicted target genes found in candidate T3 plants showing robust ABA insensitive seed germination phenotypes in the T2 screen and subsequently in the T3 generation.

Number of sequenced T3 plants	amiRNA sequence	Target genes	Gene name
18	TGGATATGCTCCAACCGGCAT	AT1G10940	SNRK2.4
		AT1G60940	SNRK2.10
		AT2G23030	SNRK2.9
		AT3G50500	SNRK2.2
		AT4G33950	SNRK2.6 (OST1)
		AT5G66880	SNRK2.3
5	TATCAACGACGTAAGACTCGT	AT2G38310	PYL4 (RCAR10)
		AT2G40330	PYL6 (RCAR9)
		AT4G17870	PYR1 (RCAR11)
1	TTAATACATGGATGCACACGT	AT3G28930	AIG2
		AT5G39720	AIG2LA
		AT5G39730	AIG2LB

Table 1.3 – (Supplemental Table 1): Comprehensive list of relevant primers used in this study.

Primer name	**Sequence**	***Reference or Source***
pha2804f	AGAGAACACGGGGGACGAG	This work
pha3479r	AAACCGGCGGTAAGGATCTG	This work
PIE1-ImiR-s	gaTAGGATTCCAGTCAGTCTCTAtctctcttttgtattcc	This work
PIE1-IImiR-a	gaTAGAGACTGACTGGAATCCTAtcaaagagaatcaatga	This work
PIE1-IIImiR*s	gaTAAAGACTGACTGCAATCCTTtcacaggtcgtgatatg	This work
PIE1-IVmiR*a	gaAAGGATTGCAGTCAGTCTTTAtctacatatatattcct	This work
dreb1_ImiR-s	gaTGCCACGTCGTGAGCACGCATtctctcttttgtattcc	This work
dreb1_IImiR-a	gaATGCGTGCTCACGACGTGGCAtcaaagagaatcaatga	This work
dreb1_IIImiR*s	gaATACGTGCTCACGTCGTGGCTtcacaggtcgtgatatg	This work
dreb1_IIVmiR*a	gaAGCCACGACGTGAGCACGTATtctacatatatattcct	This work
prxcb1-I_miR-s	gaTTTCCCAAAGGAACCGTCCAGtctctcttttgtattcc	This work
prxcb1-I_II_miR-a	gaCTGGACGGTTCCTTTGGGAAAtcaaagagaatcaatga	This work
prxcb1-I_III_miR-s	gaCTAGACGGTTCCTATGGGAATtcacaggtcgtgatatg	This work
prxcb1-I_IV_miR-a	gaATTCCCATAGGAACCGTCTAGtctacatatatattcct	This work

Table 1.4 – (Supplemental Table 2): Comprehensive list of relevant plasmids used in this study.

Plasmids	***Description***	***Reference or Source***
pFH0032	$Spec^r$, Cam^r, pGreen derivative containing 35Sp gateway ocst	(Hauser et al., 2013)
pFH0332	$Spec^r$, pGreen derivative containing 35Sp amiRNA AT1G12610; AT2G35700; AT4G16750; AT4G32800; AT5G11590; AT5G25810 ocst	This work
pFH0333	$Spec^r$, pGreen derivative containing 35Sp amiRNA AT2G18140; AT2G18150; AT3G32980; AT3G49120 ocst	This work
pFH0334	$Spec^r$, pGreen derivative containing 35Sp amiRNA AT2G28290; AT3G12810 ocst	This work

Table 1.5 – (Supplemental Table 3): Comprehensive list of new amiRNAs designed and cloned in this study.

Lines	***amiRNA sequence***
P8l1257/amiRNA-AIG	TTAATACATGGATGCACACGT
amiRNA1	TTATAGAACATACTCAGACAC
amiRNA2	TACAATAACCTAGCTAGACAC
amiRNA3	TTCTATACAAGTGATAGGCGT
amiRNA4	TTAATACATGGATACAGACGC
amiRNA5	TTAATACATGGATACAGACGA
P9l22	TGTAATCATCGATATTTGCTG
pab2mutpab1amiRNA	TCATTAGTTATTGAGAGGCAC
pag1amiRNA	TTTTTACTCGACTTCAGGCAA

Table 1.6 – (Supplemental Table 4): AmiRNA sequences and predicted target genes found in candidate T3 plants which showed a putative ABA insensitive seed germination phenotype in the T2 screen and in the T3 generation.
(1) No: The amiRNA was cloned, transformed into Arabidopsis, independent lines were selected and the T2 seeds were tested for insensitivity to abscisic acid in seed germination. The cotyledon emergence phenotype was not clearly different from wild type i.e. the phenotype observed in the T2 screen and the assay with the T3 seeds could not be reproduced. NA: no independent lines were generated.

Number of T3 plants	amiRNA sequence	Target genes	Gene name	Reproduced in independent transformants(1)
1	TAGGATTCCAGTCAGTCTCTA	AT3G12810	PHOTOPERIOD-INDEPENDENT EARLY FLOWERING 1 (PIE1); (chr13); (SRCAP)	No
		AT2G28290	CHROMATIN REMODELING COMPLEX SUBUNIT R 3 (CHR3); SPLAYED (SYD)	No
1	ATCTTGAGCGATTTGACGTTC	AT4G40030	Histone superfamily protein	NA
		AT1G75600	Histone superfamily protein	NA
		AT5G65360	Histone superfamily protein	NA
		AT5G10400	Histone superfamily protein	NA
		AT1G13370	Histone superfamily protein	NA
		AT5G65350	HISTONE 3 11 (HTR11)	NA
1	TTGAGGACATCTCCCAACCAA	AT2G44020	Mitochondrial transcription termination factor	NA
		AT2G21710	embryo defective 2219	NA
1	TTTCCCAAAGGAACCGTCCAG	AT2G18140	Peroxidase	No
		AT2G18150	Peroxidase	No
		AT3G32980	Peroxidase	No
		AT3G49120	PEROXIDASE CB (PRXCB)	No
1	TTAAAGACCATACTTACGCTT	AT3G02590	Fatty acid hydroxylase	NA
		AT3G02580	STEROL 1 (BR synthesis)	NA
5	TGCCACGTCGTGAGCACGCAT	AT4G32800	ERF/AP2 transcription factor	no
		AT4G16750	ERF/AP2 transcription factor	
		AT1G12610	DWARF AND DELAYED FLOWERING 1 (DDF1)	
		AT2G35700	ERF FAMILY PROTEIN 38 (ERF38)	
		AT5G25810	TINY	
		AT5G11590	TINY2	
1	TTTAGTCCTACCTTGAAACCT	AT2G39550 AT5G40280	Prenyltransferase family protein/ERA1	NA
1	TCATTACGATTTGTTTCGCTC	AT5G10100 AT1G35910	TREHALOSE-6-PHOSPHATE PHOSPHATASE	NA
1	TTACACTATGTCCTTGTTCTC	AT3G43670 AT2G06830 AT1G09970	Copper amine oxidase family protein	NA

References

Alonso JM, Stepanova AN, Leisse TJ, Kim CJ, Chen H, Shinn P, Stevenson DK, Zimmerman J, Barajas P, Cheuk R, Gadrinab C, Heller C, Jeske A, Koesema E, Meyers CC, Parker H, Prednis L, Ansari Y, Choy N, Deen H, Geralt M, Hazari N, Hom E, Karnes M, Mulholland C, Ndubaku R, Schmidt I, Guzman P, Aguilar-Henonin L, Schmid M, Weigel D, Carter DE, Marchand T, Risseeuw E, Brogden D, Zeko A, Crosby WL, Berry CC, Ecker JR. 2003. Genome-wide Insertional mutagenesis of Arabidopsis thaliana. Science **301**, 653 657.

Baumeister W, Walz J, Zühl F, Seemüller E. 1998. The Proteasome: Paradigm of a Self-Compartmentalizing Protease. Cell **92**, 367 380.

Brodersen P, Sakvarelidze-Achard L, Bruun-Rasmussen M, Dunoyer P, Yamamoto YY, Sieburth L, Voinnet O. 2008. Widespread translational inhibition by plant miRNAs and siRNAs. Science **320**, 1185 1190.

Clough S, Bent A. 1998. Floral dip: a simplified method for Agrobacterium-mediated transformation of Arabidopsis thaliana. The Plant journal **16**, 735 743.

Cutler SR, Ehrhardt DW, Griffitts JS, Somerville CR. 2000. Random GFP::cDNA fusions enable visualization of subcellular structures in cells of Arabidopsis at a high frequency. Proceedings of the National Academy of Sciences of the United States of America **97**, 3718 3723.

Edwards K, Johnstone C, Thompson C. 1991. A simple and rapid method for the preparation of plant genomic DNA for PCR analysis. Nucleic acids research **19**, 1349 1349.

Fujii H, Zhu J-K. 2009. Arabidopsis mutant deficient in 3 abscisic acid-activated protein kinases reveals critical roles in growth, reproduction, and stress. Proceedings of the National Academy of Sciences of the United States of America **106**, 8380 8385.

Gamborg O, Miller R, Ojima K. 1968. Nutrient requirements of suspension cultures of soybean root cells. Experimental cell research **50**, 151 158.

Hashimoto M, Negi J, Young J, Israelsson M, Schroeder JI, Iba K. 2006. Arabidopsis HT1 kinase controls stomatal movements in response to CO2. Nature Cell Biology **8**, 391 397.

Hauser F, Chen W, Deinlein U, Chang K, Ossowski S, Fitz J, Hannon G, Schroeder JI. 2013. A genomic-scale artificial microRNA library as a tool to investigate the functionally redundant gene space in Arabidopsis. The Plant Cell **25**, 2848 2863.

Koncz C, Schell J. 1986. The promoter of TL-DNA gene 5 controls the tissue-specific expression of chimaeric genes carried by a novel type of Agrobacterium binary vector. Molecular Genetics and Genomics **204**, 383 396.

Kurepa J, Smalle JA. 2008. Structure, function and regulation of plant proteasomes. Biochimie

90, 324 335.

Lindsey BE, Rivero L, Calhoun CS, Grotewold E, Brkljacic J. 2017. Standardized Method for High-throughput Sterilization of Arabidopsis Seeds. Journal of visualized experiments : JoVE.

Livak K, Schmittgen T. 2001. Analysis of relative gene expression data using real-time quantitative PCR and the 2(T)(-Delta Delta C) method. Methods **25**, 402 408.

Ma Y, Szostkiewicz I, Korte A, Moes D, Yang Y, Christmann A, Grill E. 2009. Regulators of PP2C Phosphatase Activity Function as Abscisic Acid Sensors. Science **324**, 1064 1068.

Matrosova A, Bogireddi H, Mateo-Peñas A, Hashimoto-Sugimoto M, Iba K, Schroeder JI, Israelsson M. 2015. The HT1 protein kinase is essential for red light-induced stomatal opening and genetically interacts with OST1 in red light and CO2 -induced stomatal movement responses. The New phytologist **208**, 1126 1137.

Merlot S, Mustilli A, Genty B, North H, Lefebvre V, Sotta B, Vavasseur A, Giraudat J. 2002. Use of infrared thermal imaging to isolate Arabidopsis mutants defective in stomatal regulation. Plant Journal **30**, 601 609.

Murashige T, Skoog F. 1962. A Revised Medium for Rapid Growth and Bio Assays with Tobacco Tissue Cultures. Physiologia Plantarum **15**, 473 497.

Mustilli A, Merlot S, Vavasseur A, Fenzi F, Giraudat J. 2002. Arabidopsis OST1 protein kinase mediates the regulation of stomatal aperture by abscisic acid and acts upstream of reactive oxygen species production. Plant Cell **14**, 3089 3099.

Oakley AJ, Yamada T, Liu D, Coggan M, Clark AG, Board PG. 2008. The identification and structural characterization of C7orf24 as γ-glutamyl cyclotransferase. An essential enzyme in the γ-glutamyl cycle. The Journal of biological chemistry **283**, 22031 22042.

Park S-Y, Fung P, Nishimura N. 2009. Abscisic acid inhibits type 2C protein phosphatases via the PYR/PYL family of START proteins. Science **324**, 1068 1071.

Reuber T, Ausubel F. 1996. Isolation of Arabidopsis genes that differentiate between resistance responses mediated by the RPS2 and RPM1 disease resistance genes. The Plant Cell **8**, 241 249.

Roelfsema M, Hanstein S, Felle H, Hedrich R. 2002. CO2 provides an intermediate link in the red light response of guard cells. The Plant journal **32**, 65 75.

Schindelin J, Arganda-Carreras I, Frise E. 2012. Fiji: an open-source platform for biological-image analysis. Nature Methods **9**, 676 682.

Schwab R, Ossowski S, Riester M, Warthmann N, Weigel D. 2006. Highly specific gene silencing by artificial microRNAs in Arabidopsis. The Plant Cell **18**, 1121 1133.

Warthmann N, Chen H, Ossowski S, Weigel D, Hervé P. 2008. Highly specific gene silencing by artificial miRNAs in rice. PLoS ONE **3**, e1829.

Yoshida R, Hobo T, Ichimura K, Mizoguchi T, Takahashi F, Aronso J, Ecker J, Shinozaki K. 2002. ABA-activated SnRK2 protein kinase is required for dehydration stress signaling in Arabidopsis. Plant Cell Physiol **43**, 1473 1483.

Chapter 2:

Identification of new *F-box* genes involved in ABA-inhibition of seed germination and ABA-induced stomatal closure in *Arabidopsis thaliana* using amiRNA-based forward genetic screen

Abstract

Unbiased forward genetic screens are key to finding new genes involved in multiple aspects of plant biology. One of the biggest limitations in forward genetic screens in *Arabidopsis thaliana* is the presence of multiple genes with overlapping functions, which can buffer the effect of single mutations. Using an amiRNA-based forward genetic screen, which specifically addresses genetic redundancy in Arabidopsis, over 10,000 amiRNA lines were screened with a germination assay in the presence of ABA. After re-screening around 300 candidates in the next generation (T3), the line *amiRNA-347* was confirmed to have impaired ABA-inhibition of seed germination. Interestingly, this line was also partially impaired in ABA-induced stomatal closure. The amiRNA transformed into *amiRNA-347* was sequenced and five putative target genes were identified, all of which encode not yet characterized F-box proteins, specifically F-box1 to F-box5. *F-box1*, *3* and *4* are expressed in fully expanded leaves whereas *F-box1* and *3* are expressed in dry seeds. Transgenic plants overexpressing dominant-negative isoforms of *F-box1* and *3* (named "decoy" lines) also showed impairment in ABA-inhibition of seed germination, lower leaf temperature in thermal imaging analysis and only a partial response to ABA-induced stomatal closure. In order to identify possible targets of these F-box proteins, negative regulators of the ABA signaling pathway such as "clade A PP2C" phosphatases and the β-subunit of a protein farnesyl transferase (ERA1) were tested in Y2H. Positive interactions between F-box1 and 3 with "clade A PP2Cs" were confirmed both *in vivo* and *in planta*. Taken together, our findings suggest a link between ABA signaling and F-box-mediated degradation of negative regulators in the ABA signaling pathway.

Introduction

Plants need to perceive, integrate and respond to both external and internal stimuli to maximize survival and growth. This process starts at the seed stage, when the decision between germinating or becoming dormant takes place. This is a key step to maximize survival of seedlings and has a major impact on crop production as it ensures that seeds will only germinate in optimal conditions. Although there are several factors that influence seed germination and dormancy, this process is mainly controlled by the balance between two plant hormones, gibberellins (GAs) and abscisic acid (ABA) (Weitbrecht *et al.*, 2011; Shu *et al.*, 2016). At the seed maturation stage, exogenous ABA from the mother plant inhibits seed germination while ABA synthesized by the seeds maintains seed dormancy (Kucera *et al.*, 2005). While maintaining seed dormancy, ABA accumulates and binds to the PYRABACTIN RESISTANCE1/PYR1-LIKE/REGULATORY COMPONENTS OF ABA RECEPTORS (PYR/PYL/RCAR) receptors and triggers a molecular signaling pathway through deactivation of PROTEIN PHOSPHATASES TYPE 2C (PP2C) and activation of SUCROSE NONFERMENTING1-RELATED SUBFAMILY2 (SnRK2) kinases (Cutler *et al.*, 2010; Hubbard *et al.*, 2010; Kim *et al.*, 2010). The PP2Cs play a key role in this pathway as negative regulators by binding to SnRK2 kinases and blocking ABA signaling (Ma *et al.*, 2009; Park *et al.*, 2009). There are nine "Clade A" PP2C phosphatases implicated in the ABA signaling pathway: ABA-INSENSITIVE1 and 2 (ABI1, ABI2), ABA-HYPERSENSITIVE1 (or AtP2C-HA, Leonhardt *et al*., 2004) and 2 (HAB1 and HAB2), ABA-HYPERSENSITIVE GERMINATION1 and 3 (AHG1 and PP2CA/AHG3), and three HIGLY ABA-INDUCED1, 2 and 3 (HAI1, AKT1-Interacting PP2C1/HAI2, and HAI3) (Schweighofer *et al.*, 2004; Bhaskara *et al.*, 2012; Hauser *et al.*, 2017). Recently, much attention has been given to the regulation of PP2C protein levels by E3 ligase-mediated degradation. The (RING domain ligase 1) RGLG1 E3 ligase

promotes nuclear degradation of PP2CA (Palazon *et al.*). In addition, PLANT U-BOX 12 and 13 (PUB12/13) target ABI1 for degradation in the proteasome (Kong *et al.*, 2015). More recently, the role of the "BTB/POZ AND MATH DOMAIN" BPM3 and BPM5 subunits of Cullin3-RING E3 ligases in targeting PP2CA, ABI1, ABI2 and HAB1 for degradation was also identified (Julian *et al.*, 2019).

Although these findings strongly suggest that PP2C protein levels have to be tightly controlled for proper ABA sensitivity, how these distinct E3-ligases are integrated in the pathway as well as whether other PP2Cs are also targeted by E3-ligases remain elusive.

Another major negative regulator of the ABA signaling pathway is the β-subunit of a farnesyl transferase named ENHANCED RESPONSE to ABA 1 (ERA1) (Cutler *et al.*, 1996). *Era1* mutants are hypersensitive to ABA in seed germination and are more drought tolerant due to lower stomatal conductance and stronger ABA-activation of guard cell anion-channels (Pei *et al.*, 1998). Interestingly, more recent work showed that ERA1 plays a role in blue light-induced stomatal opening, suggesting that ERA1 function goes beyond ABA signaling (Jalakas *et al.*, 2017).

Using an artificial microRNA (amiRNA)-based forward genetic screen which circumvents genetic redundancy in plants (Hauser *et al.*, 2013, 2018), over 10,000 amiRNA lines were screened for seed germination in the presence of ABA. A new line, named *amiRNA-347*, was isolated and confirmed to be less sensitive to both ABA-inhibition of seed germination and ABA-induced stomatal closure. The amiRNA transformed in *amiRNA-347* targets five *F-box* genes (*F-box1* to *F-box5*), which belong to a gene family composed of 692 members in Arabidopsis (Xu *et al.*, 2009). Protein-protein interaction analyses in Yeast Two Hybrid (Y2H) and in *Nicotiana benthamiana* plants suggest that F-box1, 2 and 3 but not F-box4 and 5 can physically interact with

"Clade A" PP2Cs and ERA1. Our data suggest that F-box1, 2 and 3 have partially overlapping function in Arabidopsis and play a role in the ABA signaling pathway.

Materials and Methods

Plant material, growth conditions and transformation

Plant growth conditions were similar to what was described in "Chapter 1". Arabidopsis accession Columbia-0 was used as the background for all amiRNA transformations. Surface-sterilized seeds (15 min 70% ethanol, 0.1% sodium dodecyl sulfate; three to four washes with ~100% ethanol; alternatively 10 min 50% bleach, 0.05% Tween-20; four to six washes with water; (Lindsey *et al.*, 2017) of Arabidopsis were cold-treated for 2–5 d at 4 °C and germinated on half-strength Murashige and Skoog basal medium supplemented with Gamborg's vitamins (Sigma-Aldrich (Murashige and Skoog, 1962; Gamborg *et al.*, 1968), 0.8% Phytoagar (Difco, Franklin Lakes, NJ, USA) and pH adjusted (pH 5.8; 2.6 mM MES titrated with potassium hydroxide). After 5–7 d, plants were transferred to plastic pots containing sterilized premixed soil (Sunshine Professional Blend LC1 RS; Sunshine; supplemented with an appropriate amount of insecticide (Marathon, Gnatrol) and propagated under the following conditions: long day (16 h light/8 h dark); 23–27 °C; 20–70% humidity, 60–100 mmol m^{-2} s^{-1} light.

Plant transformation by floral dip was performed as described elsewhere (Clough and Bent, 1998) with the following modifications. *Agrobacterium tumefaciens* GV3101::pMP90 (Koncz and Schell, 1986) was grown under selection of all markers, i.e. genomic (rifampicin), Ti-plasmid (gentamicin), pSOUP (tetracycline) and T-DNA plasmid (spectinomycin). The infiltration medium for resuspension of the bacteria and floral dip contained 5% sucrose (w/v) and 0.02% (v/v) Silwet L-77 (Clough and Bent, 1998).

Herbicide-resistant plants were transferred to soil and grown to full maturity and T2 seeds collected from individual plants. When appropriate, media for growth of bacteria or plant selection

contained the following concentrations of antibiotics (mg ml^{-1}): carbenicillin 100, gentamycin 25, kanamycin 30, rifampicin 50, spectinomycin 100, tetracycline 10, and phosphinotricin 15.

Screen for abscisic acid-insensitive cotyledon emergence phenotype and germination assay

For the pooled screening, approximately 10–50 seeds of 90 individual T2 plants were mixed, surface sterilized and sprinkled onto agar plates (3 μM (±)-ABA; Sigma-Aldrich). As a control for ABA insensitivity, *abi4-1* (ABRC, CS8104) was used and Col-0 was used as a wild-type control. A putative ABA-insensitive phenotype was scored in a binary manner for similarity to the *abi4-1* or *abi5-1* phenotype and difference from wild-type after 5–8 d using green cotyledons as the indicator (Kuhn *et al.*, 2006). For lines that showed a putative ABA insensitivity, the seed germination assay was repeated by propagating individual T2 seedlings to the next generation (T3) and using seeds of the T3 generation for ABA sensitivity assays. This time, seeds were placed on plates with and without ABA (with indicated concentration of (±)-ABA; Sigma-Aldrich) and images were taken daily for 7 d and emergence of radicles and cotyledons was counted manually using Fiji (Schindelin *et al.*, 2012). For candidates of the individual screen the T2 seeds were used for repetition of the germination assay.

Identification of amiRNA sequences and testing reproducibility

Genomic DNA from candidates with a robust and reproducible phenotype was isolated as described elsewhere (Edwards *et al.*, 1991) and the sequence of the amiRNA present was determined by sequencing of the PCR product (primers pha2804f and pha3479r; see Supplementary Table S1). Using the Target Search function available on the WMD3 website (Ossowski *et al.*, 2008), putative amiRNA target genes were predicted. For independent

confirmation of the phenotype, independent lines were generated by cloning the identified amiRNA into pFH0032 (Supplementary Table S2; (Hauser *et al.*, 2013) and transforming it into Arabidopsis Col-0. Confirmed phenotypes were further analysed by using single knock-out mutants, higher order mutants generated by crossing and/or generating amiRNAs that target subsets of the initial target genes (see Supplementary Table S3).

Gas exchange analyses

Stomatal conductance of H_2O (g_s) was measured in leaves of 5- to 6-week-old plants using portable gas exchange systems (LI-6400 and LI-6800, LI-COR, Lincoln, NE, USA), starting 2 h after growth chamber light onset. For intact single leaf ABA treatments, the method used was previously described in (Ceciliato *et al.*, 2019). Briefly, a LED light source set at 150 µmol m^{-2} s^{-1} (10% blue) and a chamber temperature of 21 °C were used. Leaves were equilibrated for 1 h at a relative humidity of 70–72%, airflow of 200 rpm and CO_2 concentration of 400 ppm. After 1 h, steady-state stomatal conductance was recorded 10 min before the addition of ABA to the petioles submerged in water at the indicated concentration. For light-response measurements, plants were kept in the dark for 18 h prior to experiments. The data presented represent $n \geq 3$ leaves with each leaf from independent plants per genotype per treatment.

Inhibition of root growth assay

In order to test ABA-inhibition of primary root growth, seeds were surface-sterilized and germinated on half-strength MS (Murashige and Skoog medium), 1 mM MES (2-(N-morpholino) ethanesulfonic acid), and 1.5% agar with the pH adjusted to 5.6 with KOH and grown vertically for four days. After this, seedlings were transferred to different media: on half-strength MS +

ETOH control or half-strength MS + 20 μM (±)-ABA; Sigma-Aldrich. Primary root growth length was measured using the software ImageJ. Bars represent average ± SD of twenty – twenty-five seedlings per genotype per treatment. The *abi1abi2hab1pp2ca* quadruple mutant was used as positive control.

qRT-PCR analysis

Total RNA (500 ng) was extracted from four-week-old leaves or dry seeds and was reverse transcribed using the first-strand cDNA synthesis kit (GE Healthcare). qRT-PCR analyses were performed using 3-fold-diluted cDNA (Maxima SYBR Green Rox/qPCR Master Mix; Thermo Fisher Scientific) on a CFX Connect PCR cycler (BioRad). The housekeeping *PDF2* gene was used as an internal control (Czechowski *et al.*, 2005). The threshold cycle (C_T) was determined by the instrument (CFX Manager Software, BioRad), and the $\Delta\Delta C_T$ method was used to calculate the fold change in each gene (Livak and Schmittgen, 2001).

Western blot analysis of F-box decoy lines

To verify the expression levels of distinct insertion events of F-box decoy lines, seedlings were first grown on half-strength MS (Murashige and Skoog medium), 1 mM MES (2-(N-morpholino) ethanesulfonic acid), and 1.5% agar with the pH adjusted to 5.6 with KOH and grown horizontally for two weeks. Total protein was extracted using protein extraction buffer (50 mM MOPS-KOH pH 7.5, 100 mM $NaCl_2$, 2.5 mM EDTA, 10 mM NaF, 2 mM DTT, 1 mM PMSF, 20 μM Leupeptin). Twenty to forty seedlings were ground using 500 μL of extraction buffer on ice and extracts were centrifuged at 14,000 rpm, 4 °C for 10 min. The supernatant was collected, and Bradford was used to quantify the protein extracts. Twenty-five μg of protein was fractionated on

10.5% SDS-PAGE gel, blotted onto a nitrocellulose membrane (Whatman Protran BA85 0.45 μm) and probed with anti-FLAG antibody (Life Tecnology) overnight at 4 °C and finally incubated with a goat anti-mouse IgG – AP (alkaline phosphatase, Santa Cruz) for 2 hours at room temperature. Membranes were incubated with NBT/BCIP (Roche) and bands were detected.

Thermal imaging of F-box decoy lines

WT Columbia-0 plants were grown side-by-side with F-box decoy insertion lines for five weeks. Plants were grown in plastic pots containing sterilized premixed soil (Sunshine Professional Blend LC1 RS; Sunshine; supplemented with insecticide (Marathon, Gnatrol)) and propagated under the following conditions: 12 h light/12 h dark); 21–22 °C; 70–85% humidity, 100 –110 mmol m^{-2} s^{-1} light in a Percival growth chamber (Ceciliato et al., 2019). A Plants were removed from the growth chamber and placed side-by-side for thermal imaging and images were taken with a FLIR T650sc thermal imaging camera (FLIR, Wilsonville, OR, USA). Thermal images were converted into Flexible Image Transport System format (fits) using the ExaminIR software (FLIR).

Protein-protein interaction in Y2H

In order to test protein-protein interactions, Y2H assays were performed using the USER-modified pGBT9 and pGADGH vectors (Clontech). Constructs were transformed into Yeast PJ69-4A cells and selected on SD-L-W medium. Three independent colonies were incubated in liquid SD-L-W medium overnight and then the OD_{600} of cultures was adjusted to 1 with water. A series of 5 μL 10- and 100-fold dilutions of transformants were spotted on SD-L-W and SD-L-W-H supplemented with ETOH control or 10 μM ABA final concentration, and grown for 5 to 6 d. For

tests in liquid media, three colonies for each transformant were grown for 48 h on SD-L-W liquid medium and the OD_{600} was measured. OD_{600} was adjusted to 0.1 and interactions were tested on SD-L-W-H liquid supplemented with ETOH control or 10 μM ABA final concentration for the indicated amount of time.

Protein-protein interaction in N. benthamiana

For Bimolecular Florescence Complementation (BiFC) experiments, the coding region of the indicated genes were inserted into the USER-modified pSPYCEmR and pSPYNER vectors (Waadt *et al.*, 2008). Optical density (OD_{600}) of transformed *Agrobacterium* cells was adjusted to 0.2 with buffer (10 mM MES, 10 mM $MgCl_2$, 100 μM acetosyringone, pH 5.6). For co-expression, equal volumes of bacterial suspensions were mixed at a final OD_{600} of 0.2 each and infiltrated into 6-week-old *N. benthamiana* leaves with a syringe. The p19 helper plasmid was also co-infiltrated. Seventy-two h after infiltration, fluorescence was observed using confocal imaging.

Results

The *amiRNA-347* line is partially insensitive to ABA-inhibition of seed germination and ABA-induced stomatal closure.

Using the amiRNA seed resource presented in "Chapter 1" and screening pools of 90 amiRNA lines (30-50 seeds per line) per round (with approximately 100 rounds total), approximately 340 putative candidates were identified in this seed germination assay. In the next generation (T3), approximately 25 of these amiRNA lines were confirmed to be less sensitive to ABA, including the line *amiRNA-347*. (Figure 1). Compared to the control line, *amiRNA-HsMYO*, the *amiRNA-347* line showed robust germination and cotyledon emergence in the presence of 1.5 μM ABA (Figure 1A). Quantification of germination rates in figure 1 showed over 75% germination in *amiRNA-347* in contrast to the control line, that showed less than 40% germination seven days after exposure to light (Figure 1B). In order to test whether the *amiRNA-347* line was less sensitive to ABA-induced stomatal closure, intact leaf gas exchange experiments were pursued. When leaves were treated with 2 μM ABA via the petiole (Ceciliato et al, 2019), a delay in ABA-induced stomatal closure in *amiRNA-347* plants was observed (Figure 1C and 1D).

AmiRNA-347 targets five F-box genes: At3G03030 (F-box1), At3G58880 (F-box2), At5G59000 (F-box3), At3G58820 (F-box4) and At5G38386 (F-box5). Using the online tool CLUSTALW (https://www.genome.jp/tools-bin/clustalw), a phylogenetic tree was generated which contained all 5 of these F-box target genes. Interestingly, the five target genes were not grouped in the same clade of the tree but spread across five distinct clades (Figure 1E). When protein identity was verified, it was observed that the five F-box proteins are less than 50%

identical to one another, whereas a sixth F-box protein (At3G03040), which is not predicted to be targeted by amiRNA-347, showed over 70% identity to F-box1 (Figure 1E, insert).

Combined, our data suggest that the *amiRNA-347* line is less sensitive to ABA in both germination assays and in ABA-induced stomatal closure, likely due to the knockdown of uncharacterized F-box genes.

New amiRNA lines targeting *F-box1* to *5* show partial insensitivity to ABA in germination assays and decrease the *F-box* gene expression levels in mature leaves.

In order to test whether new amiRNAs targeting the same five *F-box* genes would confer an ABA-phenotype, two new amiRNAs were designed and transformed into Arabidopsis. These new lines were named amiRNA 1 and amiRNA 2 (Figure 2A). In the T2 generation, three independent insertion events each of amiRNA 1 and amiRNA 2 (labeled as #1, #2 and #3 respectively) were tested in germination assays in the presence of ABA. Interestingly, and as highlighted in "Chapter 1", a large variation was observed between distinct amiRNA insertion events. In the presence of 0.5 μM ABA, amiRNA 1 insertion events #2 and #3 and amiRNA 2 insertion event #2 showed higher germination and cotyledon emergence rates compared to control lines (Figure 2B and 2C). The amiRNA lines that showed the strongest phenotypes in germination assays were chosen for further characterization (amiRNA 1, insertion #3 and amiRNA 2 insertion #2).

To further investigate the phenotypes conferred by the *F-box* knockdown lines, ABA-inhibition of primary root growth assays were performed. In the presence of 20 μM ABA, both the originally isolated *amiRNA-347* line and the new amiRNA lines 1 and 2 showed WT-like responses to ABA in primary root growth (Figure 2D).

The expression levels of *F-box* genes *1* to *5* were quantified using qRT-PCR in both mature leaves and dry seeds in the wildtype parent accession Col-0. It was observed that *F-box1*, *3* and *4* were more highly expressed in leaves (Figure 2E) and *F-box1* and *3* in dry seeds (Figure 2F). In addition, a robust decrease in gene expression levels of *F-box 1*, *3* and *4* was observed in mature leaves of *amiRNA-347* and amiRNA 2 insertion #2 (Figure 2E).

Next, we isolated T-DNA insertion lines of *F-box1*, and *4* as these are more highly expressed in mature leaves and seeds (Figures 2E and 2F). In the case of *F-box3*, we could not find a T-DNA insertion in any of the exons, but T-DNA lines for *F-box1* and *4* were isolated. Single T-DNA insertion mutants for *F-box1* and *4* were tested in germination assays and showed WT-like responses to ABA-inhibition of seed germination (Figure 3A). As these *F-box* genes might have overlapping functions, a *F-box1*/*F-box4* double mutant (*f1f4* double) was generated and tested in ABA-inhibition of seed germination assays. As previously observed in the single mutants, the *f1f4* double mutant showed WT-like sensitivity to ABA (Figure 3B), suggesting that higher order mutants might be needed for further investigation. The *f1f4* double mutant was also tested in ABA-inhibition of root growth assays. The quadruple mutant of PP2Cs (*abi1/abi2/hab1/pp2ca)*, (Li *et al.*, 2016) and WT plants were used as controls. It was observed that *f1f4* double mutants have WT-like responses to ABA in root growth assays (Figure 3C).

Our data suggest that amiRNA lines knocking down the *F-box* genes *1* to *5* have lower sensitivity to ABA in germination assays and that these F-box proteins might have overlapping functions.

The *F-box1* and *F-box3* decoy lines have lower sensitivity to ABA in germination assays, and knockdown of *F-box3* gene in the *f1f4* double mutant background decreases ABA sensitivity.

During the development of this project, Dr. Joshua Gendron (Yale University) established a method to characterize plant E3 ligases. Using dominant negative F-box proteins (denominated "decoy"), it is possible to stabilize the targets of E3 ligases instead of causing their degradation (Feke *et al.*, 2019). In addition, this technique presents an unbiased method for identifying putative interactors of E3 ligases using mass spectrometry-based immuno-precipitation (IP/MS).

When I first contacted Dr. Gendron for a collaboration, his laboratory had decoy lines for both F-box1 and F-box3. In the T2 generation, germination assays were used to test whether F-box1 decoy and/or F-box3 decoy lines have distinct sensitivity to ABA. As described above, three independent insertion events were used in these experiments for each of these lines, named F-box1 decoy #1, #2 and #3 and F-box3 decoy #1, #2 and #3. Seeds for these experiments were freshly harvested simultaneously. In the presence of 1.5 μM ABA, the insertion events F-box1 decoy #1 and F-box3 decoy #1, #2 and #3 showed higher cotyledon emergence rates compared to control lines (Figures 4A and 4B). As the variation in germination rates between independent insertion events of F-box1 decoy lines was very high, western blot was used to detect the presence of F-box1 decoy proteins in all three insertion events. It was observed that F-box1 decoy #1 line had the strongest expression of the F-box1 decoy protein (Figure 4C).

The data from F-box3 decoy lines in germination assays suggest that F-box3 might play a role in ABA-inhibition of seed germination. In order to test this hypothesis, a new amiRNA was designed to specifically target the *F-box3* gene. This new amiRNA was transformed in two distinct backgrounds: WT (named *amiRNA-F-box3*) and *f1f4* double mutant (named *f1f4*double/*amiRNA-F-box3*). In germination assays, in the presence of 1.5 μM ABA, *amiRNA-HsMYO* control lines showed on average less than 10% germination. By averaging ten independent insertion lines, *amiRNA-F-box3* plants showed around 20% germination and the *f1f4double/amiRNA-F-box3*

plants showed over 35% germination in the same condition, seven days after exposure to light (Figure 4D).

When fully developed, F-box1 and 3 decoy plants appeared to be larger than parallel-grown WT plants, in particular in terms of leaf area (Figure 5A). Using infrared thermal imaging, the canopy leaf temperatures of F-box1 and 3 decoy lines were compared to WT. The canopy leaf temperatures in F-box1 decoy#3 and F-box3 decoy#2 were very similar to WT canopy leaf temperature (Figure 5B, upper panels). Interestingly, F-box1 decoy#1 and F-box3 decoy#1 plants showed lower canopy leaf temperature compared to WT control plants (Figure 5B, lower panels). This prompted us to test whether these decoy lines have affected ABA-induced stomatal closure responses. Using intact leaf gas exchange, leaves from F-box1 decoy#1 (Figures 5C and 5D) and F-box3 decoy#1 (Figures 5E and 5F) were treated with 1.0 μM ABA and stomatal conductance was measured and compared to WT leaves treated in parallel. It was observed that leaves from F-box3 decoy#1 line had higher steady-state stomatal conductance and delayed response to ABA (Figure 5E and 5F).

Taken together, our data indicate that these F-box proteins targeted in *amiRNA-347* line have (partial) overlapping functions and that F-box3 could be important for the observed ABA phenotype.

F-box proteins 1, 2 and 3, but not 4 and 5, interact with clade A PP2Cs in Y2H assays.

F-box proteins are the substrate-recognition units of a protein complex known as "Skp1-Rbx1-Cul1-F-box protein" (SCF) ubiquitin ligases. As such, F-box proteins bind to their target(s) and ultimately drive their degradation via the 26S proteasome (Xu *et al.*, 2009). To better understand how the recently discovered F-box proteins 1 to 5 interact with the ABA signaling

pathway, the identification of their targets was crucial. By using three distinct methods to decrease gene expression/function of F-box1 to 5 (amiRNA lines, F-box decoy lines and T-DNA insertion lines), it was observed that all of them led to hyposensitivity to ABA (Figures 1, 2 and 4). This suggests that the F-box proteins could be targeting negative regulator(s) of the ABA signaling pathway. In this context, there would be a decrease in degradation of these negative regulators in our mutants and plants would become more resistant to ABA. To test this hypothesis, two major classes of negative regulators of the ABA signaling pathway were chosen: the nine "clade A" type 2C protein phosphatases (PP2Cs) (Fuchs *et al.*, 2013) and the β-subunit of a farnesyltransferase called Enhanced Response to ABA1 (ERA1) (Cutler *et al.*, 1996).

To verify whether our newly identified F-box proteins physically interact with PP2Cs and/or ERA1, we first used Yeast-Two-Hybrid (Y2H) assays. Two positive controls were selected: the interaction between the GTP exchange factor RopGEF1 and the PP2C ABI1, which is ABA-independent in yeast (Li *et al.*, 2016), and the interaction between the ABA receptor PYR1 and the PP2C HAB1, which is ABA-dependent (Park *et al.*, 2009). First, we tested putative interactions using F-box1 and F-box3 as protein baits. Our data indicated potential positive interactions between F-box1 and all nine PP2C phosphatases tested (Figure 6A). Interestingly, the addition of ABA to the plates where these interactions were tested seemed to enhance the growth of yeast co-transformed with F-box1 and PP2Cs, especially for the following combinations: F-box1+ABI1, F-box1+HAB1, F-box1+HAI2 and F-box1+HAI1 (Figure 6A). F-box1 also showed positive interaction with ERA1 in Y2H assays, although in a weaker manner. This interaction, however, was not remarkably enhanced by the addition of ABA (Figure 6B). Similar experiments were performed using F-box3 as bait. In these experiments, we did not observe a clear interaction between F-box3 and the PP2Cs (Figure 7A) or with ERA1 (Figure 7B).

From the data obtained in Figures 6 and 7, we hypothesized that some F-box proteins might interact more or less strongly with their targets. Furthermore, we needed to test whether ABA truly has a quantitative effect on these interactions. In order to better visualize these differences in the strength of putative interactions between F-box proteins and negative regulators of the ABA signaling pathway, we performed the next Y2H experiments in liquid media. Interactions could then be indirectly quantified by determining the time-dependent growth of the yeast cultures using OD_{600} measurements. In addition, we tested putative interactions in the absence (ethanol control) and presence of ABA. When the control interaction between PYR1 and HAB1 was tested, the yeast culture was observed to grow rapidly, with a maximum OD_{600} of 1.38 achieved within 50 hours of incubation, but only in the presence of ABA (Figure 8A). In the absence of ABA, the maximum OD_{600} achieved was 0.36 for the same period of time which served as a control for background interaction. With this experimental set up, the putative interactions between each of the 5 F-box proteins with the PP2Cs ABI1, HAI1, HAI2 and HAI3 were tested in the presence and absence of ABA. When F-box1 was used as a bait, positive interactions were observed for all interactions tested, including ERA1 (Figure 8B to 8F). However, the maximum growth of yeast was observed only about 70 hours after the start of the experiment, which was slower than the ABA-induced PYR1-HAB1 interaction (Figure 8A). The presence of ABA had a small effect in interactions between F-box1 and HAI3 (Figure 8B) and F-box1 and HAI1 (Figure 8D). When F-box2 was used as bait, a measurable interaction above background was only observed with HAI2 (Figure 9). In the case of F-box3, positive interactions were detected for the following combinations: F-box3+HAI1, F-box3+HAI2 and F-box3+ERA1 (Figure 10). Interestingly, F-box4 and F-box5 did not strongly interact with the tested PP2Cs or ERA1, even after over 90 hours of yeast growth (Figures 11 and 12).

With data gathered from Figures 8 to 12, an interaction network could be determined in which F-box1, 2 and 3 interact with HAI2, F-box1 and 3 interact with ERA1 and F-box4 and 5 do not strongly interact with any of the tested targets (Figure 13).

F-box1, but not F-box4, interacts with HAI2 in planta.

To further test whether F-box1 can physically interact with HAI2 and/or ERA1, we tested these putative interactions *in planta* using heterologous expression in *Nicotiana benthamiana.* For these analyses, we used Bimolecular Florescence Complementation assays (BiFC), fusing the N-terminal of YFP with F-box proteins and the C-terminal of YFP with the putative targets. Since F-box1 showed positive interaction with all PP2Cs tested in Y2H (Figures 6 and 8), another phosphatase, APD7, which does not belong to "clade A" of PP2Cs (Fuchs *et al.*, 2013), was used as a control in these experiments. Interestingly, F-box1 seemed to interact with HAI2 and APD7, but not with ERA1 (Figure 13A). HAI2 is only 28% identical to APD7 and 24% identical to ERA1 (Figure 13, insert). The F-box4 protein did not interact with HAI2 or ERA1 in Y2H experiments (Figure 11). In BiFC experiments, we also observed that F-box4 does not interact with HAI2 or ERA1 (Figure 13B), consistent with Y2H experiments.

Next, we tested whether the closest homolog of F-box1 protein could interact with HAI2 and/or ERA1. This F-box gene (At3G03040) is 71% identical to F-box1 (Figure 13, insert) and was named F-box03040. We did not detect positive interactions between F-box03040 and the tested targets (Figure 13C). The known interaction between RopGEF1 and ABI1 was used as a positive control (Figure 13D).

Together, our data suggest that F-box1 can interact with HAI2 *in planta*, but also with an unrelated phosphatase (APD7), indicating that further experiments need to be performed in order

to test the physiological relevance of such interactions. In the future, BiFC experiments will be conducted in parallel with negative controls and the data will be quantified. The ubiquitination profile of putative targets will also be evaluated in both amiRNA and F-box decoy lines.

Discussion

Forward genetic screens can lead to the isolation and identification of new genes in an unbiased fashion, but overlapping functions of homologous genes, often referred to as functional genetic redundancy makes it less useful as redundancy buffers the effect of single gene mutations. By using an amiRNA-based forward genetic screen (Hauser *et al.*, 2013, 2018), we isolated a new amiRNA line (amiRNA-347) which was less sensitive to ABA in both ABA-inhibition of seed germination and ABA-induced stomatal closure (Figure 1A to 1D). This amiRNA has five target genes, all of which encode F-box proteins. Given the fact that the F-box gene family is one of the largest gene families in Arabidopsis, with over 690 members (Xu *et al.*, 2009), our finding suggests that amiRNAs are indeed capable of circumventing genetic redundancy. Our amiRNA library was designed to target multiple genes within a given gene family, based on sequence similarity (Hauser *et al.*, 2013). The five *F-box* genes targeted by amiRNA-347 do not belong to the same branch of the phylogenetic tree generated using protein sequences (Figure 1E). This suggests that maybe some of these targeted genes might not be redundant and were targeted by the same amiRNA based on mRNA sequence similarities. Although the "amiRNA-Ax347" and "amiRNA2" do not have any predicted possible off targets based on sequence analyses, "amiRNA1" shows low binding affinity to the mRNA of another F-box gene (At3G58590). In combination with the fact that the five amiRNA target genes are spread out in the F-box gene family, this indicates that the amiRNAs used in this project might have off targets not yet considered.

When two new amiRNAs were designed to target the same five *F-box* genes (*F-box1* to *F-box5*), partial insensitivity to ABA-inhibition of seed germination was once more observed (Figure 2A to 2C). Interestingly, the phenotypes observed in these new amiRNA lines were very much insertion event dependent. This has been observed before in amiRNA lines (Hauser *et al.*, 2018),

and it is likely due to changes in the amiRNA expression levels and efficiency in gene knockdown. In fact, the insertion event "amiRNA 2 #2" showed strong impairment in ABA-inhibition of seed germination (Figure 2B and 2C) and robust reduction of gene expression levels of *F-box1* to *F-box5* (Figure 2E).

In order to further investigate the roles of these five *F-box* genes identified in our genetic screen, T-DNA insertion mutants of *F-box1* and *F-box4* were obtained (Alonso *et al.*, 2003). Single mutants for both *F-box1* and *F-box4* as well as the *f-box1/f-box4* double mutant showed WT-like responses to ABA in both germination assays and primary root growth assays (Figure 3). These data suggest that either: 1- *F-box1* and *F-box4* genes do not have overlapping function in the ABA-signaling pathway or 2- There is/are more gene(s) that have overlapping function with *F-box1* and *F-box4*.

To better understand the roles of the *F-box* genes 1 to 5 in ABA-signaling, a second approach for tackling genetic redundancy was used. In this case, F-box decoy lines were generated for F-box1 and F-box3. F-box decoy proteins were constitutively expressed but lacked the F-box domain, causing a dominant negative phenotype by stabilizing their targets (Lee *et al.*, 2018; Feke *et al.*, 2019). Three independent insertion events of F-box1 decoy and F-box3 decoy were tested in germination assays. Interestingly, for F-box1, only one insertion event (F-box1 decoy #1) showed impaired responses to ABA-inhibition of seed germination (Figure 4A and 4B). In the case of F-box3 decoy, all three tested insertion lines showed an ABA-phenotype (Figure 4A and 4B).

Distinct insertion events may affect the expression levels of the transgene, and to check whether the distinct phenotypes observed in F-box1 decoy lines correlate with expression of the transgene, western blot was used (Figure 4C). As expected, F-box1 decoy #1 showed higher levels of F-box1 decoy protein. The fact that F-box3 decoy lines showed impaired responses to ABA

(Figures 3 and 4) led us to isolate a *f-box1/f-box3/f-box4* triple mutant. As exonic T-DNA insertion lines for *F-box3* were not available, an amiRNA was designed to target this gene. When the amiRNA for *F-box3* was expressed in the *f-box1/f-box4* double mutant, an impairment in ABA-inhibition of seed germination was observed (Figure 4D), suggesting that F-box3 is an essential F-box in the molecular pathway. In the future, *f-box1/f-box3* double mutants will be isolated using CRISPR/Cas9- mediated deletion of *F-box3.* In addition, F-box3 decoy lines have higher steady-state stomatal conductance and delayed ABA-induced stomatal closure responses (Figure 5).

Knock down of the isolated F-box genes led to a decrease in ABA-sensitivity. We attempted to identify the putative targets of these F-box proteins by testing protein-protein interactions in Y2H. We selected negative regulators in the ABA signaling pathway as putative targets, such as Clade A PP2C phosphatases (Kong *et al.*, 2015) and the beta subunit of a protein farnesyl transferase ERA1 (Cutler *et al.*, 1996; Pei et al., 1998). It has been shown that the deletion of *ERA1* caused both ABA hypersensitivity of anion channel activation in guard cells and of stomatal closing, decreasing water loss through leaf transpiration in drought assays. In addition, *era1* mutants are hypersensitive to ABA in seed germination assays.

At first, putative interactions between F-box1 and F-box3 and negative regulators of the ABA pathway in Y2H were tested in semi-solid media in the absence and presence of ABA. Interestingly, positive interactions between F-box1, clade A PP2Cs and ERA1 (Figure 6), but not F-box3 (Figure 7), were found and they seemed to be enhanced by the presence of ABA. To better visualize differences in protein interaction strength in Y2H, the next experiments were performed in liquid media and yeast growth was measured using Optical Density (OD_{600}) measurements. Although positive putative interactions between F-box1 and Clade A PP2Cs were once again verified, the presence of ABA in the media did not significantly affect yeast growth rate (Figure

8). Similar experiments were performed with the other four F-box proteins (F-box2 to F-box5, Figures 9 to 12) and it was verified that F-box4 and 5 do not interact with the same putative targets (Summarized in Figure 13). These data suggest that F-box1, 2 and 3 might have overlapping functions whereas F-box4 and 5 might be targeted by the same amiRNA solely based on mRNA sequence similarities. In fact, protein-protein interactions *in planta* using BiFC (Bimolecular Florescence Complementation) showed putative positive interactions between F-box1 and HAI2 but not F-box4 and HAI2 (Figure 14A and 14B). HAI2 is a key negative regulator of the ABA signaling pathway and physically interacts with the ABA receptors PYR1 and RCAR11 in an ABA-dependent manner. Consistently, *hai2* loss of function mutants have increased seed dormancy and are hypersensitive to ABA in seed germination assays (Kim *et al*., 2013). It is of notice that a non-related phosphatase, Arabidopsis PP2C Clade D 7 (APD7) also showed positive interaction with F-box1 (Figure 14A). APD7 is a negative regulator of Arabidopsis leaf senescence and interacts with the receptor-like kinase SENESCENCE-ASSOCIATED RECEPTOR-LIKE KINASE (AtSARK), a positive regulator of leaf senescence (Xiao et al., 2015).

Taken together, our data suggest that F-box1 and 3 (and possibly F-box2) have partially overlapping function and are important ABA signaling components. These F-box proteins interact with negative regulators of the ABA signaling pathway both in yeast and in preliminary experiments *in planta*.

Future goals: In the future, key experiments will be performed: **A-** new amiRNAs targeting subsets of the five F-box targeted genes as well as CRISPR/Cas9 constructs will be designed and transformed in Arabidopsis (e.g. targeting *F-box1*, *2* and *3*), **B-** BiFC experiments will be repeated and putative interactions will be quantified and **C-** In order to test protein-protein interactions *in planta*, Co-IP experiments will be performed **D-** degradation assays in both

Nicotiana benthamiana and in Arabidopsis with stable lines will be conducted, **E-** IP/MS experiments using our F-box decoy lines will be performed both under control and ABA-treatment and **F-** ubiquitination assays will be performed to test whether these F-box proteins can indeed direct PP2Cs for degradation.

Chapter 2 is coauthored with Hauser, G; Gendron, J; Schroeder, JI. The dissertation author was the primary author of this chapter.

Figure 2.1 – The amiRNA-347 line is less sensitive to exogenous ABA treatment in germination assay and ABA-induced stomatal closure and targets 5 F-box genes. (A) Seedlings of the control amiRNA line, which targets a gene not found in Arabidopsis (*amiRNA-HsMYO* control), and an amiRNA line that targets five *F-box* genes (*amiRNA-347*) germinated in the presence of 1.5 μM ABA. Photographs were taken after 7 d of exposure. (B) Germination in "A" was counted and presented as percentage of germination. (C) Time-resolved stomatal conductance to H_2O (g_s) in response to application of 2 μM ABA to the transpiration stream (red arrows) is shown in the amiRNA control line (*amiRNA-HsMYO*) and in the amiRNA line targeting five F-box genes (*amiRNA-347*). Stomatal conductance was analysed using whole leaf gas exchange. (C) Stomatal conductance in mol m^{-2} s^{-1}. (D) Data from (C) were normalized to stomatal conductance at the beginning of the experiment. Data are the mean of n=3 leaves per genotype ±SEM. (E) Phylogenetic analyses of the F-box targeted genes in amiRNA-347 line. The phylogenetic tree was generated using the CLUSTALW (https://www.genome.jp/tools-bin/clustalw). The five targeted genes, F-box1 to F-box5 are highlighted in bold. The protein identity between F-box1 and the other four F-box proteins was analyzed (right insert). A non-targeted F-box highlighted by the red arrowhead (At3G03040) was included in the analyses.

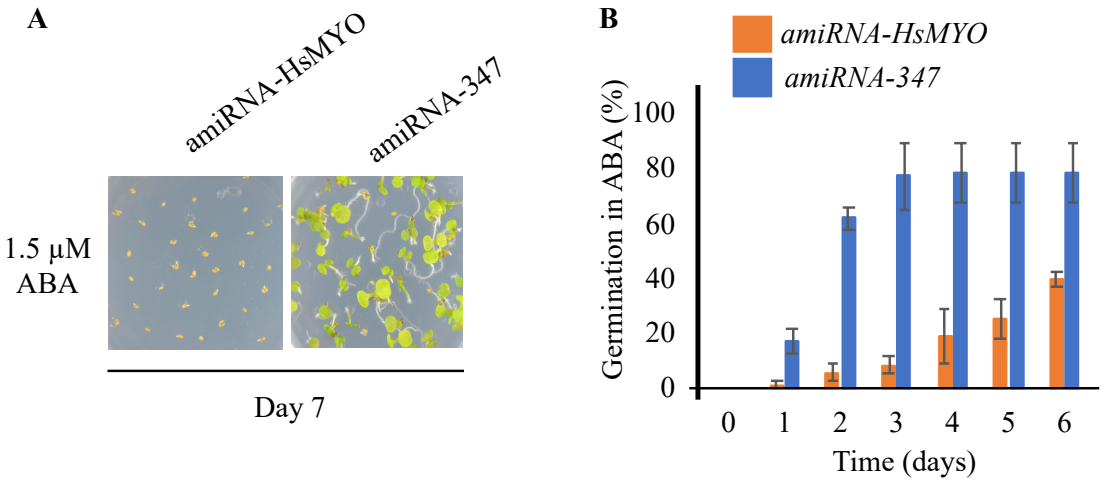
A
amiRNA-HsMYO
amiRNA-347
1.5 µM ABA
Day 7
B
amiRNA-HsMYO
amiRNA-347
Germination in ABA (%)
100
80
60
40
20
0
0 1 2 3 4 5 6
Time (days)

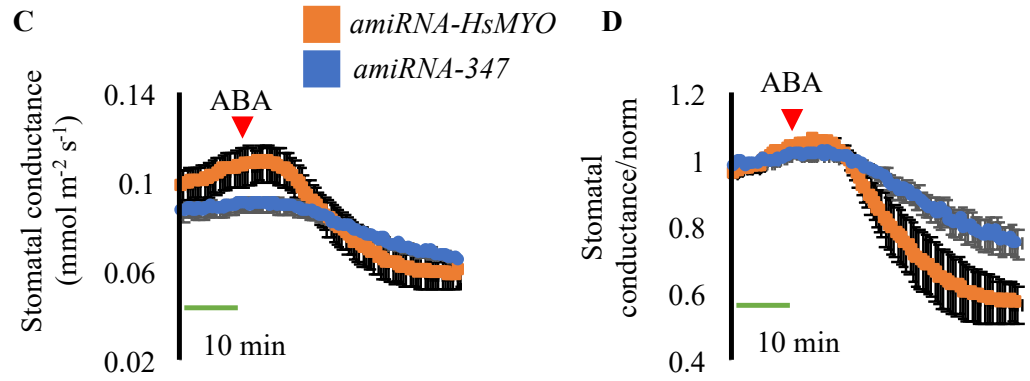
C
amiRNA-HsMYO
amiRNA-347
Stomatal conductance (mmol m-2 s-1)
0.14
0.1
0.06
0.02
ABA
10 min
D
Stomatal conductance/norm
1.2
1
0.8
0.6
0.4
ABA
10 min

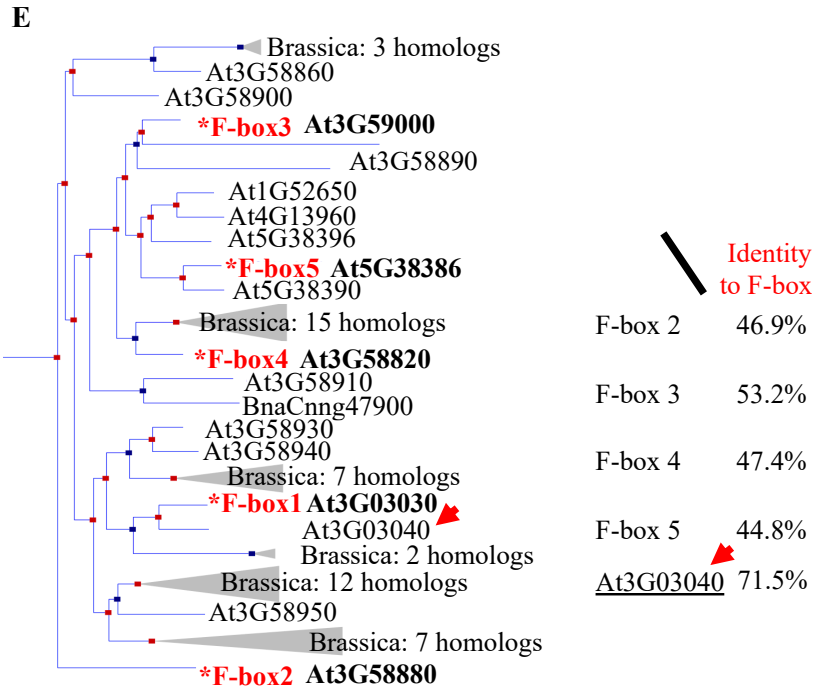
E
Brassica: 3 homologs
At3G58860
At3G58900
*F-box3 At3G59000
At3G58890
At1G52650
At4G13960
At5G38396
*F-box5 At5G38386
At5G38390
Brassica: 15 homologs
*F-box4 At3G58820
At3G58910
BnaCnng47900
At3G58930
At3G58940
Brassica: 7 homologs
*F-box1 At3G03030
At3G03040
Brassica: 2 homologs
Brassica: 12 homologs
At3G58950
Brassica: 7 homologs
*F-box2 At3G58880
Identity to F-box1
F-box 2 46.9%
F-box 3 53.2%
F-box 4 47.4%
F-box 5 44.8%
At3G03040 71.5%

Figure 2.2 – The new amiRNA lines targeting the five F-box genes are less sensitive to ABA in germination assay and F-box1 and 3 genes are expressed in leaves and in dry seeds. (A) Two new amiRNAs targeting all five F-box genes were designed and transformed in Arabidopsis. The 21nt long amiRNA sequences are given. Wild-type (WT), the control amiRNA line (*amiRNA-HsMYO* control), and three independent insertion events of amiRNA lines 1 and 2 that targets five *F-box* genes (*amiRNA 1 and amiRNA 2*) germinated in the presence of 0 or 0.5 μM ABA. (B) Germination after 4 days of exposure to light and (C) cotyledon emergence after 8 days of exposure to light. (D) Primary root growth assay was performed using the amiRNA control line (*amiRNA-HsMYO*), the *amiRNA-347* and *amiRNA 1* and *2* lines. Seedlings were grown for four days before transferring to either 1⁄2 MS plates or 20 μM ABA plates. Images on the left were taken using representative images from the 7th day of growth after transfer. Bar graphs are average of 25 seedlings/genotype/treatment ± SD. (E) The expression levels of all five F-box genes was measured in Arabidopsis leaves (four-week-old) in the control amiRNA line (*amiRNA-HsMYO* control), the *amiRNA-347* and in the *amiRNA 2* line. (F) The expression levels of all five F-box genes was measured in Arabidopsis dry seeds in the control amiRNA line (*amiRNA-HsMYO* control). qRT-PCR was performed using total RNA and the *PDF2* gene expression was used as an internal control. The graph shows data from three biological replicates with two technical replicates each. Bars show mean ± SD.

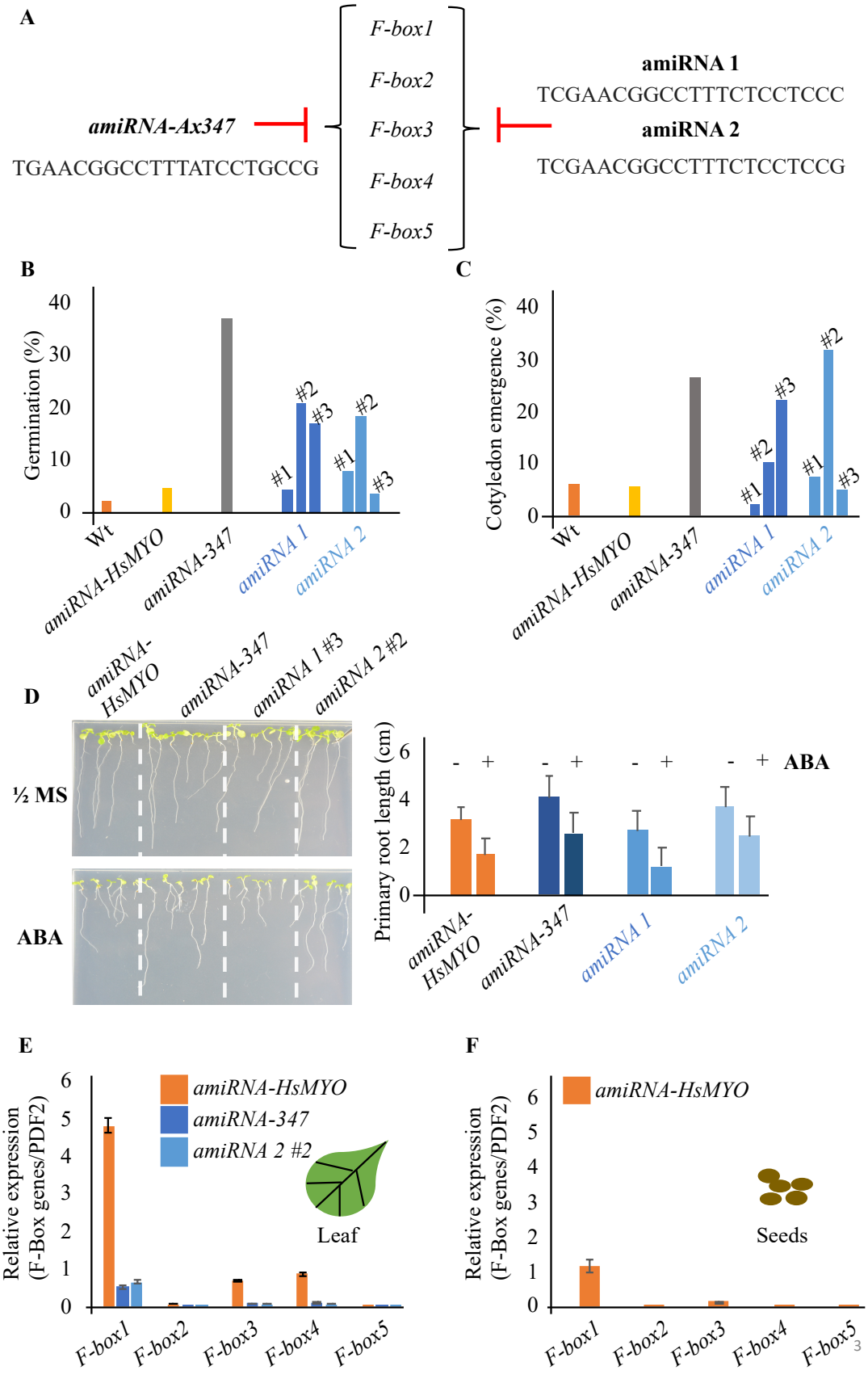
A
amiRNA-Ax347
TGAACGGCCTTTATCCTGCCG
F-box1
F-box2
F-box3
F-box4
F-box5
amiRNA 1
TCGAACGGCCTTTCTCCTCCC
amiRNA 2
TCGAACGGCCTTTCTCCTCCG
B
Germination (%)
Wt
amiRNA-HsMYO
amiRNA-347
amiRNA 1
amiRNA 2
C
Cotyledon emergence (%)
D
½ MS
ABA
Primary root length (cm)
E
Relative expression (F-Box genes/PDF2)
amiRNA-HsMYO
amiRNA-347
amiRNA 2 #2
Leaf
F-box1
F-box2
F-box3
F-box4
F-box5
F
Seeds

Figure 2.3 – Single T-DNA insertion mutants for *F-box1* and *F-box4* genes and the *f1/f4* double mutants are not insensitive to ABA in germination and root growth assay. (A) Germination assay was performed using T-DNA insertion lines for *F-box 1* (SALK 094197) and *F-box 4* (SALK 037281). Wild-type (WT), the control amiRNA line (*amiRNA-HsMYO* control), and the amiRNA-347 lines were used as controls. Germination was evaluated in the presence 1.5 µM ABA. Picture was taken 14 days after exposure to light. (B) The *f1f4* double mutant was evaluated in a germination assay. The seeds of WT, *abi4-1*, and two lines of *f1f4* double mutant were sown on ½ MS plates or 1.5 µM ABA. (C) Primary root growth assay was performed using WT seedlings, the *pp2c4x* mutant and the *f1f4* double mutant. Seedlings were grown for four days before transferring to either 1⁄2 MS plates or 20 µM ABA plates. Images on the left were taken using representative images from the 7th day of growth after transfer. Bar graphs are the average of 25 seedlings/genotype/treatment ± SD.

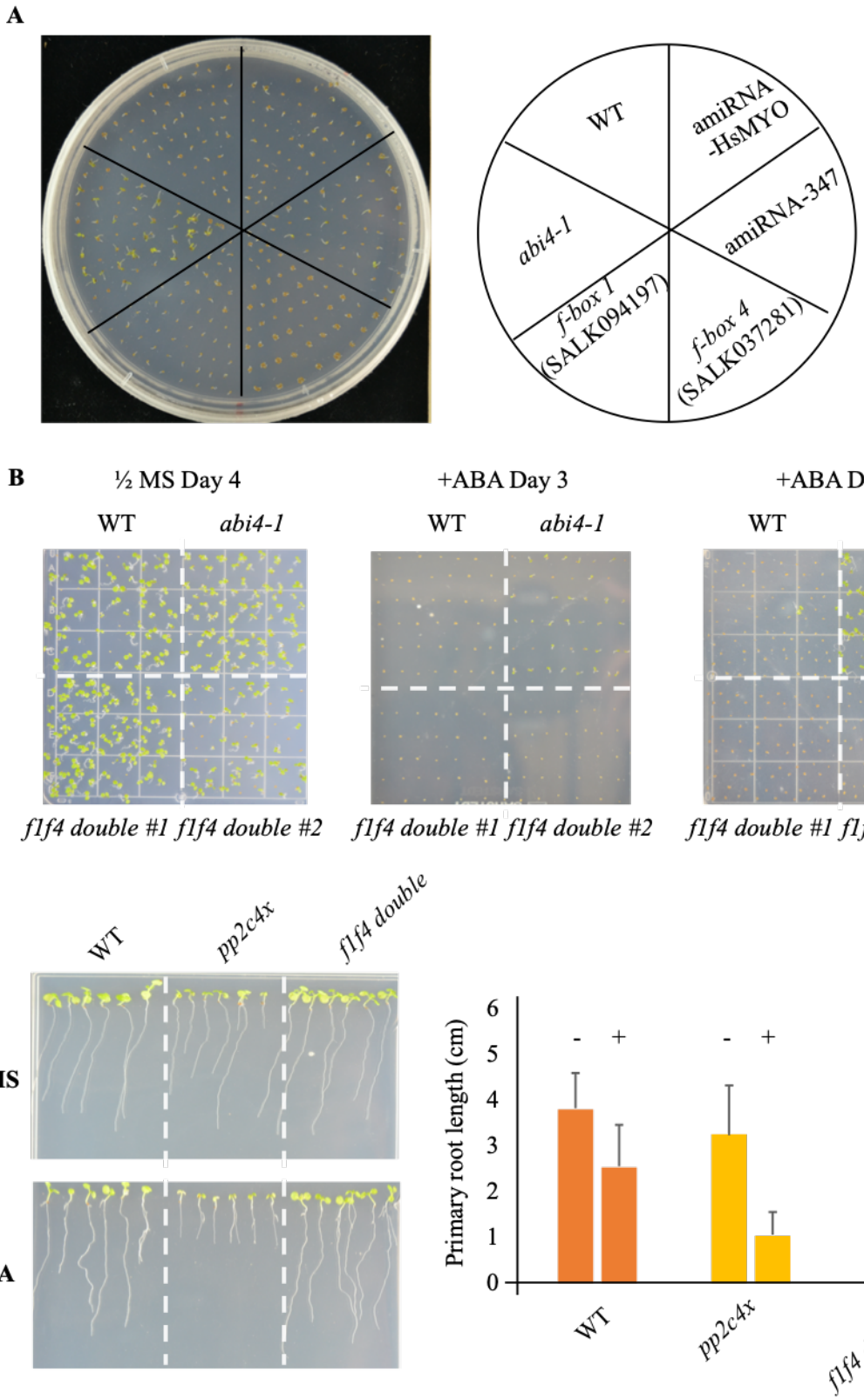
A
WT
amiRNA -HsMYO
abi4-1
amiRNA-347
f-box 1 (SALK094197)
f-box 4 (SALK037281)
B
½ MS Day 4
+ABA Day 3
+ABA Day 8
WT
abi4-1
f1f4 double #1
f1f4 double #2
WT
pp2c4x
f1f4 double
½ MS
ABA
Primary root length (cm)
0
1
2
3
4
5
6
-
+
ABA
WT
pp2c4x
f1f4 double

Figure 2.4 – The F-box decoy lines 1 and 3 are partially insensitive to ABA in germination assay, suggesting that F-box 3 is important for ABA-inhibition of seed germination. (A) Germination assay was performed with three independent lines from each decoy line. WT, the control amiRNA line (*amiRNA-HsMYO* control) and amiRNA-347 lines were used as controls. Cotyledon emergence was evaluated in the presence 1.5 μM ABA. The picture was taken 14 days after exposure to light. (B) Quantification of cotyledon emergence in "A". (C) Western blot on the right was performed using seedlings and detected with anti-FLAG antibody. Ponceau was used to dye the loading control. (D) Germination assay was performed using the amiRNA control line (*amiRNA-HsMYO* control) and 10 independent insertion events of *amiRNA-F-box3* and *f1f4*double /*amiRNA-F-box3* in the presence of 1.5 μM ABA. Data were calculated after seven days of exposure to light.

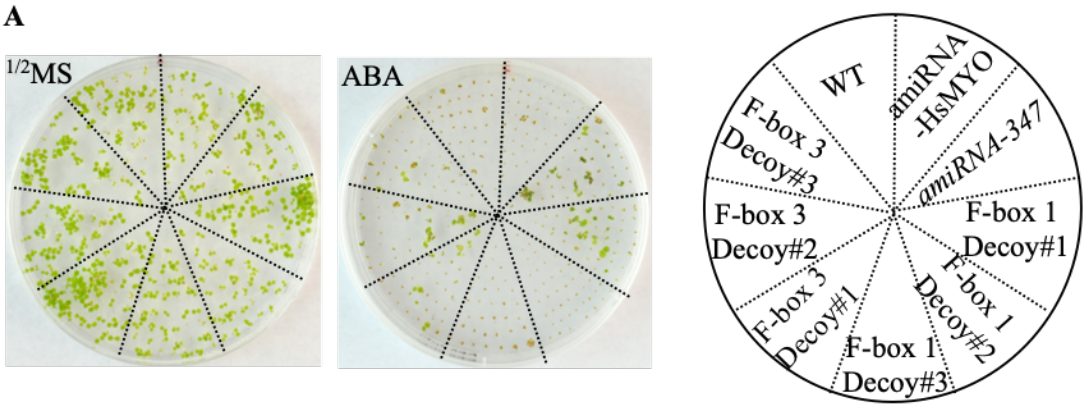
A
1/2MS
ABA
WT
amiRNA -HsMYO
amiRNA4-347
F-box 1 Decoy#1
F-box 1 Decoy#2
F-box 1 Decoy#3
F-box 3 Decoy#1
F-box 3 Decoy#2
F-box 3 Decoy#3

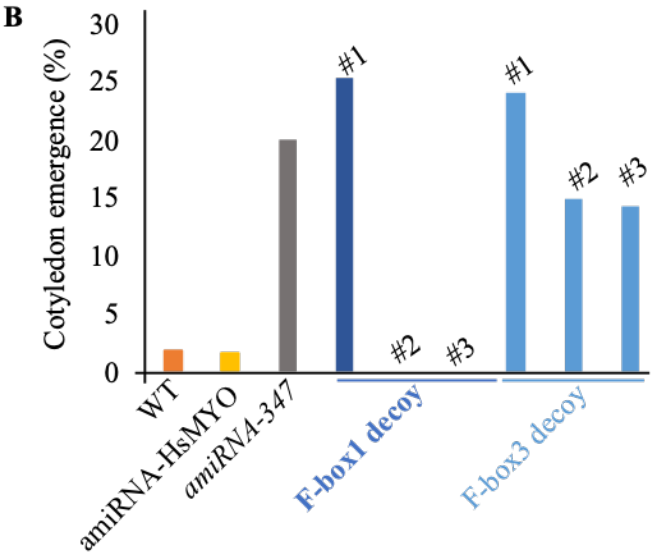
B
Cotyledon emergence (%)
30
25
20
15
10
5
0
#1
#2
#3
#1
#2
#3
WT
amiRNA-HsMYO
amiRNA-347
F-box1 decoy
F-box3 decoy

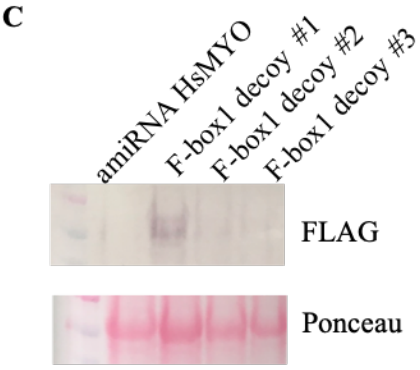
C
amiRNA HsMYO
F-box1 decoy #1
F-box1 decoy #2
F-box1 decoy #3
FLAG
Ponceau

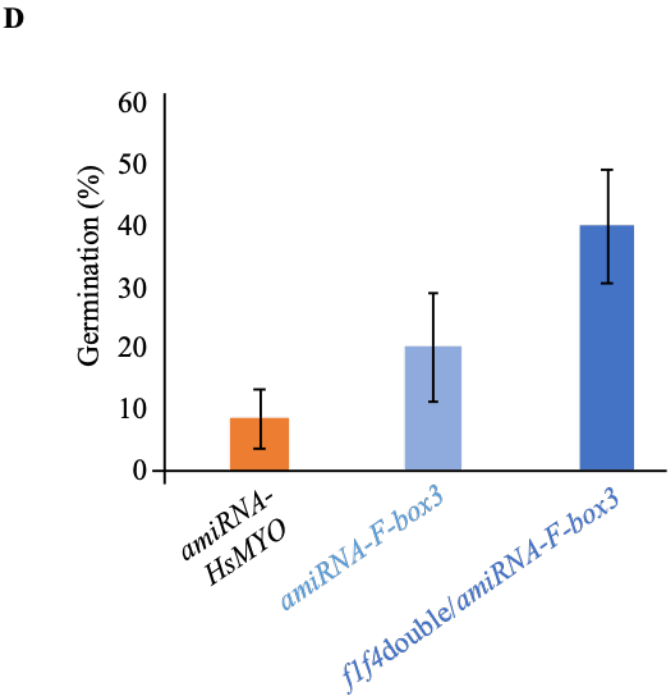
D
Germination (%)
60
50
40
30
20
10
0
amiRNA-HsMYO
amiRNA-F-box3
f1f4double/amiRNA-F-box3

Figure 2.5 – The F-box decoy lines have colder leaf temperate compared to wild-type and F-box 3 decoy lines have delayed ABA-induced stomatal closure. (A) F-box1 and 3 decoy lines were grown side-by-side with WT control plants and images were taken five weeks after transferring the seedlings to pots. (B) Two independent insertion events of F-box1 and 3 decoy lines grown for five weeks were used in infrared thermal imaging analyses of canopy leaf temperature. The bars on the left side show correlation between pseudo-colors and temperature. (C) Time-resolved stomatal conductance to H_2O (g_s) in response to application of 2 μM ABA to the transpiration stream (red arrows) is shown in WT control plants and in the two F-box decoy lines. Stomatal conductance was analyzed using whole leaf gas exchange. (C and E) Stomatal conductance in mol m^{-2} s^{-1}. (D and F) Data from (C and E) were normalized to stomatal conductance at the beginning of the experiment. Data are the mean of *n*=3 leaves per genotype ±SEM.

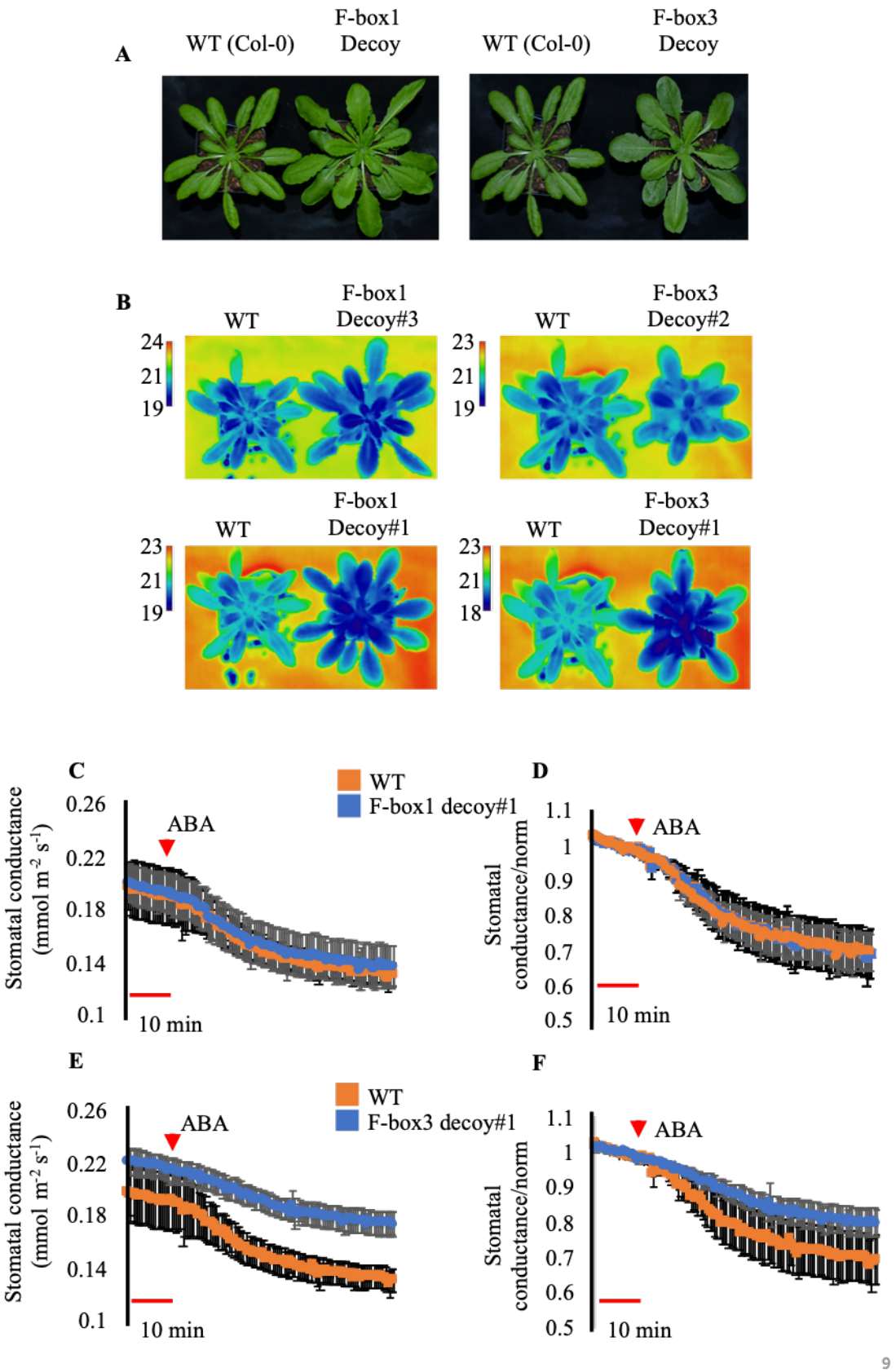
A
WT (Col-0)
F-box1 Decoy
WT (Col-0)
F-box3 Decoy
B
WT
F-box1 Decoy#3
24
21
19
WT
F-box3 Decoy#2
23
21
19
WT
F-box1 Decoy#1
23
21
19
WT
F-box3 Decoy#1
23
21
18
C
WT
F-box1 decoy#1
Stomatal conductance (mmol m-2 s-1)
0.26
0.22
0.18
0.14
0.1
ABA
10 min
D
Stomatal conductance/norm
1.1
1
0.9
0.8
0.7
0.6
0.5
ABA
10 min
E
WT
F-box3 decoy#1
Stomatal conductance (mmol m-2 s-1)
0.26
0.22
0.18
0.14
0.1
ABA
10 min
F
Stomatal conductance/norm
1.1
1
0.9
0.8
0.7
0.6
0.5
ABA
10 min

9

Figure 2.6 – F-box 1 interacts with "clade A" PP2Cs and ERA1 in Y2H assay. (A) GAL4-based yeast two-hybrid assays suggest that F-box 1 interacts with members of the "Clade A" PP2C family in yeast. Yeast colonies were grown on −L−W−H (lacking leucine, tryptophan, and histidine) selective plates with or without ABA (10 μM) for 5 d. (B) F-box 1 interacts with the β-subunit of ERA1 in yeast two-hybrid assays. Yeast colonies were grown on −L−W−H (lacking leucine, tryptophan, and histidine) selective plates with or without ABA (10 μM) for 5 d. AD, activation domain; BD, binding domain. For semi-quantitative analysis, transformed yeast colonies were grown in liquid media and diluted to an OD of 0.4 (presented as 1X). These cultures were than diluted 50X and 200X.

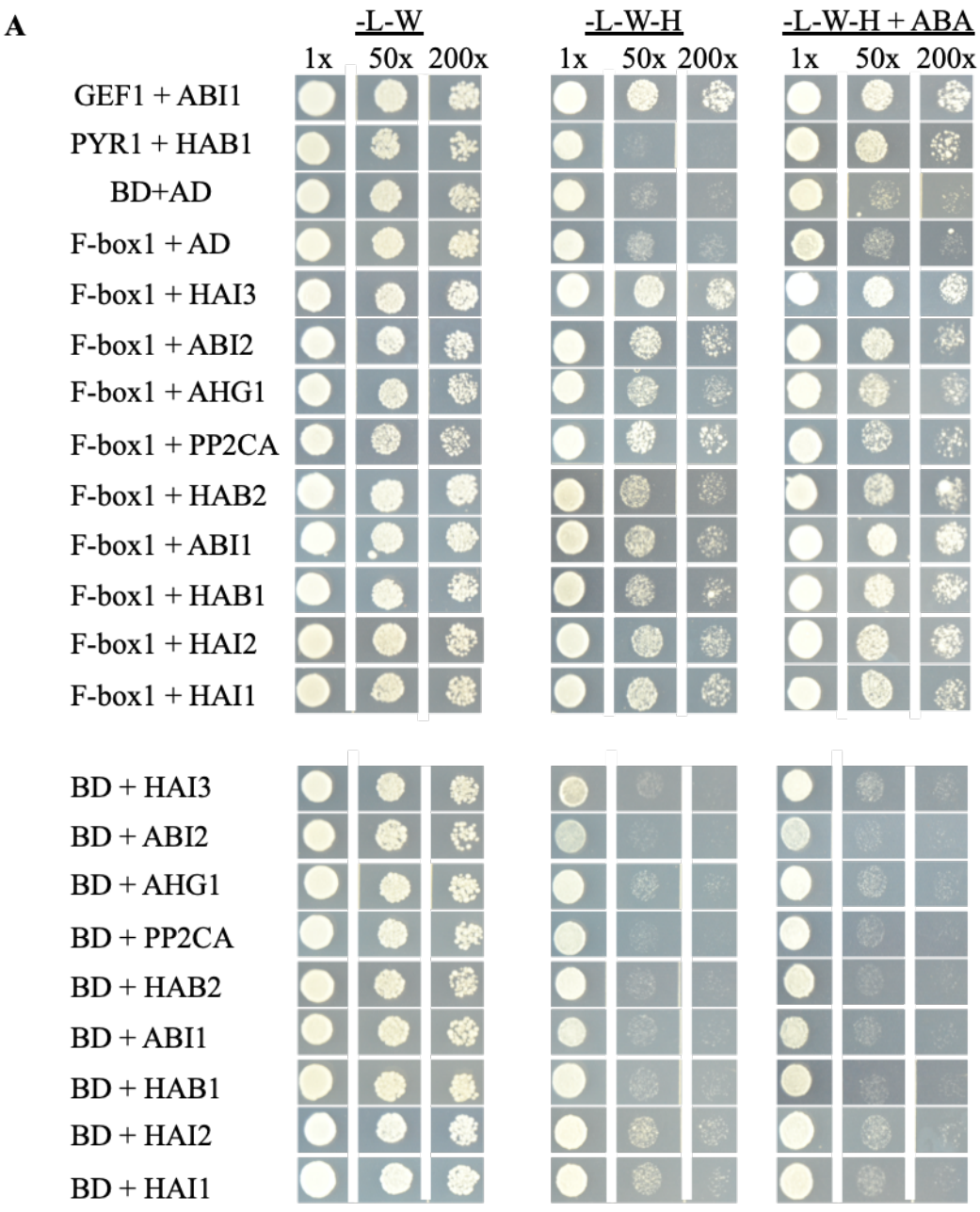
A
-L-W
-L-W-H
-L-W-H + ABA
1x 50x 200x
GEF1 + ABI1
PYR1 + HAB1
BD+AD
F-box1 + AD
F-box1 + HAI3
F-box1 + ABI2
F-box1 + AHG1
F-box1 + PP2CA
F-box1 + HAB2
F-box1 + ABI1
F-box1 + HAB1
F-box1 + HAI2
F-box1 + HAI1
BD + HAI3
BD + ABI2
BD + AHG1
BD + PP2CA
BD + HAB2
BD + ABI1
BD + HAB1
BD + HAI2
BD + HAI1
B
-L-W
-L-W-H
-L-W-H + ABA
1x 50x 200x
F-box1 + ERA1
BD + ERA1

Figure 2.7 – F-box 3 does not interact with "clade A" PP2Cs and ERA1 in Y2H assay. (A) GAL4-based yeast two-hybrid assays suggest that F-box 3 does not strongly interacts with members of the "Clade A" PP2C family in yeast. Yeast colonies were grown on −L−W−H (lacking leucine, tryptophan, and histidine) selective plates with or without ABA (10 μM) for 5 d. (B) F-box 3 does not strongly interacts with the β-subunit of ERA1 in yeast two-hybrid assays. Yeast colonies were grown on −L−W−H (lacking leucine, tryptophan, and histidine) selective plates with or without ABA (10 μM) for 5 d. AD, activation domain; BD, binding domain. For semi-quantitative analysis, transformed yeast colonies were grown in liquid media and diluted to an OD of 0.4 (presented as 1X). These cultures were than diluted 50X and 200X.

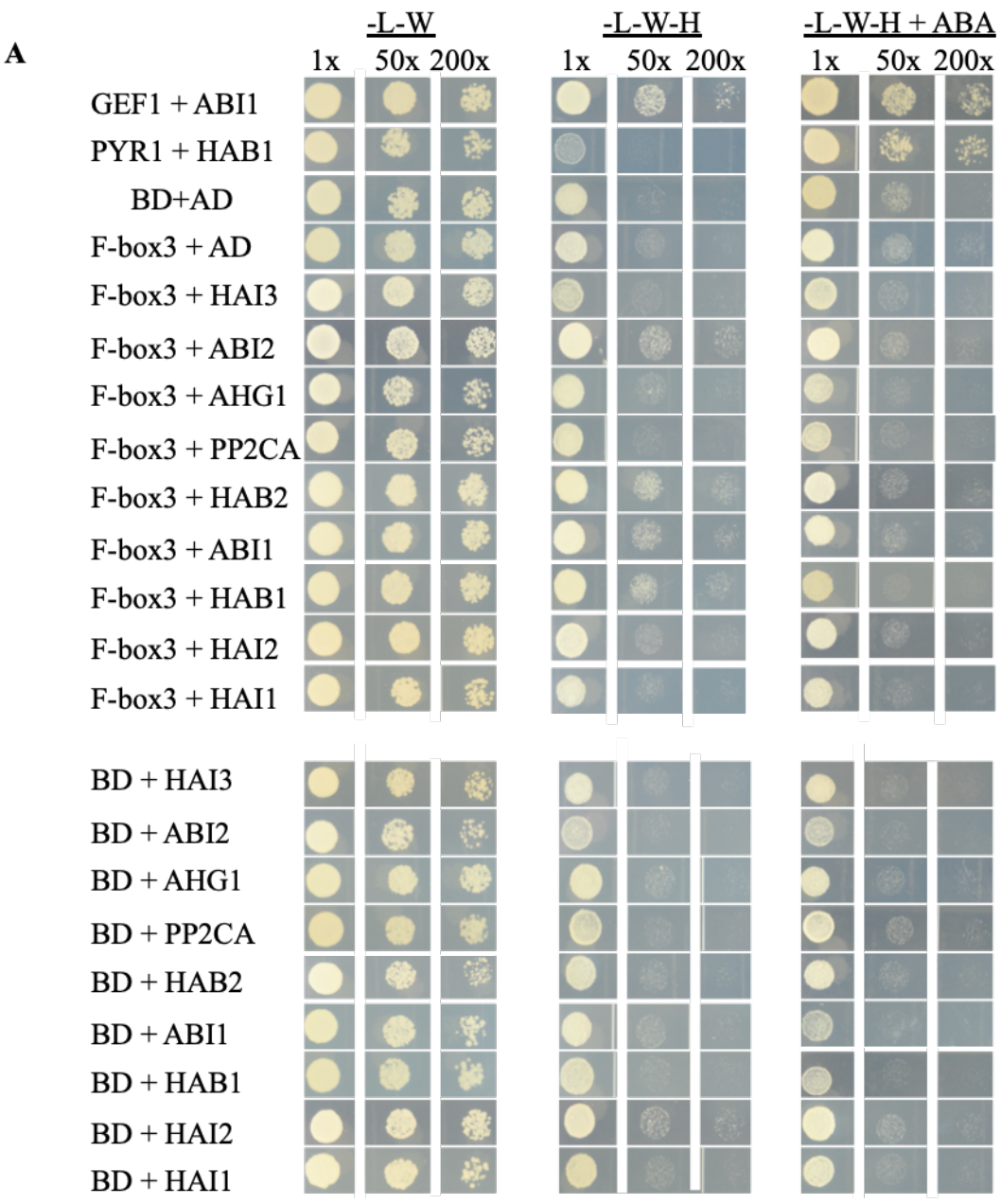
A
-L-W
-L-W-H
-L-W-H + ABA
1x 50x 200x
GEF1 + ABI1
PYR1 + HAB1
BD+AD
F-box3 + AD
F-box3 + HAI3
F-box3 + ABI2
F-box3 + AHG1
F-box3 + PP2CA
F-box3 + HAB2
F-box3 + ABI1
F-box3 + HAB1
F-box3 + HAI2
F-box3 + HAI1
BD + HAI3
BD + ABI2
BD + AHG1
BD + PP2CA
BD + HAB2
BD + ABI1
BD + HAB1
BD + HAI2
BD + HAI1
B
-L-W
-L-W-H
-L-W-H + ABA
1x 50x 200x
F-box3 + ERA1
BD + ERA1

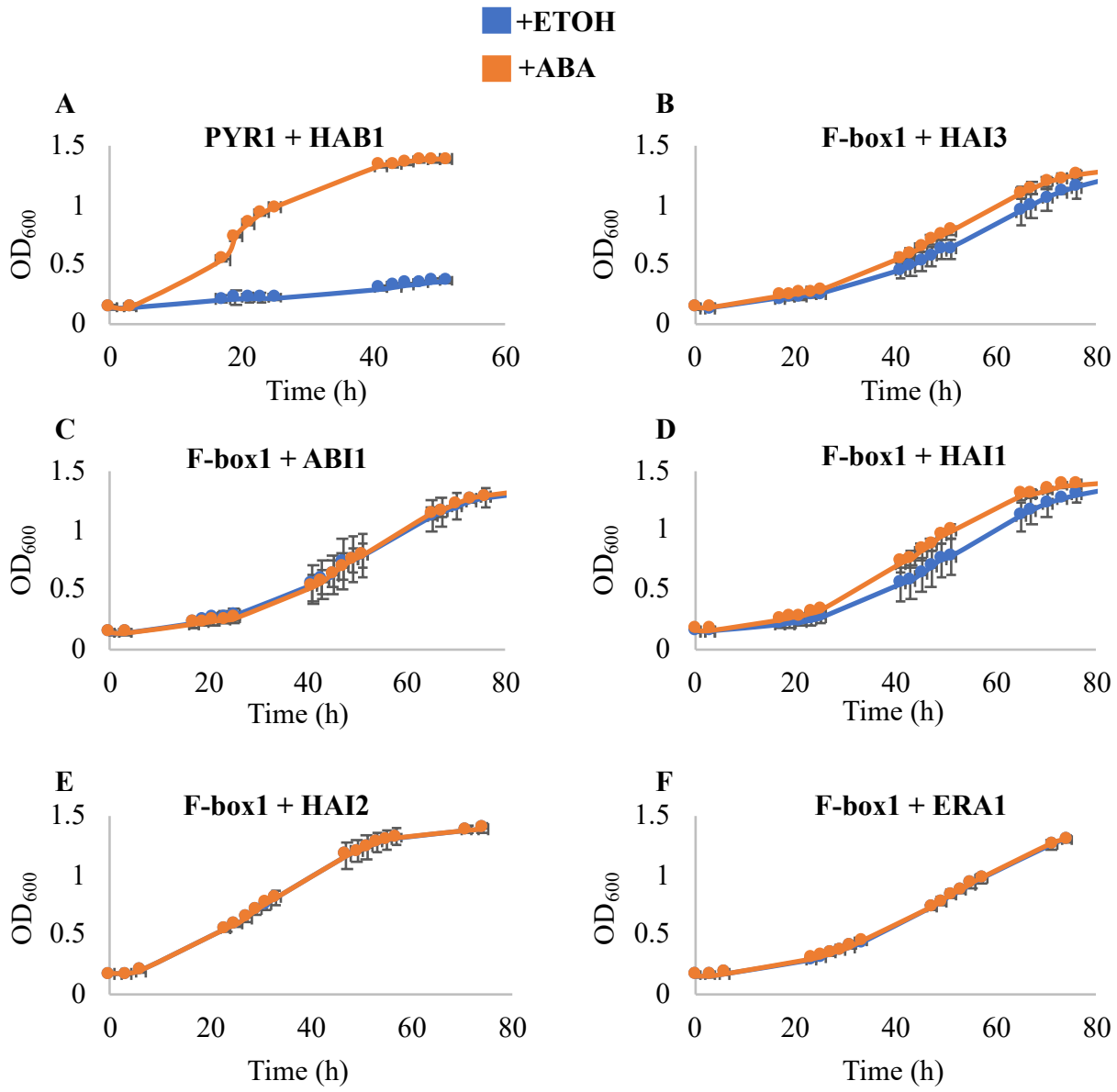

Figure 2.8 – F-box1 interacts with "clade A" PP2Cs and ERA1 in Y2H assay in liquid media. GAL4-based yeast two-hybrid assays show that F-box1 interacts with members of the "Clade A" PP2C family in yeast. Yeast colonies were grown in −L−W (lacking leucine, tryptophan) liquid selective media. After all the tested combinations were diluted to a final concentration of $O.D_{600}$ 0.1, interactions were tested in -L-W-H (lacking leucine, tryptophan, and histidine) with or without ABA (10 µM). (A) PYR1+HAB1 interaction was used as a control. (B) F-box1+HAI3. (C) F-box1+ ABI1. (D) F-box1+ HAI1. (E) F-box1+ HAI2. (F) F-box1+ERA1.

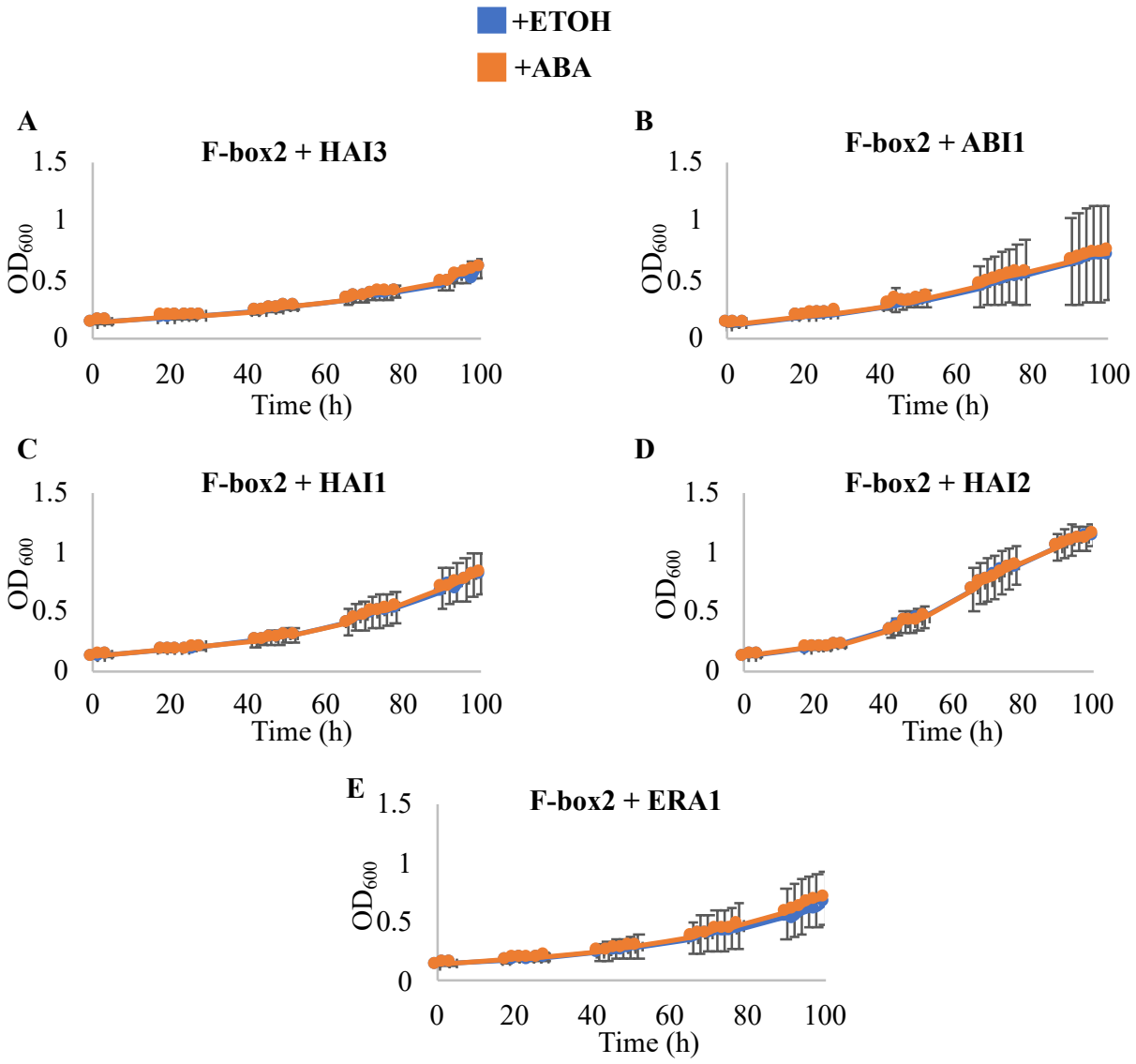

Figure 2.9 – F-box2 interacts with HAI2 in Y2H assay in liquid media. GAL4-based yeast two-hybrid assays show that F-box2 interacts with HAI2 in yeast. Yeast colonies were grown in −L−W (lacking leucine, tryptophan) liquid selective media. After all the tested combinations were diluted to a final concentration of $O.D_{600}$ 0.1, interactions were tested in -L-W-H (lacking leucine, tryptophan, and histidine) with or without ABA (10 µM). (A) F-box2+HAI3. (C) F-box2+ ABI1. (D) F-box2+ HAI1. (E) F-box2+ HAI2. (F) F-box2+ERA1.

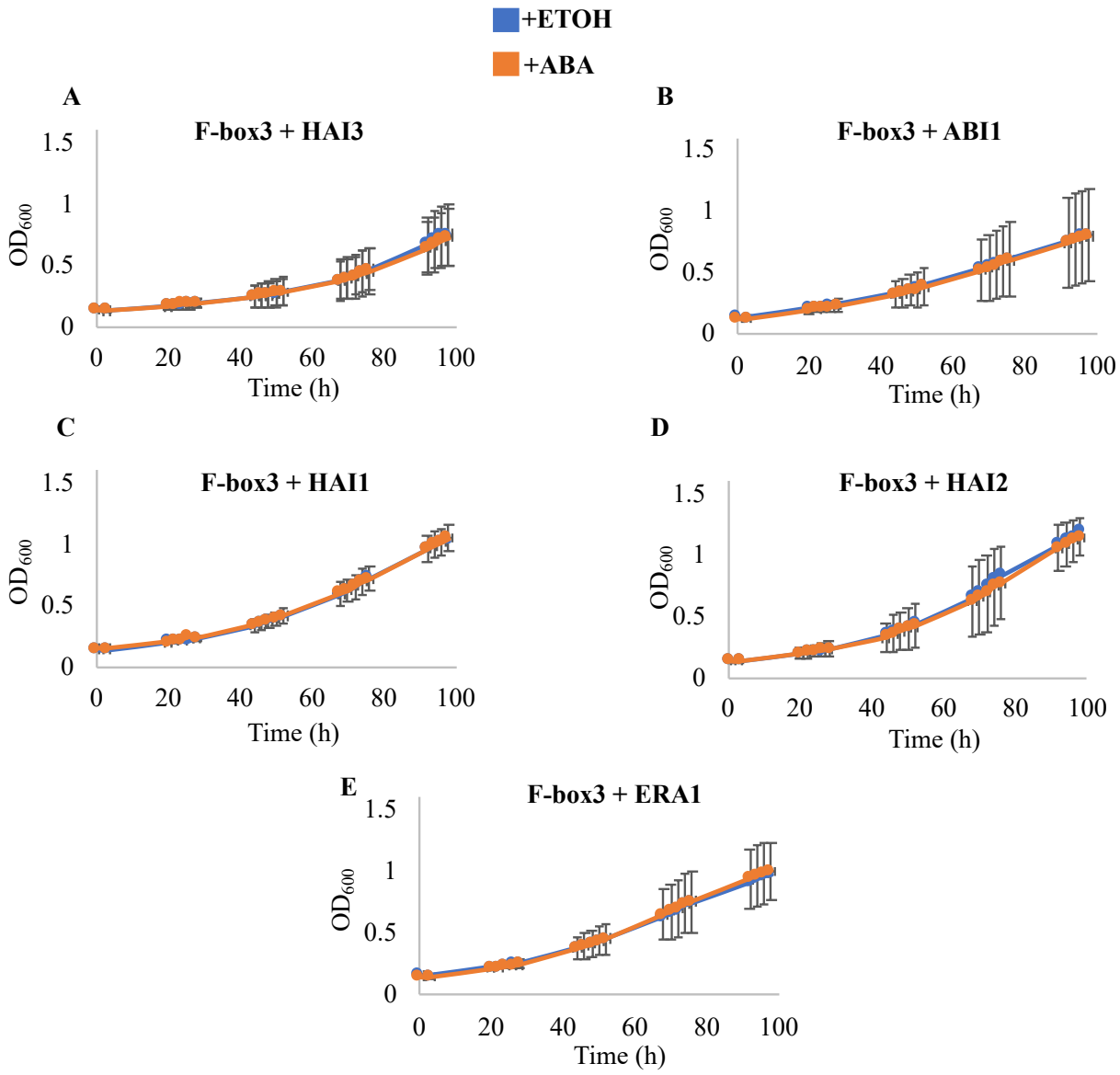

Figure 2.10 – F-box3 interacts with HAI2 in Y2H assay in liquid media. GAL4-based yeast two-hybrid assays show that F-box3 interacts with HAI2 in yeast. Yeast colonies were grown in −L−W (lacking leucine, tryptophan) liquid selective media. After all the tested combinations were diluted to a final concentration of O.D$_{600}$ 0.1, interactions were tested in -L-W-H (lacking leucine, tryptophan, and histidine) with or without ABA (10 µM). (A) F-box3+HAI3. (C) F-box3+ ABI1. (D) F-box3+ HAI1. (E) F-box3+ HAI2. (F) F-box3+ERA1.

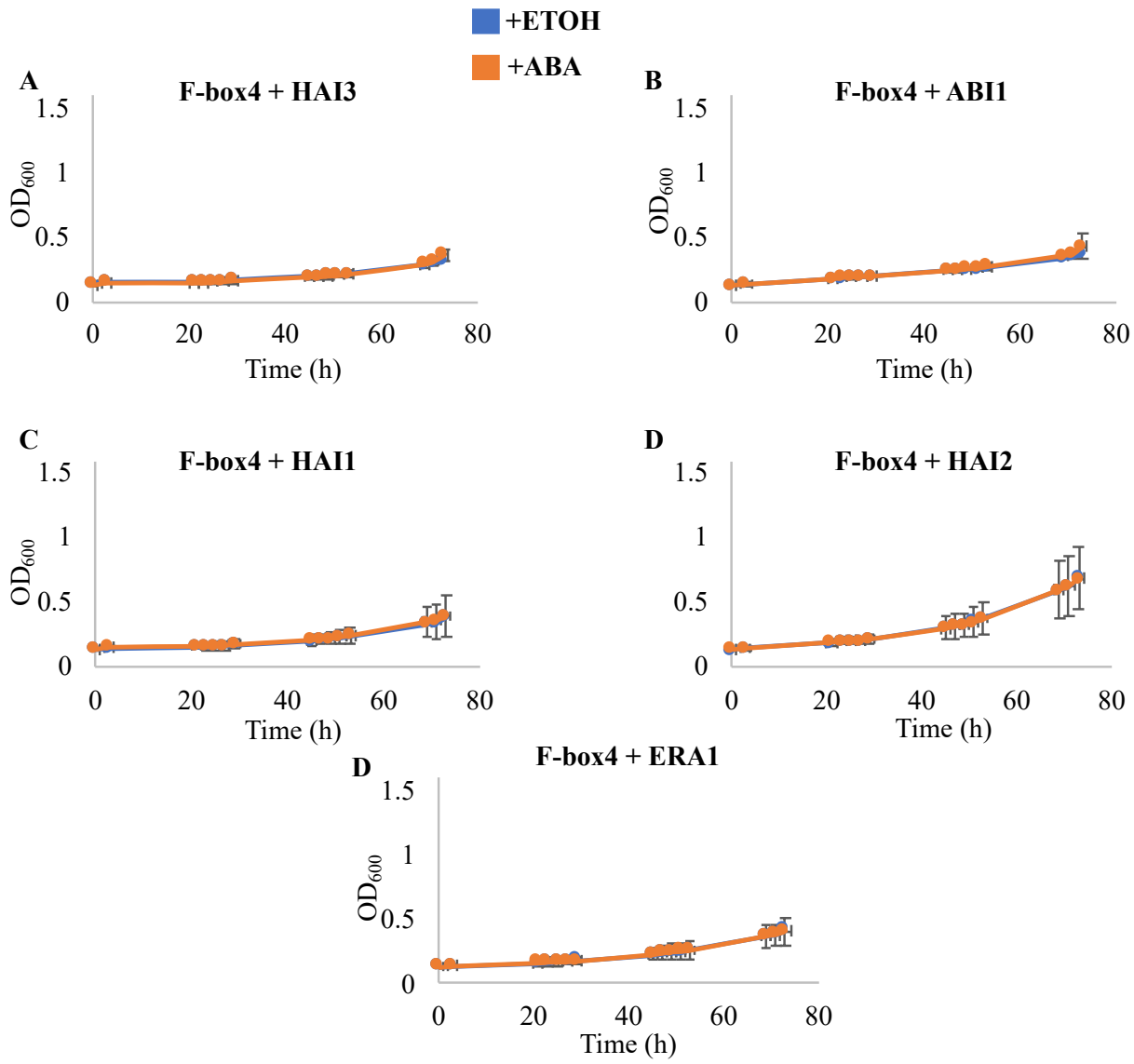

Figure 2.11 – F-box4 does not interact with "clade A" PP2C in Y2H assay in liquid media. GAL4-based yeast two-hybrid assays show no positive interaction between F-box4 and "clade A" PP2Cs in yeast. Yeast colonies were grown in −L−W (lacking leucine, tryptophan) liquid selective media. After all the tested combinations were diluted to a final concentration of $O.D_{600}$ 0.1, interactions were tested in -L-W-H (lacking leucine, tryptophan, and histidine) with or without ABA (10 µM). (A) F-box4+HAI3. (C) F-box4+ ABI1. (D) F-box4+ HAI1. (E) F-box4+ HAI2. (F) F-box4+ERA1.

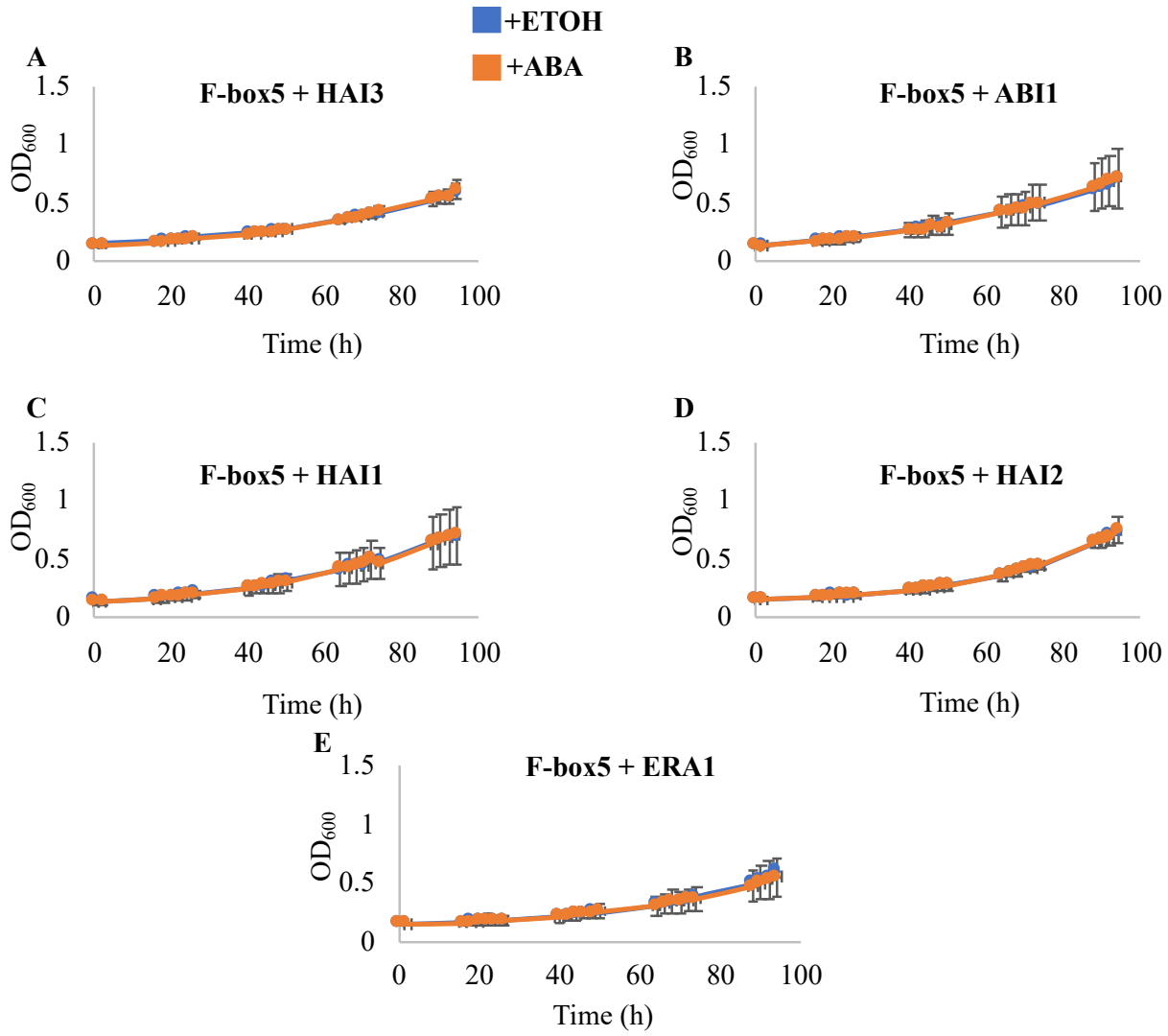

Figure 2.12 – F-box5 does not interact with "clade A" PP2C in Y2H assay in liquid media. GAL4-based yeast two-hybrid assays show no positive interaction between F-box5 and "clade A" PP2Cs in yeast. Yeast colonies were grown in −L−W (lacking leucine, tryptophan) liquid selective media. After all the tested combinations were diluted to a final concentration of $O.D_{600}$ 0.1, interactions were tested in -L-W-H (lacking leucine, tryptophan, and histidine) with or without ABA (10 µM). (A) F-box5+HAI3. (C) F-box5+ ABI1. (D) F-box5+ HAI1. (E) F-box5+ HAI2. (F) F-box5+ERA1.

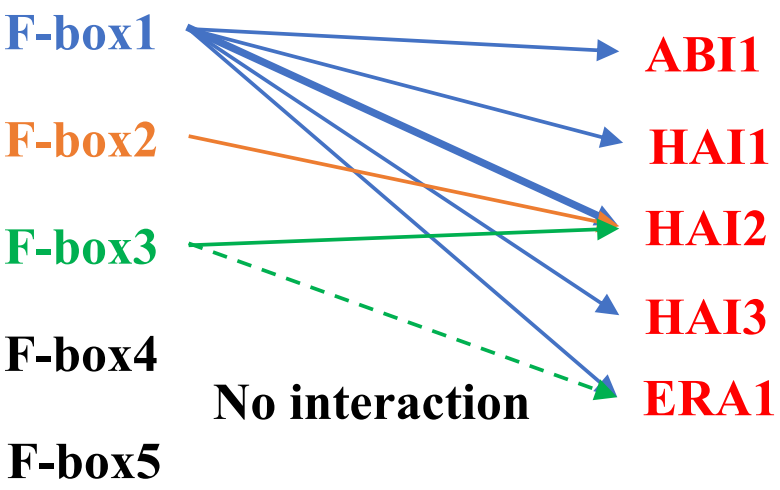

Figure 2.13 - Interactions between F-box proteins and negative regulators of ABA signaling are represented in this network. F-box1, 2 and 3 interact with clade A PP2Cs but not F-box4 and 5. Thicker lines indicate strongest interactions. Dotted lines represent weak interactions.

Figure 2.14 – F-box 1 but not F-box 4 interacts with HAI2 in BiFC. Interactions of F-box 1, F-box 4 or F-box03040 with HAI2, ERA1, APD7 proteins in *N. benthamiana* leaf cells. Confocal images of transiently transformed *N. benthamiana* leaf cells co-expressing either (A) F-box 1-YFP^{N}, (B) F-box 4-YFP^{N} or (C) F-box03040 and the indicated PP2C or ERA1-^{C}YFP protein. Interaction of GEF1-^{N}YFP and ABI1-^{C}YFP was used as control.

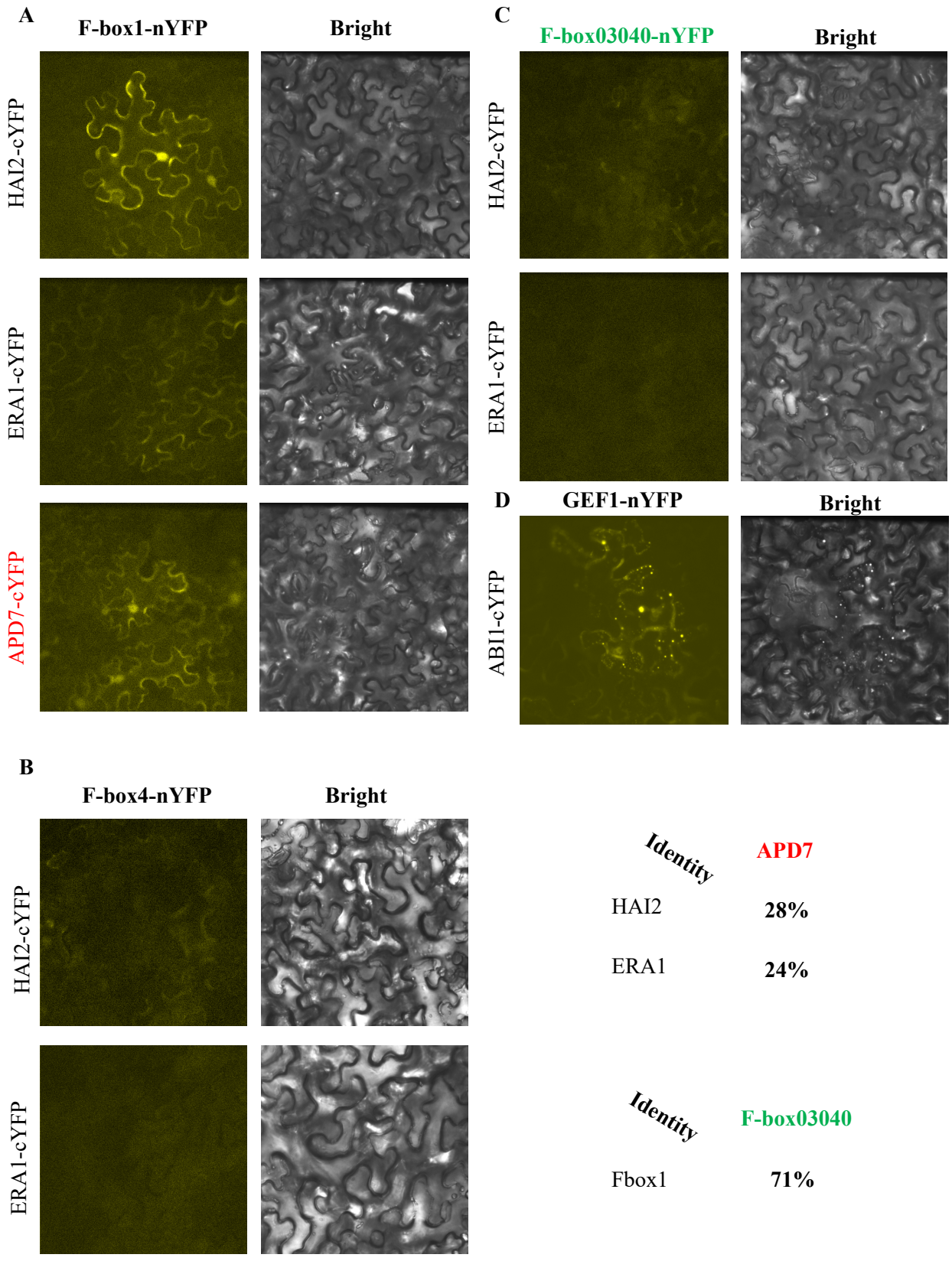
A
F-box1-nYFP
Bright
HAI2-cYFP
ERA1-cYFP
APD7-cYFP
B
F-box4-nYFP
Bright
HAI2-cYFP
ERA1-cYFP
C
F-box03040-nYFP
Bright
HAI2-cYFP
ERA1-cYFP
D
GEF1-nYFP
Bright
ABI1-cYFP
Identity
APD7
HAI2
28%
ERA1
24%
Identity
F-box03040
Fbox1
71%

References

Alonso JM, Stepanova AN, Leisse TJ, Kim CJ, Chen H, Shinn P, Stevenson DK, Zimmerman J, Barajas P, Cheuk R, Gadrinab C, Heller C, Jeske A, Koesema E, Meyers CC, Parker H, Prednis L, Ansari Y, Choy N, Deen H, Geralt M, Hazari N, Hom E, Karnes M, Mulholland C, Ndubaku R, Schmidt I, Guzman P, Aguilar-Henonin L, Schmid M, Weigel D, Carter DE, Marchand T, Risseeuw E, Brogden D, Zeko A, Crosby WL, Berry CC, Ecker JR. 2003. Genome-wide Insertional mutagenesis of Arabidopsis thaliana. Science **301**, 653.

Bhaskara G, Nguyen T, Verslues PE. 2012. Unique Drought Resistance Functions of the Highly ABA-Induced Clade A Protein Phosphatase 2Cs. Plant Physiol **160**, 379 395.

Ceciliato PH, Zhang J, Liu Q, Shen X, Hu H, Liu C, Schäffner AR, Schroeder JI. 2019. Intact leaf gas exchange provides a robust method for measuring the kinetics of stomatal conductance responses to abscisic acid and other small molecules in Arabidopsis and grasses. Plant Methods **15**, 1 10.

Clough SJ, Bent AF. 1998. Floral dip: a simplified method for Agrobacterium -mediated transformation of Arabidopsis thaliana. Plant J **16**, 735 743.

Cutler S, Ghassemian M, Bonetta D, Cooney S, McCourt P. 1996. A Protein Farnesyl Transferase Involved in Abscisic Acid Signal Transduction in Arabidopsis. Science **273**, 1239 1241.

Cutler SR, Rodriguez PL, Finkelstein RR, Abrams SR. 2010. Abscisic Acid: Emergence of a Core Signaling Network. Annual Review of Plant Biology **61**, 651 679.

Czechowski T, Stitt M, Altmann T, Udvardi MK, Scheible W-R. 2005. Genome-wide identification and testing of superior reference genes for transcript normalization in Arabidopsis. Plant Physiology **139**, 5 17.

Edwards K, Johnstone C, Thompson C. 1991. A simple and rapid method for the preparation of plant genomic DNA for PCR analysis. Nucleic acids research **19**, 1349 1349.

Feke A, Liu W, Hong J, Li M-W, Lee C-M, Zhou EK, Gendron JM. 2019. Decoys provide a scalable platform for identification of plant E3 ubiquitin ligases that regulate circadian function. eLife **8**, e44558.

Fuchs S, Grill E, Meskiene I, Schweighofer A. 2013. Type 2C protein phosphatases in plants. The FEBS journal **280**, 681 693.

Gamborg O, Miller R, Ojima K. 1968. Nutrient requirements of suspension cultures of soybean root cells. Experimental cell research **50**, 151 158.

Hauser F, Ceciliato PH, Lin Y-C. 2018. A seed resource for screening functionally redundant

genes and isolation of new mutants impaired in CO2 and ABA responses. Journal of experimental botany **70**.

Hauser F, Chen W, Deinlein U, Chang K, Ossowski S, Fitz J, Hannon G, Schroeder JI. 2013. A genomic-scale artificial microRNA library as a tool to investigate the functionally redundant gene space in Arabidopsis. The Plant Cell **25**, 2848 2863.

Hauser F, Li Z, Waadt R, Schroeder JI. 2017. SnapShot: Abscisic Acid Signaling. Cell **171**, 1708 1708.e0.

Hubbard K, Nishimura N, Hitomi K, Getzoff E, Schroeder J. 2010. Early abscisic acid signal transduction mechanisms. Genes Dev **24**, 1695 1708.

Jalakas P, Huang Y-C, Yeh Y-H, Zimmerli L, Merilo E, Kollist H, Brosché M. 2017. The Role of ENHANCED RESPONSES TO ABA1 (ERA1) in Arabidopsis Stomatal Responses Is Beyond ABA Signaling. Plant Physiol **174**, 665 671.

Julian J, Coego A, Lozano-Juste J. 2019. The MATH-BTB BPM3 and BPM5 subunits of Cullin3-RING E3 ubiquitin ligases target PP2CA and other clade A PP2Cs for degradation. Proc Natl Acad Sci U S A **116**, 201908677.

Kim T, Böhmer M, Hu H, Nishimura N, Schroeder JI. 2010. Guard cell signal transduction network: advances in understanding abscisic acid, CO2, and Ca2+ signaling. Annual Review of Plant Biology **61**, 561 591.

Kim W, Lee Y, Park J, Lee N, Choi G. HONSU, a Protein Phosphatase 2C, Regulates Seed Dormancy by Inhibiting ABA Signaling in Arabidopsis. Plant and Cell Physiol **54**, 555 572.

Koncz C, Schell J. 1986. The promoter of TL-DNA gene 5 controls the tissue-specific expression of chimaeric genes carried by a novel type of Agrobacterium binary vector. Molecular Genetics and Genomics **204**, 383 396.

Kong L, Cheng J, Zhu Y. 2015. Degradation of the ABA co-receptor ABI1 by PUB12/13 U-box E3 ligases. Nature Communications **6**, 8630.

Kucera B, Cohn M, Leubner-Metzger G. 2005. Plant hormone interactions during seed dormancy release and germination. Seed Science Research **15**, 281 307.

Kuhn J, Boisson-Dernier A, Dizon M, Maktabi M, Schroeder J. 2006. The protein phosphatase AtPP2CA negatively regulates abscisic acid signal transduction in Arabidopsis, and effects of abh1 on AtPP2CA mRNA. Plant Physiol. **140**, 127 39. Epub 2005 Dec 16.

Lee C-M, Feke A, Li M-W, Adamchek C, Webb K, Pruneda-Paz J, Bennett EJ, Kay SA, Gendron JM. 2018. Decoys untangle complicated redundancy and reveal targets of circadian clock F-box proteins. Plant Physiol **177**, pp.00331.2018.

Li Z, Waadt R, Schroeder JI. 2016. Release of GTP Exchange Factor Mediated Down-Regulation of Abscisic Acid Signal Transduction through ABA-Induced Rapid Degradation of RopGEFs. PLoS Biol **14**, e1002461.

Lindsey BE, Rivero L, Calhoun CS, Grotewold E, Brkljacic J. 2017. Standardized Method for High-throughput Sterilization of Arabidopsis Seeds. Journal of visualized experiments : JoVE.

Livak K, Schmittgen T. 2001. Analysis of relative gene expression data using real-time quantitative PCR and the 2(T)(-Delta Delta C) method. Methods **25**, 402 408.

Ma Y, Szostkiewicz I, Korte A, Moes D, Yang Y, Christmann A, Grill E. 2009. Regulators of PP2C Phosphatase Activity Function as Abscisic Acid Sensors. Science **324**, 1064 1068.

Murashige T, Skoog F. 1962. A Revised Medium for Rapid Growth and Bio Assays with Tobacco Tissue Cultures. Physiologia Plantarum **15**, 473 497.

Ossowski S, Schwab R, Weigel D. 2008. Gene silencing in plants using artificial microRNAs and other small RNAs. The Plant journal **53**, 674 690.

Palazon B, Julian J, Coego A, Wu Q, Zhang X, Batistic O, Alquraishi SA, Kudla J, An C, Rodriguez PL. ABA inhibits myristoylation and induces shuttling of the RGLG1 E3 ligase to promote nuclear degradation of PP2CA. Plant J **98**.

Park S-Y, Fung P, Nishimura N. 2009. Abscisic acid inhibits type 2C protein phosphatases via the PYR/PYL family of START proteins. Science **324**, 1068 1071.

Pei Z-M, Ghassemian M, Kwak CM, McCourt P, Schroeder JI. 1998. Role of Farnesyltransferase in ABA Regulation of Guard Cell Anion Channels and Plant Water Loss. Science **282**, 287–290.

Schindelin J, Arganda-Carreras I, Frise E. 2012. Fiji: an open-source platform for biological-image analysis. Nature Methods **9**, 676 682.

Schweighofer A, Hirt H, Meskiene I. 2004. Plant PP2C phosphatases: emerging functions in stress signaling. Trends in Plant Science **9**, 236 243.

Shu K, Liu X, Xie Q, He Z. 2016. Two Faces of One Seed: Hormonal Regulation of Dormancy and Germination. Molecular plant-microbe interactions **9**, 34 45.

Waadt R, Schmidt L, Lohse M, Hashimoto K, Bock R, Kudla J. 2008. Multicolor bimolecular fluorescence complementation reveals simultaneous formation of alternative CBL/CIPK complexes in planta. Plant J **56**, 505 516.

Weitbrecht K, Müller K, Leubner-Metzger G. 2011. First off the mark: early seed germination. Journal of Experimental Botany **62**, 3289 3309.

Xiao D, Cui Y, Xu F, Xu X, Gao G, Wang Y, Guo Z, Wang D, Wang N.N. SENESCENCE-SUPPRESSED PROTEIN PHOSPHATASE Directly Interacts with the Cytoplasmic Domain of SENESCENCE-ASSOCIATED RECEPTOR-LIKE KINASE and Negatively Regulates Leaf Senescence in Arabidopsis. Plant Phys **169**, 1275 1291.

Xu G, Ma H, Nei M, Kong H. 2009. Evolution of F-box genes in plants: Different modes of sequence divergence and their relationships with functional diversification. Proc Natl Acad Sci U S A **106**, 835 840.

Chapter 3:

Intact leaf gas exchange provides a robust method for measuring the kinetics of stomatal conductance responses to abscisic acid and other small molecules in Arabidopsis and grasses

Abstract

Background

Guard cells perceive external and internal stimuli and regulate stomatal conductance in plants. With the use of gas exchange analyzers, time-resolved stomatal conductance responses to light intensity, [CO_2] concentration and relative humidity changes can be measured. This is more difficult to achieve when measuring stomatal responses to small soluble molecules such as the plant hormone abscisic acid (ABA) or the bacterial peptide flagellin 22 (flg22), in particular when investigating mutants with response phenotypes.

Results

A method to evaluate the dynamic effects of small molecules on stomatal conductance in a time-resolved fashion using gas exchange analyzers is presented here. ABA-induced stomatal closure was investigated by adding ABA to the transpiration stream of intact leaves placed in a microcentrifuge tube containing water. Strong ABA responses were resolved in time- and in a dose-dependent manner in wild-type Arabidopsis leaves, whereas the same response was not observed in leaves of the ABA-insensitive mutant *open stomata 1-3* (*ost1-3*). Moreover, when leaves of the Plasma membrane Intrinsic Protein (PIP) aquaporin quadruple mutant *pip1;1 pip1;2 pip2;1 pip2;2* were tested, robust wild-type-like responses to ABA were observed. When the bacterial peptide flg22 was added to the transpiration stream of intact wild-type leaves, a strong flg22-induced stomatal closure effect was observed. Finally, the proposed technique was further developed and optimized for evaluation of stomatal conductance responses to small molecules in leaves of grasses using the reference plant *Brachypodium distachyon*.

Conclusions

Due to the variable size of stomata in Arabidopsis and the limited dynamic response of stomata in isolated epidermal strips, evaluation of the effect of small molecules on stomatal physiology has been challenging and has led in some cases to inconsistent results. Moreover, potential signals from the mesophyll are missing when using epidermal peels to evaluate stomatal aperture responses. Here we propose a less invasive technique which allows for time-resolved measurements of stomatal conductance responses to small molecules optimized for both Arabidopsis and Brachypodium distachyon leaves. This work was published in Plant Methods (https://doi.org/10.1186/s13007-019-0423-y).

Introduction

Plants respond to environmental change in order to maximize growth and reproduction. Stomata are specialized pores found on the surface of leaves that can both perceive and respond to external stimuli. Stomata gate CO_2 uptake for photosynthesis and water loss through transpiration. Stomatal movements are ultimately controlled by guard cell turgor changes.

Stomatal movements can be controlled by external stimuli such as light intensity/quality (Assmann, 1993; Kinoshita and Shimazaki, 1999; Kinoshita *et al.*, 2001; Inoue *et al.*, 2008), relative humidity (Bauer *et al.*, 2013; Kollist *et al.*, 2018; Merilo *et al.*, 2018) and CO_2 concentration [CO_2] changes (Young *et al.*, 2006; Engineer *et al.*, 2016). With the use of gas exchange analyzers, these parameters can be tightly controlled, and time-resolved stomatal conductance analyses have become a standard for investigating responses to these signals. On the other hand, small molecules such as the plant hormone abscisic acid (ABA) (Weiner *et al.*, 2010) and the bacterial peptide flagellin 22 (flg22) (Deger *et al.*, 2015) can also affect stomatal movements but quantifying kinetic responses to small molecules is more difficult as these cannot be reliably added to a gas exchange chamber. Leaf epidermal peels can be isolated and treated with these and other molecules and stomatal apertures can be measured (Weyers and Travis, 1981). Although this technique is broadly used, there are limitations that have to be considered, including: (a) the small and variable size of the stomata in species such as Arabidopsis thaliana, (b) the small area of the leaf that is evaluated by using microscopic images, (c) the invasive method of removing the epidermal peels, lacking putative important signals from the mesophyll (Mott *et al.*, 2008; Lawson *et al.*, 2014) and other parameters including mechanical constraints (Kollist *et al.*, 2018; Merilo *et al.*, 2018) and (d) time-resolved measurements of the same individual stomata is labor-intensive.

Here, we propose an optimized method, which allows for time-resolved measurements of stomatal conductance and thus the kinetic response of the ensemble of hundreds of stomata in parallel to small molecules in intact leaves of both Arabidopsis and the grass model *Brachypodium distachyon*. The proposed technique is described here in detail and can provide a potent alternative for measuring the effect of small molecules on both the magnitude and the dynamics of stomatal movement responses.

Materials and Methods

Plant material and growth conditions

Arabidopsis thaliana, accession Columbia-0 (Col-0) and *Brachypodium distachyon* accession Bd21-3 were used as wild type references. *Arabidopsis* seeds were surface sterilized as described elsewhere (Lindsey *et al.*, 2017) and cold-treated for 48 h at 4 °C. Seeds were germinated on half strength Murashige and Skoog (Murashige and Skoog, 1962; Gamborg *et al.*, 1968) basal medium supplemented with Gamborg's vitamins (Sigma-Aldrich), 0.8% Phytoagar (Difco, Franklin Lakes, NJ, USA), 4-Morpholinoethane sulfonic acid (2.6 mM; Sigma-Aldrich) and the pH was adjusted to 5.8. Seedlings were transferred from plates to pots containing sterilized premixed soil (Sunshine Professional Blend LC1 RS; Sunshine) after 7–10 days and grown under the following conditions: 12 h light/12 h dark, 21 °C, 85–90% humidity and 90–110 μmol m^{-2} s^{-1} light. Growth of plants at this relatively high humidity was found to be helpful for investigating stimulus-induced stomatal closing in the present study.

In order to promote the growth of the leaves and the development of long and thick petioles, seedlings were kept under a transparent tray dome (7'' height, vented humidity dome) for 2 weeks and fertilized (technigro® sunshine fertilizer, 0.66 g $L^{-1}$of water) twice before the beginning of the experiments: first, after seedlings were transferred to pots, and second, after removing the humidity domes. Plants were ready for experiments 5–6 weeks after being transferred to pots. The *pip* quadruple mutant *pip1;1 pip1;2 pip2;1 pip2;2* was generated by crossing *pip1;1* (GK_437B11), *pip1;2* (SALK_019794), *pip2;1* (SM_3_35928), *pip2;2* (SAIL_169A03) single mutants.

For *Brachypodium*, seeds were cold-treated for 4–5 days at 4 °C, transferred to pots containing premixed soil (Sunshine Professional Blend LC1 RS; Sunshine) and kept under a tray

dome for 2 weeks. Plants were fertilized once a week (technigro®sunshine fertilizer, 0.66 g L^{-1} of water) and kept at the following conditions: long day (16 h light/8 h dark); 23–25 °C; 20–50% humidity, 150–250 µmol m^{-2} s^{-1} light. Plants were used 6–7 weeks after being transferred to pots.

Leaf preparation and gas exchange

For intact leaf gas exchange analyses using *Arabidopsis* leaves, petioles are first cut using a new razor blade and the cut surface of the petioles was immediately transferred to a petri dish filled and submerged in milli-Q water (Fig. 1aI). Petioles are cut a second time under water using a razor blade. The second cut under water is a crucial step of the proposed technique and can be difficult to make. For the second cut it is recommended: (a) approximately one-third of the petiole should be cut but no more. Longer petioles are better for the following steps; (b) the razor blade should be positioned perpendicular to the petiole and at an oblique angle; (c) the cut should be made by gently moving the razor blade back and forth and not by pressing the blade against the petiole and (d) a microcentrifuge tube filled with milli-Q water and closed with plastic paraffin film (Parafilm M) should be prepared in advance. After the parafilm is placed on the tube, two holes are made using fine tweezers, one for the petiole and the second for adding the treatment to the water. After the second cut is made the petiole, with a droplet of water on its cut end, is immediately transferred to the microcentrifuge tube filled with milli-Q water (Fig. 1a, II). The droplet on the end of the petiole is essential to avoid xylem embolism. Leaves are placed inside the gas exchange chamber (Fig. 1a, III) and equilibrated for 45–90 min to reach a stable stomatal conductance before the beginning of the experiments. Experiments were started at least 1 h after growth chamber light onset.

For intact leaf gas exchange in *Brachypodium*, the petioles are first cut 1.5–2.0 cm below the junction between two leaves using a razor blade and immediately placed in a petri dish filled with milli-Q water (Fig. 1b, I). The second cut is made under water using a razor blade positioned perpendicular to the petiole and in an oblique angle and the petiole is transferred to a microcentrifuge tube filled with milli-Q water and closed with parafilm. A second pair of leaves is prepared as described above and added together to the first pair in the same hole in the microcentrifuge tube (Fig. 1b, II). The leaves are taped together using surgical tape (micropore 3 M), leaving the middle area of the leaves free for placement into the gas exchange chamber (Fig. 1b, III), where they equilibrate for 2 h before the beginning of the experiments.

Stomatal conductance to water (gsw) was measured using a portable gas exchange system (LI6400 and LI-6800, LI-COR, Lincoln, Nebraska) with the following conditions: the LED light source was set at 150 μmol m^{-2} s^{-1} (10% blue light), gas exchange temperature was 21 °C, relative humidity in the chamber was kept between 74 and 78% as high relative humidity is very important in these experiments for analyzing petiole-fed small molecules-induced stomatal closing. Airflow was set to 200 revolutions per minute (rpm) and the CO_2 concentration at 400 ppm. After allowing the stomatal conductance to settle at a steady state level, steady-state stomatal conductance was recorded for 10 min prior to the addition of the treatment at the indicated concentrations. The data represent $N \geq 3$ leaves per genotype per treatment.

RT-PCR analysis of pip mutants

Total RNAs from 4-week-old plants were extracted using the TRIzol Reagent (Invitrogen, Carls-bad, CA, USA) or the innuPREP Plant RNA kit (Analytik Jena, Jena, Germany) and reverse transcribed using the M-MLV reverse transcriptase (Promega or Qiagen, Hilden, Germany)

according to the manufacturer's instructions. The presence of functional transcripts was assessed by RT-PCR using primer pairs flanking the insertion site of each mutant (**PIP1;1F**-CAGAGCTTTACAATTTCTCTCTACA, **PIP1;1R**-CACAGTGTTAGCTCCTCCTCCT; **PIP1;2F**- CTGGTTTCTCCGATCTAACGA, **PIP1;2R**-GCATTTTGATCCGATGTTACAA; **PIP2;1F**- AACATATAACGTTGGCAAAAA, **PIP2;1R**-TGGTTAAGACAGGGTTAGTCA; **PIP2;2F**-AAGTTATAGAAATGGCCAAAGAC, **PIP2;2R**- CTCAAACGTTGGCTGCACTTCTG). Expression levels of the housekeeping gene *TUB9* was used as control for cDNA synthesis (**TUB9F-** GTACCTTGAAGCTTGCTAATCCTA, **TUB9R-**GTTCTGGACGTTCATCATCTGTTC).

Stomatal aperture measurements

Three-week-old *Arabidopsis* plants were grown in a growth chamber at 21 °C at 70% humidity, 16 h light/8 h dark regime with a white light intensity 80 µmol m^{-2} s^{-1}. Leaf epidermal layers were pre-incubated in opening buffer (10 mM MES, 10 mM KCl and 10 mM $CaCl_2$ at pH 6.15) for 2 h in a growth chamber with a light intensity of 150 µmol m^{-2} s^{-1} at 21 °C and then incubated with buffers supplemented with 10 µM ABA for 1 h. Stomata were tracked, and apertures were measured using ImageJ. Stomatal assays were conducted as genotype-blinded.

Results

Intact leaf gas exchange enables time-resolved evaluation of ABA effects on stomatal movements

To monitor abscisic acid (ABA) responses in intact leaves, five-week-old leaves from wildtype (Col-0) plants were excised and the petioles were immediately submerged into water. Then, their petioles were cut a second time under water and placed in a microcentrifuge tube with the petiole tips submerged in water. Leaves were clamped in a gas exchange chamber for time-resolved measurements of stomatal conductance (Fig. 1a). Leaves were equilibrated for 70 min inside the gas exchange chamber, before the addition of mock treatment or abscisic acid (ABA). ABA was applied to the water in the microcentrifuge tube in three final concentrations: 0.1, 0.5 and 1.0 μM. For all three concentrations tested, a decrease in stomatal conductance was observed within 5–10 min of ABA addition (Fig. 2a, b). The slope of the stomatal conductance change (from 8 to 15 min after the addition of ABA) was calculated for all treatments and compared to mock treatments. All three ABA concentrations tested showed significant changes in the negative slope of the stomatal conductance when compared to the ethanol mock treatment (Slope of mock treatments: average = 0.0002 mol m^{-2} s^{-1} min^{-1} ± 0.001, slope of 0.1 μM ABA treatment: average = − 0.0005 mol m^{-2} s^{-1} min^{-1} ± 0.0001, slope of 0.5 μM ABA treatment: average = − 0.0016 mol m^{-2} s^{-1} min^{-1} ± 0.0004 and slope of 1.0 μM ABA treatment: average = − 0.0020 mol m^{-2} s^{-1} min^{-1} ± 0.0008. One-Way ANOVA, p value ≤ 0.05). Moreover, a more rapid decrease in stomatal conductance was consistently observed for 0.5 and 1.0 μM of ABA when compared to the 0.1 μM ABA treatment. Note that steady-state stomatal conductance values for the mock treatment in Fig. 2 are slightly higher than the values observed in ABA-treated leaves.

This variation in steady-state stomatal conductance is often observed between plants grown at separate batches as done here (mock) (Azoulay-Shemer *et al.*, 2016).

To test whether steady-state stomatal conductance levels were comparable between intact and cut leaves, the same three independent leaves from three plants were evaluated before and after cutting their petioles. Leaves were first equilibrated inside the gas exchange chamber for 70 min and stomatal conductance was recorded for 10 min in intact plants. The same leaves were then cut as described above and inserted into the gas exchange chamber to again equilibrate for 70 min. Steady-state stomatal conductance of cut leaves was recorded for 10 min after equilibration in the gas exchange chamber and were very similar to steady-state stomatal conductance values of intact leaves (Fig. 3).

The protein kinase "OPEN STOMATA1" (OST1) is a key component of ABA signal transduction in guard cells and the *ost1-3* mutant is strongly impaired in ABA-induced stomatal closure (Mustilli, 2002; Yoshida *et al.*, 2002). To measure ABA responses in intact leaves of the *ost1-3* mutant, ABA was added to the microcentrifuge tubes containing WT (Col-0) or *ost1-3* leaves at a final concentration of 2 μM. Stomatal conductance in *ost1-3* leaves was not strongly affected by the addition of ABA, whereas the same treatment in parallel-grown WT (Col-0) leaves strongly reduced stomatal conductance (Fig. 4a). The steady-state stomatal conductance of *ost1-3* mutants before the treatment with ABA was higher than the steady-state stomatal conductance in WT under the imposed conditions from parallel grown plants (Fig. 4a). To better compare and visualize the effect of ABA on stomatal conductance, the data were normalized to the average stomatal conductance values during the first 10 min, before the addition of ABA (Fig. 4b).

Together, these data suggest that the measurable decrease in stomatal conductance by the addition of ABA to the transpiration stream of intact leaves is mediated by ABA and this protocol

enables analyses of the time-resolved ensemble average of hundreds of stomatal apertures in intact leaves in each experiment.

Aquaporin *pip1;1 pip1;2 pip2;1 pip2;2* quadruple mutant leaves show a WT-like response to ABA in intact leaves

Aquaporins are physiologically relevant water channels that facilitate the passage of water across cell membranes. As guard cells use cell turgor to regulate and fine-tune stomatal apertures, guard cell-expressed aquaporins play an important role in this process by facilitating water diffusion (Uehlein *et al.*, 2003; Kaldenhoff *et al.*, 2008; Maurel *et al.*, 2008; Chaumont and Tyerman, 2014; Heinen *et al.*, 2014). However, the large gene family of the plasma membrane intrinsic protein (PIP) aquaporins (Quigley *et al.*, 2002) have rendered it difficult to investigate the role of plasma membrane aquaporins in ABA-induced stomatal closing. Moreover, whether single mutant alleles in the *pip2;1*gene impair ABA-induced stomatal closing remains a matter of debate (Grondin *et al.*, 2015; Wang *et al.*, 2016).

We therefore generated a *pip* quadruple mutant (*pip1;1 pip1;2 pip2;1 pip2;2*) using the same *pip2;1-2* mutant allele used in previous research (Grondin *et al.*, 2015; Wang *et al.*, 2016) to test whether higher order *pip* mutant leaves have impaired responses to ABA in intact leaves. RT-PCR analyses did not detect transcripts of *PIP1;2, PIP2;1* and *PIP 2;2*, whereas the detection of *PIP1;1* was substantially lower in the single mutants used to generate the quadruple mutant, when compared to WT (Fig. 5a). In stomatal aperture measurements using isolated epidermal strips, little difference was noted in response to ABA (10 μM) between *pip* quadruple mutant and WT leaves (One-Way ANOVA, p value > 0.05) (Fig. 5b). However, the stomatal response in stomatal aperture experiments was quite small. In intact leaf gas exchange analyses, the steady-

state stomatal conductance of *pip* quadruple mutant leaves was similar to WT leaves under the imposed conditions (Fig. 5c). When ABA (2 μM) was applied to the transpiration stream of intact *pip* quadruple mutant leaves, a WT-like decrease in stomatal conductance was observed (Fig. 5c, d). Our results show that intact quadruple mutant leaves of these *pip* aquaporins are highly responsive to ABA treatments in stomatal conductance and indistinguishable from the wild type response in intact leaves both in terms of the time-dependent kinetics of the response and the magnitude of the ABA response.

The defense elicitor peptide flagellin 22 leads to a rapid decrease in stomatal conductance when applied to the transpiration stream of *Arabidopsis* leaves

Microbe-associated molecular patterns (MAMPs) are molecules recognized by plants during pathogen infection that trigger several defense-related responses, which includes stomatal closure. The bacterial peptide flagellin 22 (flg22) is recognized by the FLAGELLIN SENSITIVE2 (FLS2) receptor kinase (Gómez-Gómez and Boller, 2000) and has been reported to lead to a stomatal closure response (Melotto *et al.*, 2006), when nano-infused in *Arabidopsis* leaves(Deger *et al.*, 2015).

To test whether the flg22 peptide could affect stomatal conductance in intact leaves, we applied 10 μM flg22 or mock treatment to the transpiration stream of *Arabidopsis* WT (Col-0) leaves. Flg22 peptide treatments clearly decreased stomatal conductance of intact leaves within 20 min, compared to mock treatment controls (Fig. 6). Our data confirm that the flg22 peptide is a strong regulator of stomatal closure and can be effective when applied to the leaf transpiration stream. These data suggest that the present method is suitable for evaluating the kinetic response of diverse molecules on stomatal conductance regulation in intact leaves.

Optimization of intact leaf gas exchange in grasses using *Brachypodium distachyon*

Understanding the dynamics of stomatal movements in response to defined stimuli is relevant in many plant species, including in the grasses that have unique dumbbell-shaped stomata (McKown and Bergmann, 2018). Although research on the reference plant, *Arabidopsis thaliana*, is crucial for developing knowledge of stomatal response mechanisms in dicotyledon plants, research is necessary to further our knowledge on stomatal responses in grasses. Recently, in the emerging model organism *Brachypodium distachyon* (Raissig *et al.*, 2016), it was observed that stomatal subsidiary cells play a key role in enhancing stomatal responsiveness (Raissig *et al.*, 2017), which can be best observed in time-resolved experiments.

In order to measure ABA-dependent stomatal closing in *Brachypodium* leaves, our protocol was adapted and optimized (Fig. 1b). ABA or mock ethanol treatment were added to the microfuge tube and stomatal conductance was recorded. Approximately 5 min after the addition of ABA, a rapid decrease in stomatal conductance was observed and a new plateau was rapidly reached within 15 min (Fig. 7). Our results suggest that this method for time-resolved kinetic evaluation of small molecules effects on stomatal conductance in intact leaves can be applied to different species with distinct leaf sizes and morphologies.

Discussion

Stomatal responses to external and internal stimuli are important for plant survival and quantifying these responses can be difficult. With the use of gas exchange analyzers, responses to a diverse range of stimuli, from light quality and light intensity to [CO_2] concentration changes, can be automatically controlled and stomatal conductance responses can be measured in time. On the other hand, small molecules such as the plant hormone ABA and the bacterial peptide flg22 have major impact on stomatal physiology (Kim *et al.*, 2010; Deger *et al.*, 2015). However, to date there has been only limited use of automated techniques to robustly measure these responses. Here we provide detailed information for a simple method in which leaf petioles are placed inside a centrifuge tube containing water and leaves are clamped into a gas exchange chamber (Fig. 1) for evaluation of stomatal conductance responses to small soluble molecules. With this technique, stomatal responses to ABA were measured in time and showed dose-dependency (Fig. 2a, b). The steady-state stomatal conductance of leaves was measured before and after the cuts of the petiole and showed similar values (Fig. 3), suggesting that the cut of the petioles pose little effect on stomatal conductance when following the described protocol. In addition, the petioles could be submerged in water for the first cut to avoid any xylem embolism and to possibly facilitate steady-state stomatal conductance recovery. ABA-dependent decrease in stomatal conductance was not observed when leaves from the *ost1-3* mutant were treated with ABA (Fig. 4).

To evaluate the contribution of four abundant plasma membrane aquaporins, we tested a *pip* (*pip1;1 pip1;2 pip2;1 pip2;2*) quadruple mutant's response to ABA in both epidermal peels and intact leaves. The expression of all four *PIP* genes affected in our mutants were evaluated using RT-PCR. This analysis confirmed the loss-of-function mutation of *PIP1;2*, *PIP2;1* and *PIP2;2*, while a low expression of the *PIP1;1* gene could still be detected

in the *pip1;1* mutant, probably through a partially correct splicing of the T-DNA insertion within an intron allele (Fig. 5a). While stomatal aperture data indicate a possible, but non-significant, reduction in ABA-responsiveness (Fig. 5b), in intact leaf gas exchange experiments the *pip* quadruple mutant leaves show WT-like responses to ABA (Fig. 5c, d). The present data suggest that time-resolved measurements are more adequate for comparing genotypes due to the large dynamic range of the intact leaf response. These findings lie in contrast to a study that suggested dramatic impairment in ABA-induced stomatal closing in leaf epidermal peels of the same single *pip2;1* mutant allele (Grondin *et al.*, 2015). In contrast, another study showed intact ABA responses in the single *pip2;1* mutant (Wang *et al.*, 2016), consistent with the present study. These data point to the hypothesis that even higher order *pip* mutants would be required to observe any noticeable phenotype in the ABA response when studying PIP contribution in a whole leaf context.

The bacterial peptide flg22 was reported to reproducibly induce stomatal closure in a SLAC1-dependent manner when flg22 was nano-infused in stomata (Deger *et al.*, 2015). Although this elegant technique clearly confirmed the effect of flg22 on stomatal closure, the effect of this peptide had not yet been investigated in stomatal conductance of intact leaves. When applied to the transpiration stream of intact leaves, flg22 peptide rapidly induced a decrease in stomatal conductance (Fig. 6). These data suggest that small peptides can travel through the xylem of leaves and reach guard cells, regulating stomatal aperture and gas exchange in intact leaves.

Similar techniques have been recently used to measure ABA-dependent stomatal closure in *Arabidopsis* (Park *et al.*; Batool *et al.*, 2018; Hauser *et al.*, 2018; Zhang *et al.*, 2018) and also in several other plant species such as *Phoenix dactylifera* (Müller *et al.*, 2017) , *Vicia faba* (Felle *et al.*, 2000), tomato (*Solanum lycopersicum*) (Wilkinson and Davies, 2008) and barley (*Hordeum*

vulgare) (Schäfer *et al.*, 2018). In the present study we provide a detailed protocol for robust small molecule response analyses. In the case of grasses, the stomata are surrounded by subsidiary cells which respond to external and internal stimuli with changes in turgor pressure that are inverted with respect to the guard cell response. Furthermore, the subsidiary cells have been shown to maximize stomatal responses (Raissig *et al.*, 2017). Measuring the effect of small molecules on stomatal conductance in grasses will be important towards understanding stomatal physiology in monocots. Our technique was optimized and rapid ABA-mediated decreases in stomatal conductance were resolved in intact leaves of the reference grass species *Brachypodium distachyon* (Fig. 7). This allowed us to quantify not only the final magnitude of ABA responses, but importantly, the time course of the ensemble average of stomata in intact leaves could be resolved.

Conclusions

Understanding how guard cells respond to stresses and signals is a subject of interest in plant biology and numerous advances have been made. Signals that modulate stomatal movements and that can be controlled by gas exchange analyzers, such as light and CO_2 concentration, have been extensively investigated. It has become a standard in this field to include time-resolved data on stomatal conductance for stimuli that can be automatically adjusted. Here we present a detailed method applying small soluble molecules that has a substantially larger dynamic range than epidermal peel experiments and enables kinetic analyses. We recommend this approach for evaluation of stomatal conductance responses to small molecules, particularly in mutants which have intermediate phenotypes. The protocol is described in detail here and optimized for two key model organisms, *Arabidopsis* and the grass *Brachypodium distachyon*.

Chapter 3, in full, is published as it may appear in Plant Methods, Ceciliato, PHO; Zhang, J; Liu, Q; Shen, X; Hu, H; Liu, C; Schäffner, AR; Schroeder JI. The dissertation author was the primary investigator and author of this paper.

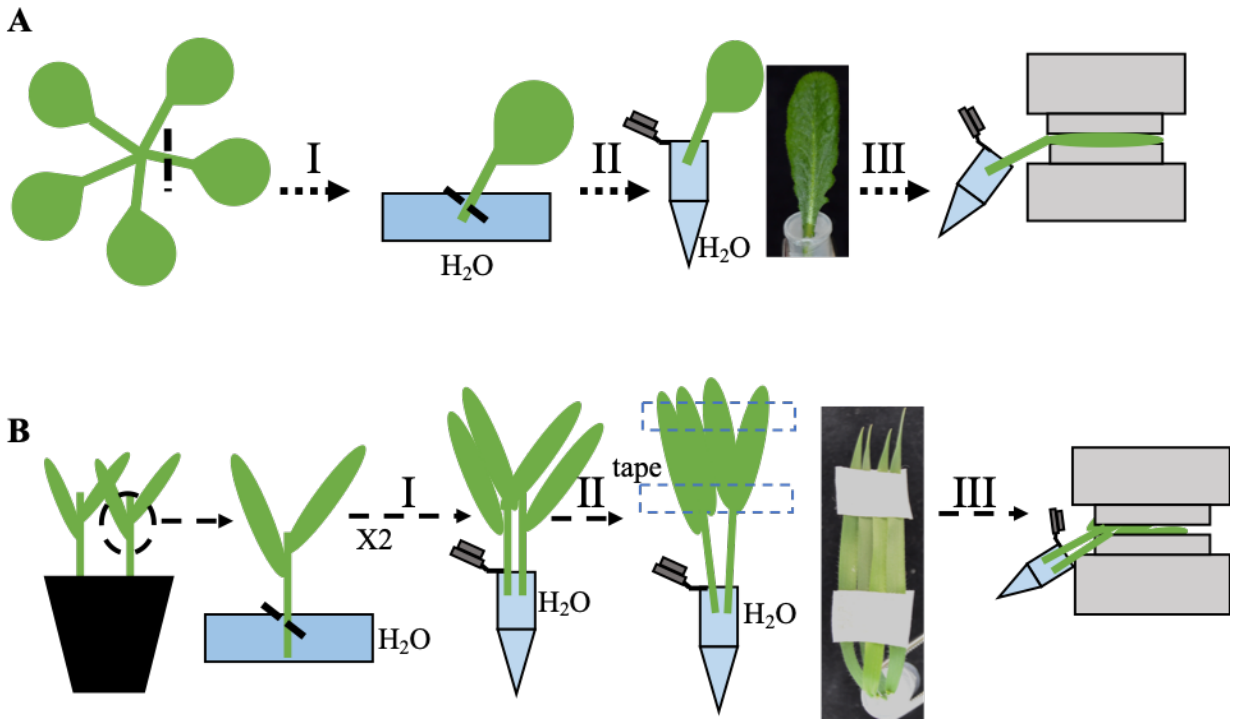

Figure 3.1 - Depiction of the methods used to perform whole-leaf time-resolved ensemble analyses of small molecule responses. (A) Depiction of the approach for investigating stomatal responses to small molecules in *Arabidopsis thaliana.* (B) Depiction of the approach for investigating stomatal ABA responses in the grass *Brachypodium distachyon*. See text for details.

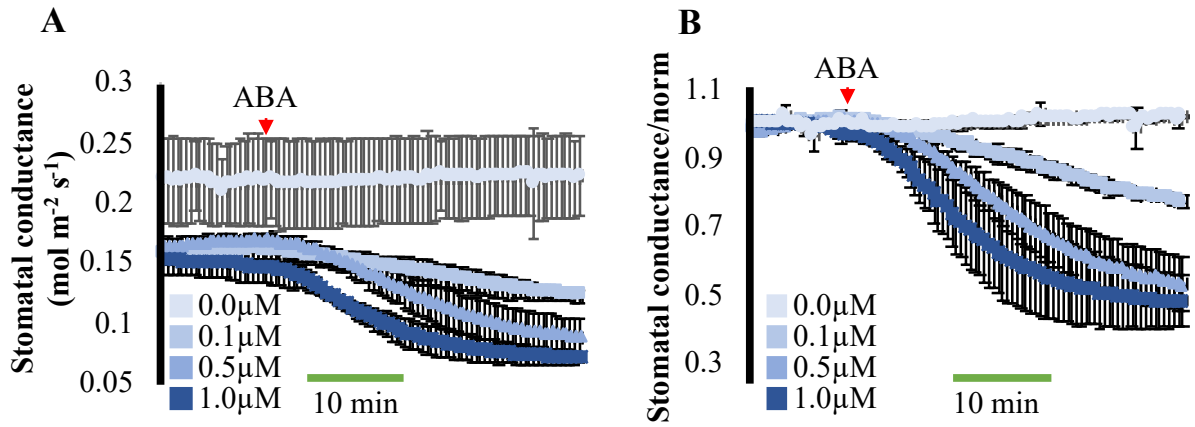

Figure 3.2 - Time-resolved stomatal conductance analysis of ABA responses in intact *Arabidopsis* leaves. Time-resolved stomatal conductance responses at the indicated ABA concentrations in wild-type (Col-0) were analyzed using whole-leaf gas exchange analyses. (A) Stomatal conductance in mol m^{-2} s^{-1}. (B) Data shown in (A) were normalized to the average of the first 10 minutes of stomatal conductance values recorded. ABA was added to the transpiration stream (red arrowhead). N=3 leaves per condition ± SD.

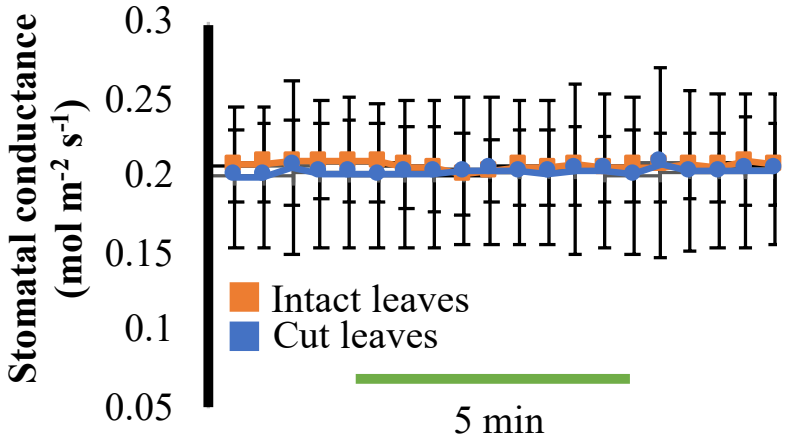

Figure 3.3 - Time-resolved stomatal conductance analysis of the same leaves before and after the cut of the petioles. The same three leaves from three plants were evaluated before (in intact plants) and after the cut of their petioles. Time resolved steady-state stomatal conductance was measured after 70 minutes of insertion of the leaves into a gas exchange analyzer chamber. N=3 leaves per condition ± SD.

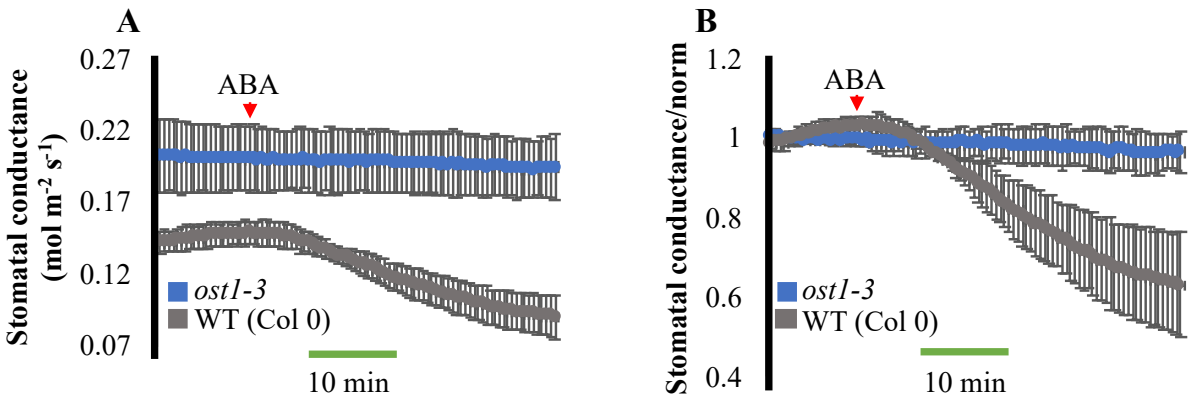

Figure 3.4 - *ost1-3* mutant is insensitive to ABA in time-resolved stomatal conductance analysis. Time-resolved stomatal conductance responses in response to ABA (2 μM) in wild-type (Col-0) and *ost1-3* (Col-0 ecotype) mutant were analyzed using a whole-leaf gas exchange analyzer. (A) Stomatal conductance in mol m^{-2} s^{-1}. (B) Data shown in (A) were normalized to the average of the first 10 minutes of stomatal conductance values recorded. ABA was added to the transpiration stream (red arrowhead). N=3 leaves per genotype ± SD.

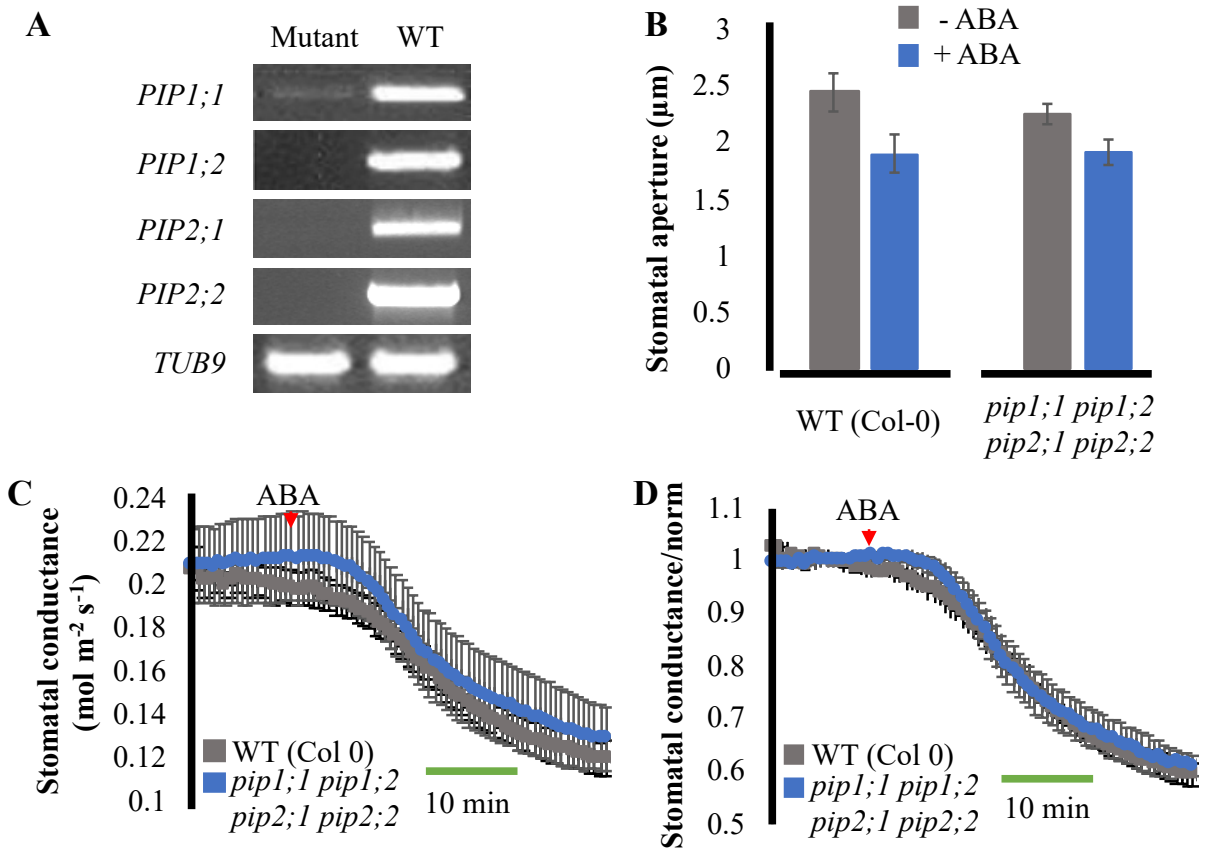

Figure 3.5 - Aquaporin *pip* quadruple mutant is responsive to ABA. (A) Expression levels of *PIP* genes in WT (Col 0) and *pip1;1, pip1;2, pip2;1 and pip2;2* mutants. Expression of tubulin 9 is shown as control. (B) Analyses of stomatal movements in response to ABA. Leaf epidermal layers were incubated with ± ABA (10 µM ABA) and the stomatal aperture was scored (N=10 stomata per genotype per treatment). (C) Stomatal conductance of detached leaves from wild type (Col-0) (n=3) and *pip1;1/pip1;2/pip2;1/pip2;2* quadruple mutant (n=4) plants in response to 2 µM ABA. (D) Normalized data shown in panel (C). Data shown in (C) were normalized to the average of the first 10 minutes of stomatal conductance values recorded. ABA was added to the transpiration stream (red arrowhead). N>3 leaves ± SEM per genotype.

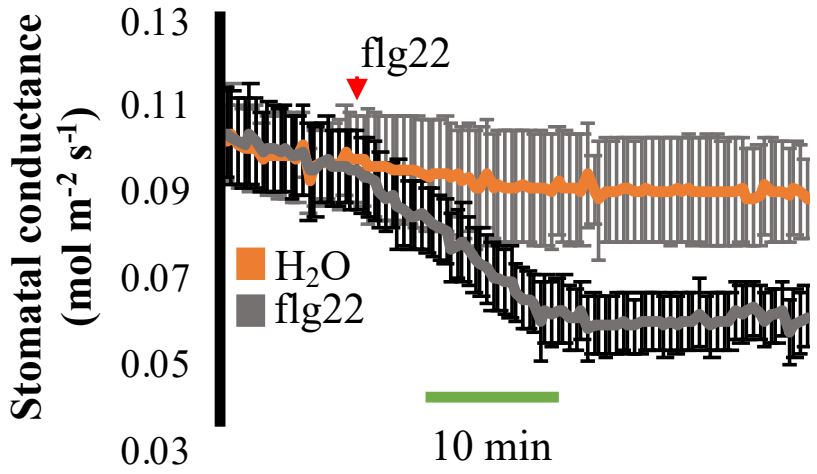

Figure 3.6 - Time-resolved analysis of stomatal responses to the defense elicitor peptide flg22 in intact leaves. Time-resolved stomatal conductance responses at a final concentration of 10 µM flagellin 22 (flg22) in wild-type (Col-0) was analyzed in intact leaves using a whole-leaf gas exchange analyzer. N=3 leaves per condition ± SD.

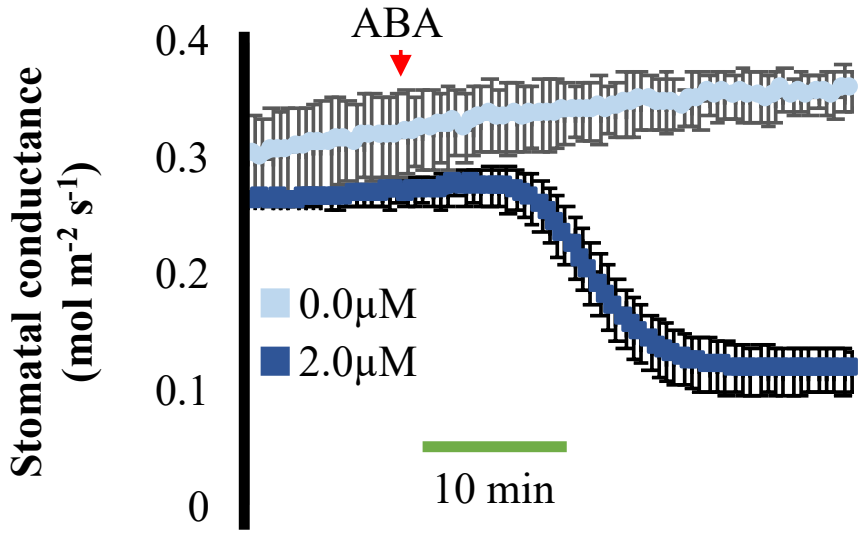

Figure 3.7 - Time-resolved analysis of stomatal conductance response to ABA in intact leaves of *Brachypodium distachyon*. Time-resolved stomatal conductance responses at the imposed ABA concentrations (0 and 2 µM) in wild-type Bd21-3 Brachypodium plants were analyzed using whole-leaf gas exchange. N= 3 experiments, 4 leaves in each experiment ± SD.

References

Assmann SM. 1993. Signal Transduction in Guard Cells. Annual Review of Cell Biology **9**, 345–375.

Azoulay-Shemer T, Bagheri A, Wang C, Palomares A, Stephan AB, Kunz H-H, Schroeder JI. 2016. Starch Biosynthesis in Guard Cells But Not in Mesophyll Cells Is Involved in CO2-Induced Stomatal Closing. Plant Physiol **171**, 788 798.

Batool S, Uslu VV, Rajab H, Ahmad N, Waadt R, Geiger D, Malagoli M, Xiang CB, Hedrich R, Rennenberg H, Herschbach C, Hell R, Wirtz M. 2018. Sulfate is Incorporated into Cysteine to Trigger ABA Production and Stomatal Closure. Plant Cell **30**, 2973 2987.

Bauer H, Ache P, Lautner S, Fromm J, Hartung W, Al-Rasheid KA, Sonnewald S, Sonnewald U, Kneitz S, Lachmann N, Mendel RR, Bittner F, Hetherington AM, Hedrich R. 2013. The stomatal response to reduced relative humidity requires guard cell-autonomous ABA synthesis. Curr Biol **23**, 53 57.

Chaumont F, Tyerman SD. 2014. Aquaporins: highly regulated channels controlling plant water relations. Plant Physiol **164**, 1600 1618.

Deger A, Scherzer S, Nuhkat M, Kedzierska J, Kollist H, Brosché M, Unyayar S, Boudsocq M, Hedrich R, Roelfsema RM. 2015. Guard cell SLAC1-type anion channels mediate flagellin-induced stomatal closure. New Phytol **208**, 162 173.

Engineer CB, Hashimoto-Sugimoto M, Negi J, Israelsson M, Azoulay-Shemer T, Rappel W-J, Iba K, Schroeder JI. 2016. CO2 Sensing and CO2 Regulation of Stomatal Conductance: Advances and Open Questions. Trends in Plant Science **21**, 16 30.

Felle HH, Hanstein S, Steinmeyer R, Hedrich R. 2000. Dynamics of ionic activities in the apoplast of the sub-stomatal cavity of intact Vicia faba leaves during stomatal closure evoked by ABA and darkness. Plant J **24**, 297 304.

Gamborg O, Miller R, Ojima K. 1968. Nutrient requirements of suspension cultures of soybean root cells. Experimental cell research **50**, 151 158.

Gómez-Gómez L, Boller T. 2000. FLS2: An LRR Receptor–like Kinase Involved in the Perception of the Bacterial Elicitor Flagellin in Arabidopsis. Mol Cell **5**, 1003 1011.

Grondin A, Rodrigues O, Verdoucq L, Merlot S, Leonhardt N, Maurel C. 2015. Aquaporins Contribute to ABA-Triggered Stomatal Closure through OST1-Mediated Phosphorylation. Plant Cell **27**, tpc.15.00421 1954.

Hauser F, Ceciliato PHO, Lin YC, Guo D, Gregerson JD, Abbasi N, Youhanna D, Park J, Dubeaux G, Shani E, Poomchongkho N, Schroeder JI. 2018. A seed resource for screening

functionally redundant genes and isolation of new mutants impaired in CO2 and ABA responses. Journal of experimental botany **70**.

Heinen RB, Bienert G, Cohen D, Chevalier AS, Uehlein N, Hachez C, Kaldenhoff R, Thiec D, Chaumont F. 2014. Expression and characterization of plasma membrane aquaporins in stomatal complexes of Zea mays. Plant Mol Biol. **86**, 335 350.

Inoue S, Kinoshita T, Matsumoto M, Nakayama KI, Doi M, Shimazaki K-I. 2008. Blue light-induced autophosphorylation of phototropin is a primary step for signaling. Proc Natl Acad Sci U S A **105**, 5626 5631.

Kaldenhoff R, Ribas-Carbo M, Sans J, Lovisolo C, Heckwolf M, Uehlein N. 2008. Aquaporins and plant water balance. Plant Cell Environ **31**, 658 666.

Kim T, Böhmer M, Hu H, Nishimura N, Schroeder JI. 2010. Guard cell signal transduction network: advances in understanding abscisic acid, CO2, and Ca2+ signaling. Annual Review of Plant Biology **61**, 561 591.

Kinoshita T, Doi M, Suetsugu N, Kagawa T, Wada M, Shimazaki K-I. 2001. phot1 and phot2 mediate blue light regulation of stomatal opening. Nature **414**, 656 660.

Kinoshita T, Shimazaki K-I. 1999. Blue light activates the plasma membrane H+-ATPase by phosphorylation of the C-terminus in stomatal guard cells. Embo Journal **18**, 5548 5558.

Kollist H, Zandalinas SI, Sengupta S, Nuhkat M, Kangasjärvi J, Mittler R. 2018. Rapid Responses to Abiotic Stress: Priming the Landscape for the Signal Transduction Network. Trends Plant Sci **24**.

Lawson T, Simkin AJ, Kelly G, Granot D. 2014. Mesophyll photosynthesis and guard cell metabolism impacts on stomatal behaviour. New Phytologist **203**, 1064 1081.

Lindsey BE, Rivero L, Calhoun CS, Grotewold E, Brkljacic J. 2017. Standardized Method for High-throughput Sterilization of Arabidopsis Seeds. Journal of visualized experiments : JoVE.

Maurel C, Verdoucq L, Luu D-T, Santoni V. 2008. Plant aquaporins: membrane channels with multiple integrated functions. Annu Rev Plant Biol **59**, 595 624.

McKown KH, Bergmann DC. 2018. Grass stomata. Curr Biol **28**, R814 R816.

Melotto M, Underwood W, Koczan J, Nomura K, He S. 2006. Plant stomata function in innate immunity against bacterial invasion. Cell **126**, 969 980.

Merilo E, Yarmolinsky D, Jalakas P, Parik H, Tulva I, Rasulov B, Kilk K, Kollist H. 2018. Stomatal VPD Response: There Is More to the Story Than ABA. Plant Physiol **176**, 851 864.

Mott K, Sibbernsen E, Shope J. 2008. The role of the mesophyll in stomatal responses to light

and CO2. Plant Cell Environ **31**, 1299 1306.

Müller HM, Schäfer N, Bauer H, Geiger D, Lautner S, Fromm J, Riederer M, Bueno A, Nussbaumer T, Mayer K, Alquraishi SA, Alfarhan AH, Neher E, Al-Rasheid KAS, Ache P, Hedrich R. 2017. The desert plant Phoenix dactylifera closes stomata via nitrate-regulated SLAC1 anion channel. New Phytol **216**, 150 162.

Murashige T, Skoog F. 1962. A Revised Medium for Rapid Growth and Bio Assays with Tobacco Tissue Cultures. Physiologia Plantarum **15**, 473 497.

Mustilli A. 2002. Arabidopsis OST1 Protein Kinase Mediates the Regulation of Stomatal Aperture by Abscisic Acid and Acts Upstream of Reactive Oxygen Species Production. The Plant Cell **14**, 3089 3099.

Park J, Kim TH, Takahashi Y, Schwab R, Dressano K, Stephan AB, Ceciliato PHO, Ramirez E, Garin V, Huffaker A, Schroeder JI. Chemical genetic identification of a lectin receptor kinase that transduces immune responses and interferes with abscisic acid signaling. Plant J **98**.

Quigley F, Rosenberg JM, Shachar-Hill Y, Bohnert HJ. 2002. From genome to function: the Arabidopsis aquaporins. Genome Biol **3**, RESEARCH0001.

Raissig MT, Abrash E, Bettadapur A, Vogel JP, Bergmann DC. 2016. Grasses use an alternatively wired bHLH transcription factor network to establish stomatal identity. Proc Natl Acad Sci U S A **113**, 8326 8331.

Raissig MT, Matos JL, Anleu Gil MX, Kornfeld A, Bettadapur A, Abrash E, Allison HR, Badgley G, Vogel JP, Berry JA, Bergmann DC. 2017. Mobile MUTE specifies subsidiary cells to build physiologically improved grass stomata. Science **355**, 1215 1218.

Schäfer N, Maierhofer T, Herrmann J, Jørgensen ME, Lind C, von Meyer K, Lautner S, Fromm J, Felder M, Hetherington AM, Ache P, Geiger D, Hedrich R. 2018. A Tandem Amino Acid Residue Motif in Guard Cell SLAC1 Anion Channel of Grasses Allows for the Control of Stomatal Aperture by Nitrate. Current Biology **28**, 1370-1379.e5.

Uehlein N, Lovisolo C, Siefritz F, Kaldenhoff R. 2003. The tobacco aquaporin NtAQP1 is a membrane CO2 pore with physiological functions. Nature **425**, 734 737.

Wang C, Hu H, Qin X, Zeise B, Xu D, Rappel W-J, Boron WF, Schroeder JI. 2016. Reconstitution of CO2 Regulation of SLAC1 Anion Channel and Function of CO2-Permeable PIP2;1 Aquaporin as CARBONIC ANHYDRASE4 Interactor. The Plant Cell **28**, 568 582.

Weiner JJ, Peterson FC, Volkman BF, Cutler SR. 2010. Structural and functional insights into core ABA signaling. Curr Opin Plant Biol **13**, 495 502.

Weyers JD, Travis AJ. 1981. Selection and Preparation of Leaf Epidermis for Experiments on Stomatal Physiology. Journal of experimental botany **32**, 837 850.

Wilkinson S, Davies WJ. 2008. Manipulation of the apoplastic pH of intact plants mimics stomatal and growth responses to water availability and microclimatic variation. Journal of experimental botany **59**, 619 631.

Yoshida R, Hobo T, Ichimura K, Mizoguchi T, Takahashi F, Aronso J, Ecker J, Shinozaki K. 2002. ABA-activated SnRK2 protein kinase is required for dehydration stress signaling in Arabidopsis. Plant Cell Physiol **43**, 1473 1483.

Young J, Mehta S, Israelsson M, Godoski J, Grill E, Schroeder J. 2006. CO(2) signaling in guard cells: calcium sensitivity response modulation, a Ca(2+)-independent phase, and CO(2) insensitivity of the gca2 mutant. Proc Natl Acad Sci U S A **103**, 7506 11. Epub 2006 May 1.

Zhang J, Wang N, Miao Y, Hauser F, McCammon AJ, Rappel W-J, Schroeder JI. 2018. Identification of SLAC1 anion channel residues required for CO2/bicarbonate sensing and regulation of stomatal movements. Proc Natl Acad Sci U S A **115**, 201807624 11137.

Chapter 4:

Towards identifying new components of CO_2-regulation of stomatal conductance in grasses using *Brachypodium distachyon*.

Abstract

In grasses, stomata are surrounded by two groups of cells: the dumbbell-shaped guard cells and the stomatal subsidiary cells. In combination, these cells respond to both external and internal stimuli, thus enabling rapid stomatal opening and closing. However, the molecular mechanisms mediating stomatal movements in grasses remain to a large degree unknown.

Using the reference grass species *Brachypodium distachyon*, a forward genetic screen was performed. Over 1,070 mutagenized lines were screened for changes in their canopy leaf temperature using real-time infra-red imaging. Differences in leaf temperature may indicate defective stomatal development or responsiveness. Using this approach, 21 mutant lines with consistent canopy leaf temperature changes compared to wild type (WT) were selected and are currently being characterized. Interestingly, two of these mutant lines named "*chill1*" and "*chill15*" have impaired responses to elevated CO_2 concentration but retain stomatal closing response to the hormone abscisic acid in intact leaf gas exchange experiments. Moreover, stomatal indices in *chill1* and *chill15* lines are similar to WT stomatal indices. Whole Genome Sequencing (WGS) data suggest that new genes in CO_2-mediated stomatal movements in grasses will be identified in these mutants.

Introduction

The global atmospheric CO_2 concentration is rising and in 2013 it surpassed 400 parts per million for the first time in human history (https://scripps.ucsd.edu/programs/keelingcurve/). Plants can sense changes in CO_2 concentration ($[CO_2]$) in leaves and adapt transpiration and water use efficiency accordingly. On the surface leaves, plants have pores called stomata which gate CO_2 uptake for photosynthesis and water loss through transpiration. Stomatal aperture is ultimately controlled by two cells, called guard cells, that surround the pore. High $[CO_2]$ has two major effects on stomata in several plant species: in the short-term it leads to stomatal closure and in the long-term it decreases stomatal density in leaves (Engineer *et al.*, 2014; Zhang *et al.*, 2018), both of which have profound effects on plant water use efficiency.

When plants are exposed to high $[CO_2]$, guard cell-expressed beta carbonic anhydrases (βCA) convert CO_2 into bicarbonate, which is an essential step for CO_2-induced stomatal closure (Hu *et al.*, 2010). In fact, the carbonic anhydrase βCA4 and the Plasma membrane Intrinsic Protein 2,1 (AtPIP2;1) interact *in planta,* which facilitates the entrance of CO_2/bicarbonate into the guard cells (Wang *et al.*, 2016). Recent work has shown that bicarbonate can directly activate Slow Anion Channel-Associated 1 (SLAC1) anion channels, which has predicted bicarbonate binding sites and leads to stomatal closure (Engineer *et al.*, 2014; Zhang *et al.*, 2018*a*). Although SLAC1 is one of the bicarbonate sensors in plants, *slac1-1* mutants do not completely abolish CO_2-mediated stomatal responses, suggesting that SLAC1 is a secondary CO_2/bicarbonate sensor and that another pathway and a primary CO_2/HCO_3- sensor is essential for WT-like responses to $[CO_2]$-shifts. In this context, there are many genes/proteins known to play an important role in CO_2-mediated stomatal movements. Double mutants for the Mitogen-Activated Protein Kinase 4 and 12 (*mpk4/mpk12*) have high steady-state stomatal conductance and are heavily impaired in CO_2-

induced stomatal closure (Hõrak *et al.*, 2016; Tõldsepp *et al.*, 2018). Also, the High leaf Temperature 1 (HT1) protein kinase is a negative regulator of CO_2 signaling and mutants *ht1-2* have low steady-state stomatal conductance and completely abolish stomatal responses to CO_2 (Hashimoto *et al.*, 2006; Matrosova *et al.*, 2015).

In addition to those CO_2-specific components of the signaling pathway, there are a few proteins that participate in CO_2-regulation of stomatal movements but also in other molecular pathways that control stomatal responses. For instance, the Open Stomata 1 (OST1) protein kinase, which has a central role in ABA-induced stomatal closure, is also crucial for normal high CO_2-dependent stomatal closure responses (Xue *et al.*, 2011). More recently, a convergence between low CO_2- and blue-light-induced stomatal opening was found. Mutants lacking the Convergence of Blue Light and CO_2 1/2 (CBC1/CBC2) kinases are impaired in both blue-light and low CO_2-induced stomatal opening (Hiyama *et al.*, 2017). In summary, many genes involved in the bicarbonate/CO_2 perception and signaling in guard cells have been identified and characterized. However, how and whether these distinct proteins interact with one another to coordinate proper CO_2-responses, as well as whether there is another CO_2 sensor in plants are still opened questions in the field. In addition, the vast majority of these findings were done in the dicot reference plant *Arabidopsis thaliana*, and our understanding of CO_2-signaling in guard cells in grasses (monocots) is limited.

Monocots have a distinct stomatal apparatus: the guard cells are dumbbell-shaped and respond to external stimuli together with surrounding subsidiary cells. When the dumbbell-shaped guard cells become more turgid for stomatal opening, the neighboring subsidiary cells deflate and vice-versa; this mechanism enhances stomatal responses in grasses compared to dicots (Raissig *et*

al., 2017; Nunes *et al.*, 2019). This intricate stomatal movement mechanism has great potential for the discovery of new genes and pathways in guard cell signaling.

Using the grass reference plant *Brachypodium distachyon*, we performed a forward genetic screen with an EMS-mutagenized seed population. We screened over 1,070 EMS lines for changes in canopy leaf temperature utilizing infra-red thermal imaging. Changes in leaf temperature could be linked to stomatal movement/development phenotypes due to changes in transpiration rates. Two CO_2-insensitive mutants and 19 mutant lines with changes in leaf temperature were identified in an unbiased fashion. Interestingly, some isolated mutants are strongly insensitive to CO_2-concentration changes but still respond to other stimuli that control stomatal aperture, including the drought hormone abscisic acid, suggesting CO_2 response specificity. Identification of new genes and mechanisms, that impair the stomatal CO_2 response in grasses, could play a key role in future engineering of improved water use efficiency or heat tolerance of crops, in light of the continuing increase in greenhouse gas concentrations and extreme climate events. Ultimately, new discoveries in this field of research could be applied to major crops in the future, mitigating the impacts of high CO_2 on food production.

Materials and Methods

Plant material and growth conditions

Brachypodium distachyon accession Bd21-3 was used as the wild type reference. Seeds were cold-treated for 4–5 days at 4 °C, transferred to 2 inch square pots containing premixed soil (Sunshine Professional Blend LC1 RS; Sunshine) and kept under a tray dome for 2 weeks. Plants were fertilized once a week (technigro®sunshine fertilizer, 0.66 g L^{-1} of water, 1 liter per tray) and watered every other week and kept at the following conditions: long day (16 h light/8 h dark); 23–25 °C; 20–50% humidity, 150–250 µmol m^{-2} s^{-1} light. For the first round of screening, plants were grown under 150 µmol m^{-2} s^{-1} light (16 h light/8 h dark). For the second round of screening, more optimum light intensities (250 µmol m^{-2} s^{-1}) was used. Plants were used for the indicated experiments 6–7 weeks after being transferred to pots.

The forward genetic screen

For this forward genetic screen, two distinct approaches were adopted. First, about 30 EMS-mutagenized lines in the M5 generation were used in a pilot screen. Five plants per line were grown as described above for 4-5 weeks together with WT Bd21-3 control plants. These plants were exposed to high CO_2 (900 ppm) in a Percival growth chamber for two hours and the canopy leaf temperature was measured with a FLIR A320 thermal imaging camera (FLIR, Wilsonville, OR, USA). Plants with lower leaf temperature compared to WT plants were selected as putative candidates. This first pilot screen resulted in the isolation of the *chill1* mutant line.

The second approach was used to screen over 1,045 EMS lines in the M5 generation and it was similar to the pilot approach, except that plants were not exposed to high CO_2 before thermal imaging data were acquired. In this case, five plants per mutant line were grown at ambient CO_2

for 4-5 weeks and thermal images were taken at the ambient (growth room) CO_2 concentration. For these experiments, 5 plants from each mutant line were placed next to parallel-grown WT Bd21-3 plants and thermal images were obtained. Lines that were selected for a second round of screening showed 3 or more out of five plants with distinct canopy leaf temperature compared to WT. These lines were selected for another test in the same generation (M5), in similar conditions. Mutant lines with robust phenotypes were selected to be re-evaluated in the next generation (M6). Using these criteria, 28 mutant lines were selected to be re-tested. For these experiments, 5-10 plants per line were grown as described above in parallel with WT control plants. These lines were individually imaged using infrared thermal imaging and canopy leaf temperature was again measured. Lines with robust phenotypes in two distinct generations (M5 and M6) will be further characterized.

Stomatal conductance measurements

Intact leaf stomatal conductance was measured using two distinct approaches. First, parallel grown WT plants and mutant candidates were used, and stomatal conductance was measured using a leaf porometer (SC-1 Porometer, decagon devices). As the leaf porometer gives a single measurement of stomatal conductance from a very small leaf area, a more robust technique was used for further investigation of stomatal conductance responses.

For intact leaf gas exchange resolved over time, stomatal conductance of H_2O (g_s) was measured in leaves of 5- to 6-week-old plants using portable gas exchange systems (LI-6400 and LI-6800, LI-COR, Lincoln, NE, USA), starting 2 h after growth chamber light onset. For intact single leaf ABA treatments, a LED light source set at 150 μmol m^{-2} s^{-1} (10% blue) and a chamber temperature of 21 °C was used. Leaves were equilibrated for 1 h at a relative humidity of 70–72%,

airflow of 200 rpm and CO_2 concentration of 400 ppm. After 1 h, steady-state stomatal conductance was recorded 10 min before the addition of ABA to the petioles submerged in water at the indicated concentration (Ceciliato *et al*., 2019). The data presented represent $n \geq 3$ leaves with each leaf from independent plants per genotype per treatment.

Stomatal index and density measurements

For stomatal imaging in Brachypodium, a new protocol was developed. First, 5-6-week-old mutant candidate plants were grown under the abovementioned conditions in parallel with WT control plants. The fifth true leaf was used for the measurements and the abaxial side of the leaf was visualized. In a microscope slide, a small drop of super glue (Loctite professional liquid) was placed and the center of the abaxial side of the leaves were placed on top of the super glue drop. By gently pressing the leaves against the microscope slide, super glue was evenly spread through the surface of the leaf. Once the super glue is dry, the leaf is peeled off and the epidermal peel of the abaxial side of the leaves were used for visualization under a Differential Interference Contrast (DIC) microscope. For each experiment, five leaves (from five different plants) were imaged per genotype, with four images per leaf. Images were later analyzed, and stomata and pavement cells were counted using the software ImageJ.

Results

A new forward genetic screen using the grass reference *Brachypodium distachyon* – isolation of new mutants impaired in CO_2-mediated stomatal movements.

With the rise in atmospheric CO_2 concentration (https://scripps.ucsd.edu/programs/keelingcurve/), new efforts toward understanding how plants perceive and respond to [CO_2] oscillation are necessary. An elevated CO_2 concentration can be perceived at the guard cell level and leads to stomatal closure in many plant species (Engineer *et al.*, 2016). In grasses, such as the model organism *Brachypodium distachyon* (hereafter referred to as Brachypodium), high CO_2-induced stomatal closure occurs rapidly, with enhanced responsiveness provided by stomatal subsidiary cells (Raissig *et al.*, 2017). As dicots, such as Arabidopsis, do not possess stomatal subsidiary cells, further research using grasses could greatly broaden our knowledge of CO_2-regulation of stomatal movements and development.

Using an EMS-mutagenized population of Brachypodium consisting of over 1,075 lines in the M5 generation, we performed a forward genetic screen aiming to find mutants impaired in CO_2-regulation of stomatal responses. First, five individual plants per line were grown side-by-side with WT (Bd21-3) control plants at ambient CO_2 for four to five weeks. These plants were then exposed to high CO_2 (900 ppm) for two hours and infrared thermal imaging was used to measure canopy leaf temperature. When plants are exposed to high [CO_2] they close their stomata, and plant transpiration decreases. After a few hours with limited transpiration, canopy leaf temperature rises. We screened for plants whose leaves were colder than WT leaves exposed to the same condition as an indication of possible decrease in high [CO_2]-induced stomatal closure. Using this approach, over 30 lines were screened in a pilot run. When plants were exposed to high CO_2 for two hours, WT control plants showed high leaf temperatures and the opposite happened

when they were exposed to low CO_2. One of our mutants, *chill1*, did not show a dramatic change in canopy leaf temperature after incubation at high or low CO_2 (Figure 1A). A leaf porometer was used to measure stomatal conductance in these plants after exposure to high and low CO_2. When WT plants were exposed to low CO_2, the steady-state stomatal conductance to water was ≈200 μmol m^{-2} s^{-1}. After high CO_2 exposure, steady-state stomatal conductance measured in the same leaves decreased by 5 times, to ≈40 μmol m^{-2} s^{-1}. The same was not observed when steady-state stomatal conductance was measured in *chill1* leaves, shifting from 180 μmol m^{-2} s^{-1} on average to 155 μmol m^{-2} s^{-1} (Figure 1B).

Next, we decided to investigate *chill1* plants at ambient [CO_2]. Infrared thermal images showed that *chill1* plants have lower leaf temperature compared to WT even at ambient [CO_2] (Figure 2A). Steady-state stomatal conductance in *chill1* plants was more than twice as high on average compared to WT steady-state stomatal conductance under the same conditions (Figure 2B). This prompted us to verify stomatal development in these plants. Interestingly, *chill1* plants have WT-like stomatal index and density measurements indicating no dramatic effect on stomatal development (Figure 2C).

Our experiments suggest that the mutant line *chill1* is defective in CO_2-regulation of stomatal movements but is not affected in stomatal development.

The *chill1* mutant line is impaired in CO_2-induced stomatal closure but not in ABA-induced stomatal closure.

To further characterize the *chill1* mutant line, seeds from plants in the M5 generation were harvested and new experiments were performed in the subsequent generation. We again observed lower canopy leaf temperature of *chill1* plants compared to WT control plants after exposure to

high CO_2 for two hours (Figure 3A). Using intact leaf gas exchange analyses, stomatal conductance responses to [CO_2] shifts were time-resolved. First, leaves were clamped in the gas exchange chamber and equilibrated for two hours. Steady-state stomatal conductance to low [CO_2] was measured for 90 minutes before changing to high CO_2 for another 60 minutes. WT control plants showed a fast-stomatal response by decreasing stomatal conductance after exposure to high [CO_2]. In contrast, in *chill1* leaves, the stomatal conductance remained steady after exposure to high CO_2 (Figure 3B). This prompted us to test whether *chill1* plants can close their stomata in response to other stimuli. Using the methodology described in "chapter three" (Ceciliato *et al.*, 2019), ABA-induced stomatal closure was tested in *chill1* plants. In these experiments, leaves were clamped in the gas exchange chamber and equilibrated for two hours at ambient [CO_2]. After this period, ten minutes of steady-state stomatal conductance was measured, and ABA was applied to a final concentration of 2 μM to the petioles of 4 excised leaves per experiment (Ceciliato *et al*., 2019). Interestingly, both WT and *chill1* leaves showed a rapid ABA-induced stomatal closure response (Figure 3C).

In summary, the mutant *chill1* is heavily impaired in [CO_2]-regulation of stomatal movement while still responsive in ABA-induced stomatal closure.

Identification of new mutants with distinct canopy leaf temperature at ambient CO_2 led to the isolation of a *chill1*-like mutant line.

The results obtained from *chill1* plants suggested that mutants with impaired stomatal responses can be isolated using infrared thermal images even at ambient [CO_2]. We continued our forward genetic screen using EMS mutagenized lines by selecting plants with distinct canopy leaf temperatures compared to WT at ambient [CO_2]. Differences in leaf temperature can be linked to

defective stomatal movements and/or development. Using this pipeline, over 1,000 EMS mutant lines that were separately stored were individually screened. We performed our screen using M5 generation plants, in roughly 50 rounds composed of 20 mutant lines each round. Each individual line was represented by 5 plants that were grown in parallel with WT Bd21-3 control plants. We were able to isolate over 50 putative mutant candidate lines with distinct canopy leaf temperatures. These first mutant candidates were individually retested by screening plants from the same seed pool as in the primary screen, and 28 mutant lines were selected for further characterization as they presented robust phenotypes in the M5 generation. Seeds from each of these 28 mutants were harvested and stored separately. In the next generation (M6), 5 to 10 individual plants were grown in parallel with WT control plants for further characterization. From the 28 mutant lines confirmed in the M5 generation, 24 were tested in the M6 generation and 12 of those lines showed strong and robust phenotypes in thermal imaging analyses (Table 1). One of these confirmed lines, named *chill15*, showed lower leaf temperature compared to WT after exposure to high CO_2 for two hours (Figure 4A). These differences in canopy leaf temperature could not be linked to defects in stomatal development, as stomatal index and density measurements showed a WT-like phenotype in *chill15* plants (Figure 4B). Intact leaf gas exchange measurements were performed and when the [CO_2] was shifted from low to high, *chill15* plants showed a weak response compared to WT plants (Figure 4C). On the other hand, *chill15* plants showed a robust response in ABA-induced stomatal closure (Figure 4D).

As previously stated, over 20 mutant lines showed robust phenotypes in infrared thermal imaging in the M5 generation and 12 of these lines in the M6 generation. These lines were also tested using intact leaf gas exchange analyses and a multitude of phenotypes were observed. In these experiments, three distinct [CO_2] were tested: 400 ppm, 150 ppm and 900 ppm.

With the information gathered from our intact leaf gas exchange experiments, different groups of mutants were identified (Figure 5 and Table 1):

Group 1- Mutants with impaired responses to [CO_2] shifts in gas exchange analyses: candidates 1, 10 and 15.

Group 2 - Mutants with distinct kinetics of stomatal responses to [CO_2] shifts: candidates 12 and potentially 13.

Group 3 - Mutants with lower steady-state stomatal conductance compared to WT: candidates 3, 11 and 12.

Group 4 - Mutants with higher steady-state stomatal conductance compared to WT: candidates 6, 9, 14, 19 and potentially 8.

Group 5 - Mutants which show a possible stomatal re-opening at high [CO_2]: candidates 2, 9 and 13.

Group 6 - Mutants presenting WT-like responses to [CO_2] shifts: candidates 2, 4, 7 and 16.

In summary, we isolated two mutants that are highly impaired in [CO_2]-regulation of stomatal movements and still responsive to ABA-induced stomatal closure. These lines have been backcrossed into the parental line (Bd21-3) for selection of the mapping population. In addition, twelve other mutants were selected and re-tested and will be further characterized.

Discussion

Although substantial knowledge has been gained regarding CO_2/bicarbonate perception and signaling in dicots (Engineer *et al.*, 2016; Zhang *et al.*, 2018*a*), in grasses our understanding of this pathway is considerably smaller. In order to identify new components that function in CO_2/bicarbonate signaling in grasses, we performed a forward genetic screen using an EMS-mutagenized population of *Brachypodium distachyon*. First, mutant lines were exposed to high [CO_2] followed by leaf thermal imaging. Changes in canopy leaf temperature may result from impairment in stomatal responsiveness and/or development. Using this approach, a CO_2-insensitive line was isolated, named *chill1* (Figure 1). *Chill1* showed impaired CO_2 responses in both canopy leaf temperature changes and stomatal conductance measurements (Figure 1 and Figure 3). Interestingly, *chill1* plants have lower canopy leaf temperature even at ambient [CO_2], which could not be explained by the number of stomata per leaf area (Figure 2A to 2C). All the infra-red thermal images were taken in our growth room, and we speculate that the [CO_2] in this room is slightly elevated compared to atmospheric [CO_2] of ≈ 410 ppm. Since *chill1* mutants are insensitive to high [CO_2], this could explain why WT control plants are warmer under our growth conditions.

Mutants defective in CO_2 responses in guard cells are often also impaired to other stimuli such as the drought hormone ABA (Xue *et al.*, 2011) or blue light (Hiyama *et al.*, 2017). Interestingly, *chill1* plants showed a robust response to ABA-induced stomatal closure (Figure 3C), suggesting specificity. Recent work indicates that ABA and CO_2 can control stomatal movements in parallel signaling pathways, although points of convergence do exist (Hsu *et al.*, 2018). Even though both *chill1* and *chill15* mutant lines showed a robust response to ABA, WT

control plants show slightly faster stomatal closing (Figures 3C and 3D). Classic work on *Xanthium strumarium L* suggest that ABA responses can be enhanced by CO_2 (Raschke., 1975).

After screening 30 mutant lines by first exposing plants to high [CO_2] before thermal imaging, we adopted a second approach, in which plants were imaged in our growth room (ambient [CO_2]). Since *chill1* showed cooler leaves under these conditions, we hypothesized that other mutants could be identified at ambient [CO_2] and more lines could be screened using this approach. After screening over 1,000 EMS lines, some interesting mutants were isolated. One of these mutant lines, named *chill15*, showed lower canopy leaf temperature in both the M5 and M6 generations. Interestingly, this line was also less sensitive to high [CO_2] in both changes in leaf temperature and stomatal conductance measurements (Figure 4A to 4C), while maintaining ABA-induced stomatal closure responses (Figure 4D). *Chill1* and *chill15* mutants have similar stomatal phenotypes and crosses are currently being performed to verify whether these two lines are allelic.

As described, over 20 mutants were isolated in this forward genetic screen and several lines were tested using stomatal conductance measurements to [CO_2]-shifts (Figure 5). Although the majority of these lines are responsive to [CO_2]-shifts, interesting phenotypes were found: mutant lines with higher steady-state stomatal conductance (*chill9*, *14* and *19*) and lines with distinct kinetics of stomatal conductance responses (*chill12* and *13*). Mutant lines such as *chill9*, *14* and *19* could have increased amounts of stomata per leaf area and are currently being characterized. In the case of *chill12* and *13*, other stimuli that control stomatal movements will be verified in the future to test whether the differences in stomatal conductance kinetics are CO_2 specific.

As we advance in characterizing the candidate lines, new information will be obtained by sequencing their genomes and performing RNA seq on the most promising mutants. This information will be crucial for us to narrow down putative mutations related to the most promising

phenotypes observed. Backcrosses for the mutant lines *chill1* and *chill15* were obtained and the F2 population will be used for bulked segregant analyses and WGS.

Chapter 4 is coauthored with Sidhom, M; Rangel, F; Zhang, L; Lopez, B; Schroeder, JI. The dissertation author was the primary author of this chapter.

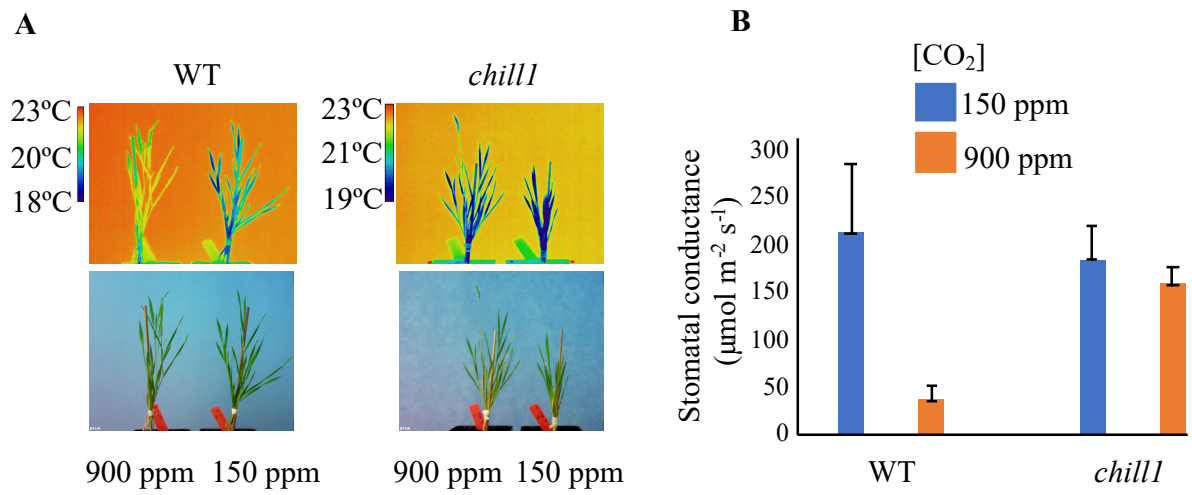

Figure 4.1 – The *chill1* mutant line has impaired responses to [CO_2] shifts. (A) Five-week old *Brachypodium distachyon* plants were exposed to high [CO_2] (900 ppm) or low [CO_2] (150 ppm) for 120 minutes. Plants were removed from CO_2 growth chamber and set side-by-side and the canopy leaf temperature was analysed by infrared thermal imaging (WT, left; *chill1* mutant, right). Note that the background temperatures between different images can vary, but this does not affect canopy leaf temperatures.(B) The stomatal conductance of WT (Bd21-3 parent line) and *chill1* *Brachypodium* leaves was analyzed using a leaf porometer after exposure to high [CO_2] (900 ppm) or low [CO_2] (150 ppm) for 120 minutes (n=3 experiments ±SEM, 4 leaves per experiment, 12 leaves total per genotype).

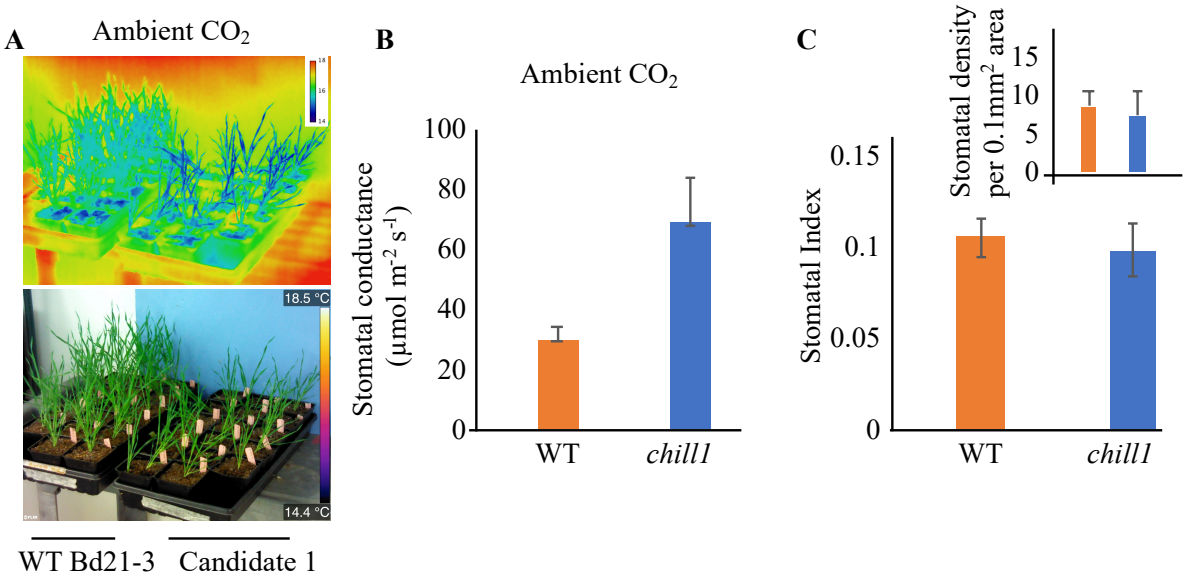

Figure 4.2 – The *chill1* mutant line has higher steady-state stomatal conductance under ambient CO_2. (A) Four-week old *Brachypodium distachyon* plants were set side-by-side and the canopy leaf temperature was analysed by infrared thermal imaging at ambient [CO_2] (WT, left; *chill1* mutant, right). (B) The stomatal conductance of WT (Bd21-3 parent line) and *chill1* *Brachypodium* leaves was analyzed at ambient [CO_2] using a leaf porometer (n=3 experiments ±SEM, 4 leaves per experiment, 12 leaves total per genotype). (C) Leaves from five-week old plants were used to calculate stomatal index (five leaves per genotype, four images per leaf). The insert shows stomatal density (five leaves per genotype, four images per leaf).

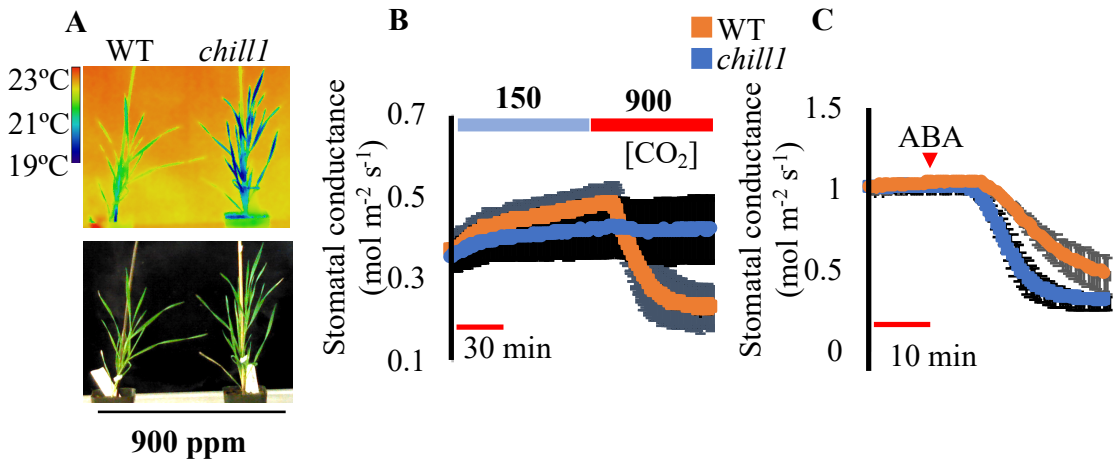

Figure 4.3 – *Chill1* mutant line has impaired responses to [CO_2] shifts in stomatal conductance responses but not to ABA. (A) Four-week old *Brachypodium distachyon* plants were exposed to high [CO_2] (900 ppm) for 120 minutes. Plants were removed from CO_2 growth chamber and set side-by-side and the canopy leaf temperature was analysed within 30 seconds by infrared thermal imaging (WT, left; *chill1* mutant, right). (B) The stomatal conductance of WT (Bd21-3 parent line) and *chill1 Brachypodium* leaves was analyzed using a gas exchange analyzer (n=3 experiments ±SEM, 4 leaves per experiment, 12 leaves total per genotype). (C) ABA-induced stomatal conductance downregulation in *chill1* mutant. ABA (2 µM) was added to the transpiration stream of intact leaves (red arrowhead). Normalized to pre-ABA conductance (n=3 independent experiments ±SEM, 4 leaves per experiment, 12 leaves total per genotype).

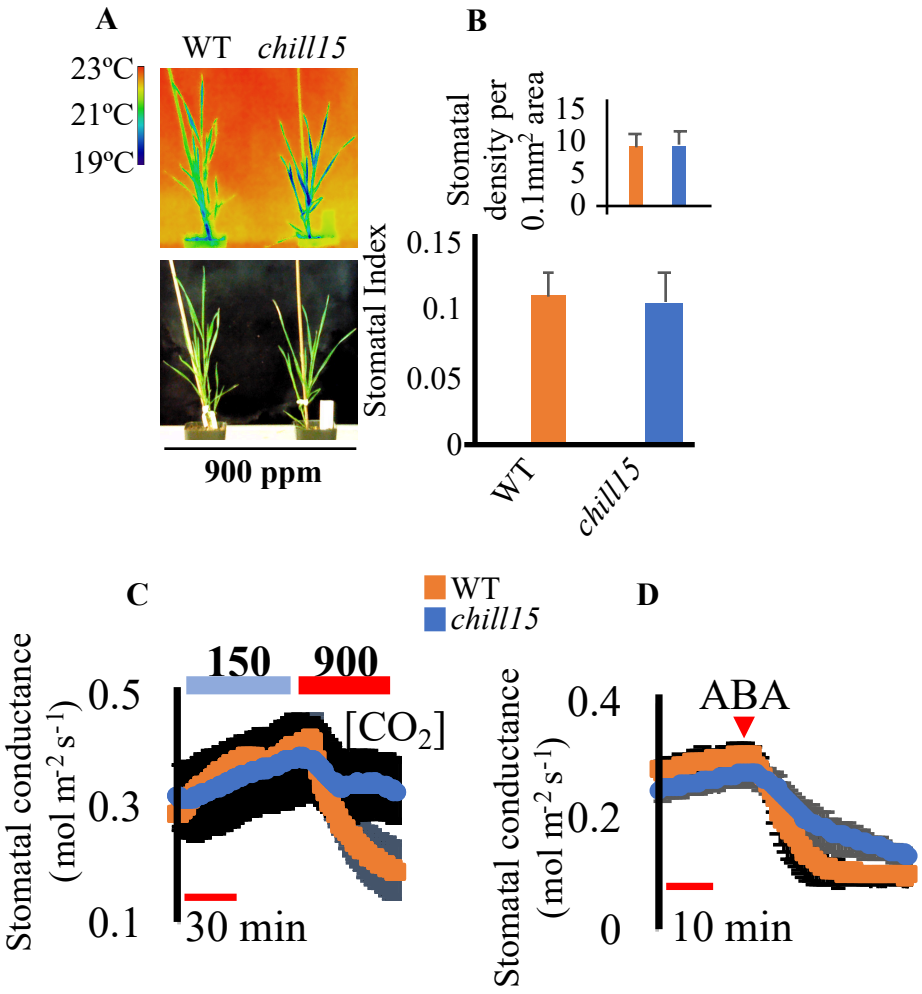

Figure 4.4 –*Chill15* mutant line shows *chill1*-like phenotype in both [CO_2] and ABA responses. (A) Four to five-week old plants were imaged at high [CO_2] (900 ppm) and canopy leaf temperature was analyzed by thermal imaging WT and *chill15*. (B) Leaves from five-week old plants were used to calculate stomatal index (five leaves per genotype, four images per leaf). The insert shows stomatal density (five leaves per genotype, four images per leaf). (C) The stomatal conductance of WT and *chill15 Brachypodium* leaves was analyzed using a gas exchange analyzer (n=3 experiments ±SEM, 4 leaves per experiment, 12 leaves total per genotype). (D) ABA-induced stomatal conductance downregulation in *chill15* mutant. ABA (2 µM) was added to the transpiration stream of intact leaves (red arrowhead), n=3 independent experiments ±SEM, 4 leaves per experiment, 12 leaves total per genotype).

Figure 4.5 – Responses to [CO_2]-shifts in *chill* mutants. The stomatal conductance (gs) of WT and indicated *chill* mutant *Brachypodium* leaves was analyzed using a gas exchange analyzer. Data are the average of n ≥ 3 ±SEM experiments, four leaves per experiment (≥12 leaves total per genotype). The data from the graphs on the left were normalized to the average gs of the 10 first minutes (plots on the right for each line).

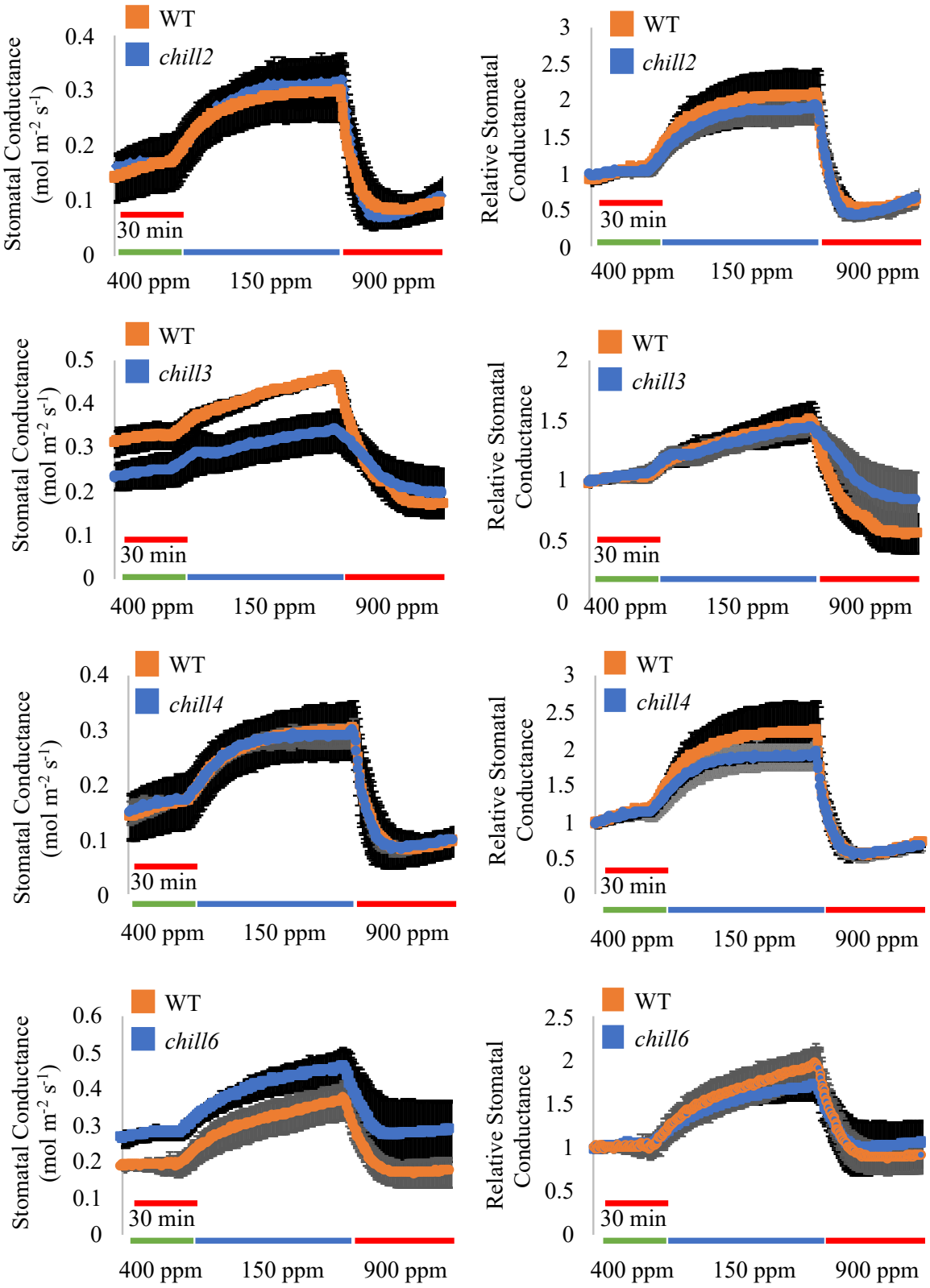
WT
chill2
Stomatal Conductance (mol m-2 s-1)
0.4
0.3
0.2
0.1
0
30 min
400 ppm
150 ppm
900 ppm
Relative Stomatal Conductance
3
2.5
2
1.5
1
0.5
0
WT
chill3
0.5
0.4
0.3
0.2
0.1
0
2
1.5
1
0.5
0
WT
chill4
0.4
0.3
0.2
0.1
0
3
2.5
2
1.5
1
0.5
0
WT
chill6
0.6
0.5
0.4
0.3
0.2
0.1
0
2.5
2
1.5
1
0.5
0

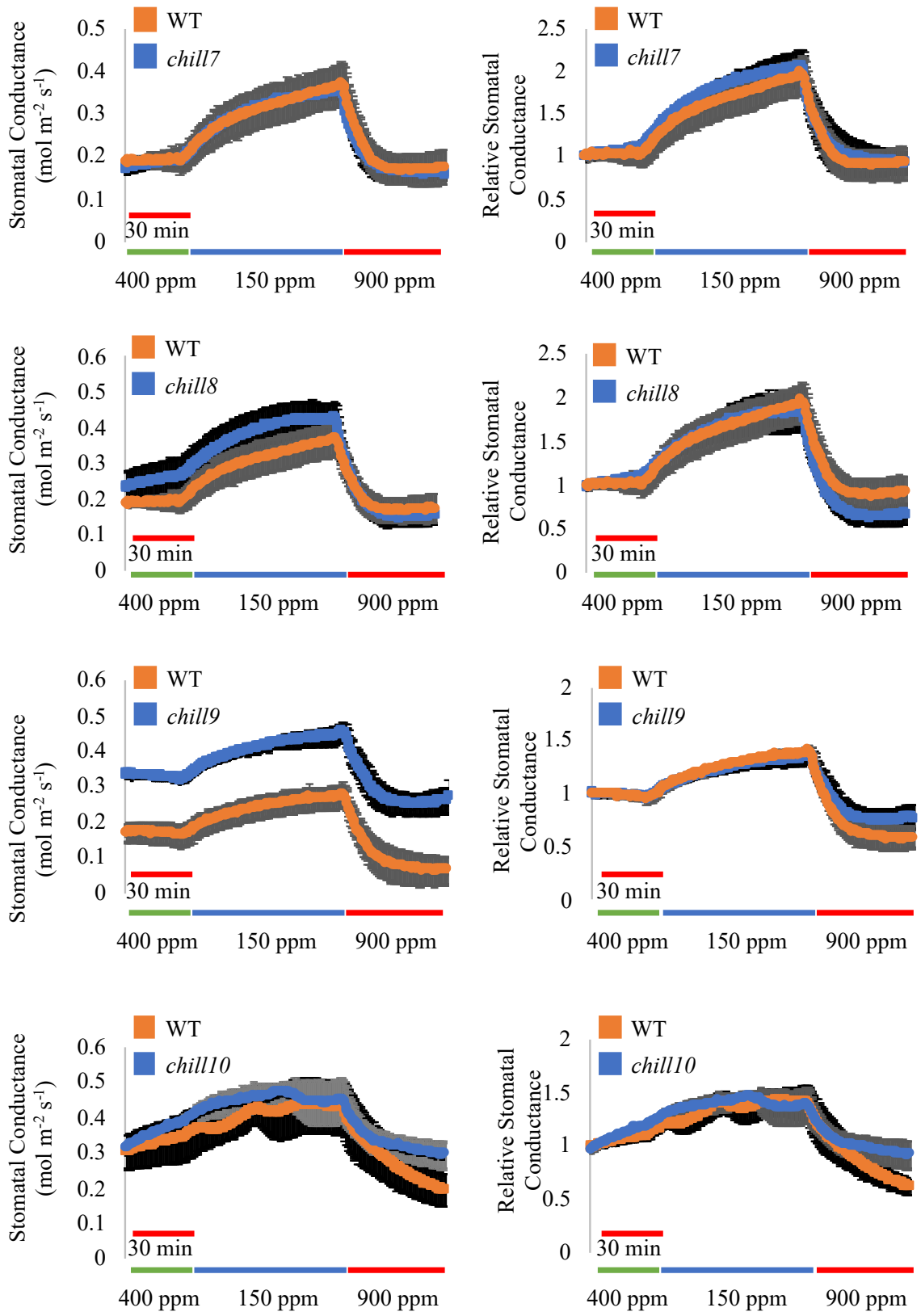

Figure 4.5 – Responses to [CO_2]-shifts in *chill* mutants (continued).

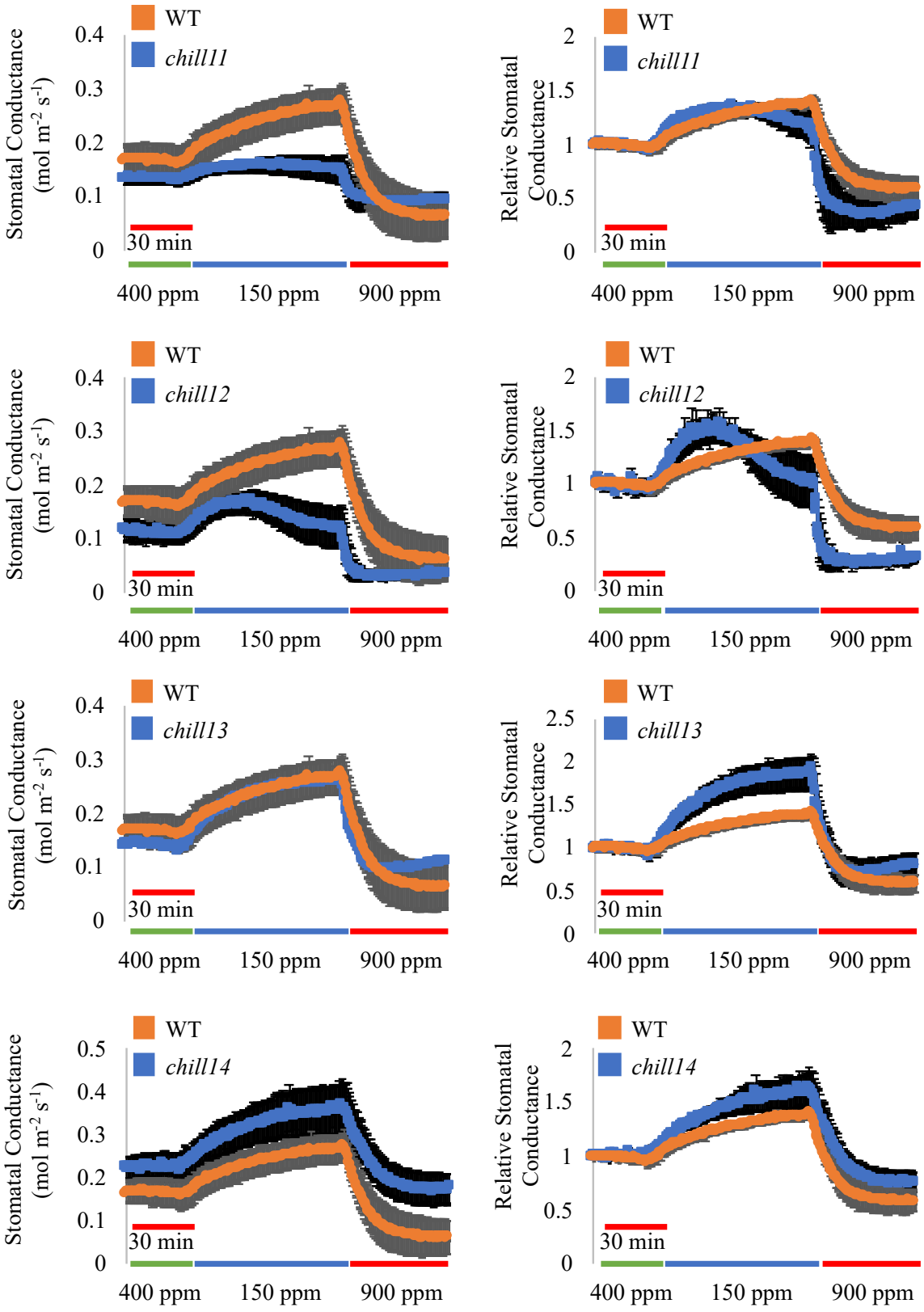

Figure 4.5 – Responses to [CO_2]-shifts in *chill* mutants (continued).

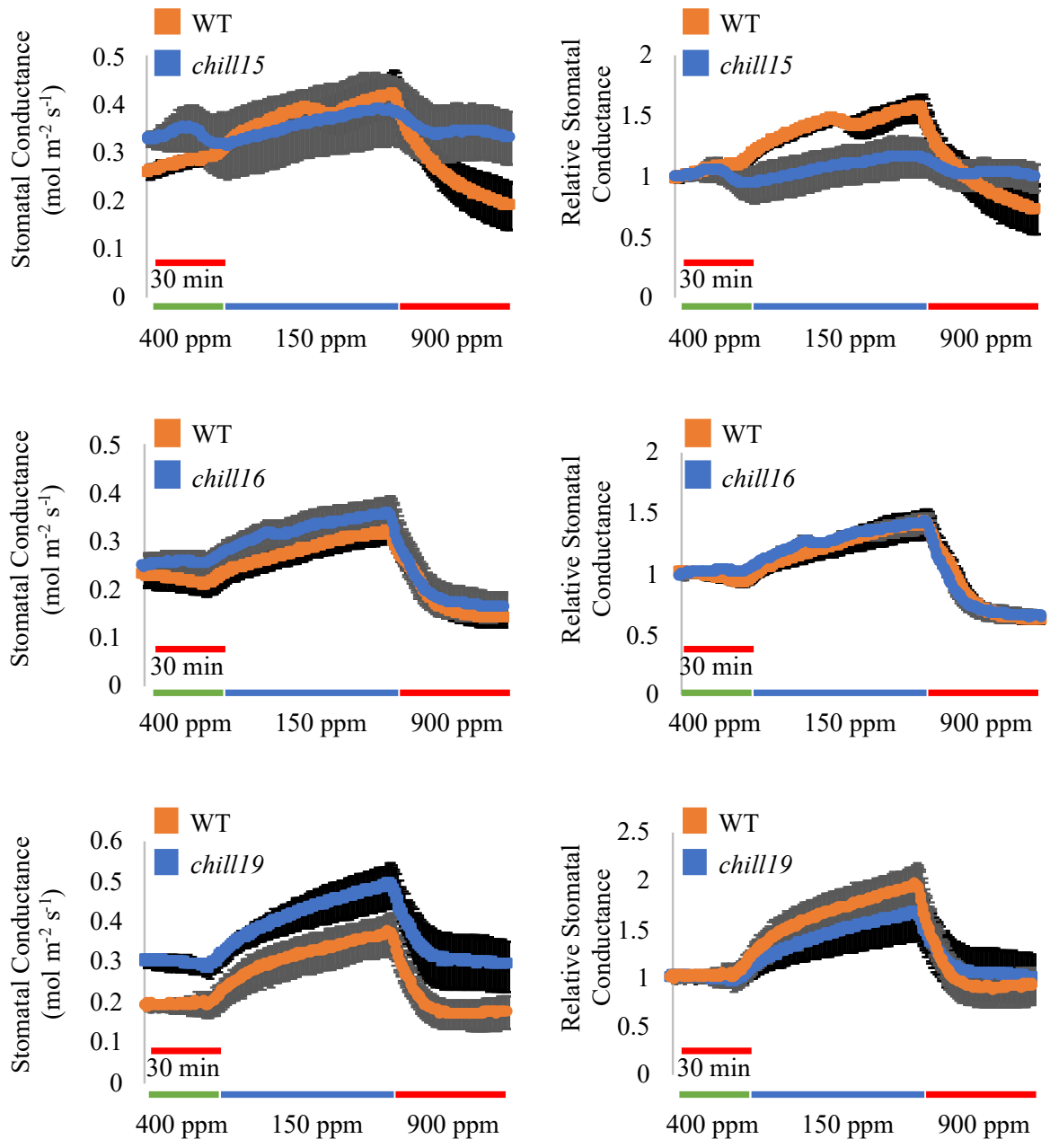

Figure 4.5 – Responses to [CO_2]-shifts in *chill* mutants (continued).

Table 4.1 - Mutant candidates and the status of the screen. In total, 12 of 24 mutants were confirmed by screening M6 generation plants and the remaining 4 of the initial 28 putative mutants are being tested in the M6 generation as described in the text. Thus, presently a total of 16 lines (12 + 4) are being investigated. Note that ABA-induced stomatal closing assays were not performed on mutants that showed no clear CO_2 response phenotype in gas exchange analyses and are labeled as "NA".
*This experiment was done once with n=3 leaves per experiment, plants grown under the non-optimized growth conditions (n=3).
**DNA extracted for WGS.

Re-tested candidates in M5 generation: Colder than Wild Type at Ambient CO_2	Confirmed in M6 generation X=confirmed No=not confirmed	*Preliminary Stomatal Density Imaging X=done	Preliminary Results on Stomatal Density	High CO_2 (900ppm) Thermal Imaging in M6 generation X=done	Results of Thermal imaging under high CO_2	LiCOR Gas Exchange (CO_2) X=done	Insensitive to CO_2	LiCOR Gas Exchange (ABA) X=done	Whole Genome Seq.
chill1	x	x	WT-like	x	colder	x	yes	x	x,x**
R6-33 (chill2)	x	x	WT-like	x	colder	x	no	NA	x
R4-45 (chill3)	x	x	WT-like	x	colder	x	no	NA	x
R5-18 (chill4)	x	x	WT-like	x	colder	x	no	NA	x
R6-18 (chill5)	x/Growing	x	WT-like	x	colder				x
R21-29 (chill6)	No	x	WT-like	x	WT-like	x	no	NA	
R21-32 (chill7)	No	x	WT-like	x	WT-like	x	no	NA	
R21-30 (chill8)	No	x	WT-like	x	WT-like	x	no	NA	
R21-33 (chill9)	No	x	WT-like	x	WT-like	x	no	NA	
R20-7 (chill10)	x	x	WT-like	x	colder	x	partial	ongoing	x**
R20-8 (chill11)	x	x	WT-like	x	WT-like	x	no	NA	
R20-18 (chill12)	x	x	WT-like	x	WT-like	x	no	NA	x**
R20-38 (chill13)	x	x	WT-like	x	WT-like	x	no	NA	x,x**
R20-40 (chill14)	x	x	WT-like	x	WT-like	x	no	NA	x
R20-41 (chill15)	x	x	WT-like	x	colder	x	yes	x	x,x**
R20-43 (chill16)	x	x	WT-like	x	colder	x	no	NA	x
R30-4 (chill17)	Growing					x	no	NA	x**
R31-1 (chill18)	Growing								
R31-34 (chill19)	No			x	WT-like	x	no	NA	x**
R31-5 (chill20)	Growing								x**
R30-7 (chill21)	Growing								x**

References

Ceciliato PH, Zhang J, Liu Q, Shen X, Hu H, Liu C, Schäffner AR, Schroeder JI. 2019. Intact leaf gas exchange provides a robust method for measuring the kinetics of stomatal conductance responses to abscisic acid and other small molecules in Arabidopsis and grasses. Plant Methods **15**, 1 10.

Engineer CB, Ghassemian M, Anderson JC, Peck SC, Hu H, Schroeder JI. 2014. Carbonic anhydrases, EPF2 and a novel protease mediate CO2 control of stomatal development. Nature **513**, 246 +.

Engineer CB, Hashimoto-Sugimoto M, Negi J, Israelsson M, Azoulay-Shemer T, Rappel W-J, Iba K, Schroeder JI. 2016. CO2 Sensing and CO2 Regulation of Stomatal Conductance: Advances and Open Questions. Trends in Plant Science **21**, 16 30.

Hashimoto M, Negi J, Young J, Israelsson M, Schroeder JI, Iba K. 2006. Arabidopsis HT1 kinase controls stomatal movements in response to CO2. Nature Cell Biology **8**, 391 397.

Hiyama A, Takemiya A, Munemasa S, Okuma E, Sugiyama N, Tada Y, Murata Y, Shimazaki K. 2017. Blue light and CO2 signals converge to regulate light-induced stomatal opening. Nature Communications **8**, 901 13.

Hõrak H, Sierla M, Tõldsepp K, Wang C, Wang YS, Nuhkat M, Valk E, Pechter P, Merilo E, Salojärvi J, Overmyer K, Loog M, Brosché M, Schroeder JI, Kangasjärvi J, Kollist H. 2016. A Dominant Mutation in the HT1 Kinase Uncovers Roles of MAP Kinases and GHR1 in CO2-Induced Stomatal Closure. The Plant Cell **28**, 2493 2509.

Hsu P-K, Takahashi Y, Munemasa S, Merilo E, Laanemets K, Waadt R, Pater D, Kollist H, Schroeder JI. 2018. Abscisic acid-independent stomatal CO2 signal transduction pathway and convergence of CO2 and ABA signaling downstream of OST1 kinase. Proc Natl Acad Sci U S A **115**, 201809204 E9980.

Hu H, Boisson-Dernier A, Israelsson M, Böhmer M, Xue S, Ries A, Godoski J, Kuhn JM, Schroeder JI. 2010. Carbonic anhydrases are upstream regulators of CO2-controlled stomatal movements in guard cells. Nature Cell Biology **12**, 87 93-sup pp 1-18.

Matrosova A, Bogireddi H, Mateo-Peñas A, Hashimoto-Sugimoto M, Iba K, Schroeder JI, Israelsson M. 2015. The HT1 protein kinase is essential for red light-induced stomatal opening and genetically interacts with OST1 in red light and CO2 -induced stomatal movement responses. The New phytologist **208**, 1126 1137.

Nunes T, Zhang D, Raissig MT. 2019. Form, development and function of grass stomata. The Plant Journal.

Raissig MT, Matos JL, Anleu Gil MX, Kornfeld A, Bettadapur A, Abrash E, Allison HR,

Badgley G, Vogel JP, Berry JA, Bergmann DC. 2017. Mobile MUTE specifies subsidiary cells to build physiologically improved grass stomata. Science **355**, 1215 1218.

Tõldsepp K, Zhang J, Takahashi Y, Sindarovska Y, Hõrak H, Ceciliato PHO, Koolmeister K, Wang YS, Vaahtera L, Jakobson L, Yeh CY, Park J, Brosche M, Kollist H, Schroeder JI. 2018. Mitogen-activated protein kinases MPK4 and MPK12 are key components mediating CO2-induced stomatal movements. Plant J **96**.

Wang C, Hu H, Qin X, Zeise B, Xu D, Rappel W-J, Boron WF, Schroeder JI. 2016. Reconstitution of CO2 Regulation of SLAC1 Anion Channel and Function of CO2-Permeable PIP2;1 Aquaporin as CARBONIC ANHYDRASE4 Interactor. The Plant Cell **28**, 568 582.

Xue S, Hu H, Ries A, Merilo E, Kollist H, Schroeder JI. 2011. Central functions of bicarbonate in S-type anion channel activation and OST1 protein kinase in CO2 signal transduction in guard cell. The EMBO Journal **30**, 1645 1658.

Zhang J, De-Oliveira-Ceciliato P, Takahashi Y, Schulze S, Dubeaux G, Hauser F, Azoulay-Shemer T, Tõldsepp K, Kollist H, Rappel WJ, Schroeder JI. 2018*a*. Insights into the Molecular Mechanisms of CO2-Mediated Regulation of Stomatal Movements. Current Biology **28**, R1356–R1363.

Zhang J, Wang N, Miao Y, Hauser F, McCammon AJ, Rappel W-J, Schroeder JI. 2018*b*. Identification of SLAC1 anion channel residues required for CO2/bicarbonate sensing and regulation of stomatal movements. Proc Natl Acad Sci U S A **115**, 201807624 11137.